NOAA OAR Special Report

PMEL Tsunami Forecast Series: Vol. NNNN
Development of a Tsunami Forecast Model for Point Reyes, California

Michael C. Spillane [1,2]

[1]Joint Institute for the Study of the Atmosphere and Ocean (JISAO), University of Washington, Seattle, WA
[2]NOAA/Pacific Marine Environmental Laboratory (PMEL), Seattle, WA

June 2011

NOTICE from NOAA

Mention of a commercial company or product does not constitute an endorsement by NOAA/OAR. Use of information from this publication concerning proprietary products or the tests of such products for publicity or advertising purposes is not authorized. Any opinions, findings, and conclusions or recommendations expressed in this material are those of the authors and do not necessarily reflect the views of the National Oceanic and Atmospheric Administration.

Contribution No. XXXX from NOAA/Pacific Marine Environmental Laboratory

Also available from the National Technical Information Service (NTIS)
(http://www.ntis.gov)

Contents

Appendix B Propagation Database: Pacific Ocean Unit Sources

Appendix C Synthetic Testing Report

List of Figures

List of Tables

This page is intentionally blank.

PMEL Tsunami Forecast Series: Vol. NNNN
Development of a Tsunami Forecast Model for Point Reyes, California

Michael C. Spillane [1,2]

Foreword

Tsunamis have been recognized as a potential hazard to United States coastal communities since the mid-twentieth century, when multiple destructive tsunamis caused damage to the states of Hawaii, Alaska, California, Oregon, and Washington. In response to these events, the United States, under the auspices of the National Oceanic and Atmospheric Administration (NOAA), established the Pacific and Alaska Tsunami Warning Centers, dedicated to protecting United States interests from the threat posed by tsunamis. NOAA also created a tsunami research program at the Pacific Marine Environmental Laboratory (PMEL) to develop improved warning products.

The scale of destruction and unprecedented loss of life following the December 2004 Sumatra tsunami served as the catalyst to refocus efforts in the United States on reducing tsunami vulnerability of coastal communities, and on 20 December 2006, the United States Congress passed the "Tsunami Warning and Education Act" under which education and warning activities were thereafter specified and mandated. A "tsunami forecasting capability based on models and measurements, including tsunami inundation models and maps." is a central component for the protection of United States coastlines from the threat posed by tsunamis. The forecasting capability for each community described in the PMEL Tsunami Forecast Series is the result of collaboration between the National Oceanic and Atmospheric Administration office of Oceanic and Atmospheric Research, National Weather Service, National Ocean Service, National Environmental Satellite Data and Information Service, the University of Washington's Joint Institute for the Study of the Atmosphere and Ocean, National Science Foundation, and United States Geological Survey.

Abstract. Operational tsunami forecasting by NOAA's Tsunami Warning Centers relies on the detection of tsunami wave trains in the open ocean, inversion of these data (telemetered via satellite) to quantify their source characteristics, and real-time modeling of the impact on threatened coastal communities. The latter phase of the process involves, for each such community, a pre-tested Forecast Model capable of predicting the impact, in terms of inundation and dangerous inshore currents, with sufficient resolution and within the time constraints appropriate to an emergency response.

In order to achieve this goal, considerable advance effort is required to tune each forecast model to the specific bathymetry and topography, both natural and manmade, of the impact area, and to validate its performance with a broad set of tsunami sources. Where possible the validation runs should replicate observed responses to historical events, but the sparse instrumental record of these rare but occasionally devastating occurrences dictates that comprehensive testing should include a suite of scenarios that represent potential future events.

During the forecast model design phase, and in research mode outside the pressures of an emergency situation, more detailed and slower-running models can be investigated. Such a model, referred to as a Reference Model, represents the most credible numerical representation of tsunami response for the study region, using the most detailed bathymetry available and without the run-time constraint of operational use. Once a reference model has been developed, the process of forecast model design is to determine where efficiencies can be gained, through reducing the grid resolution and increasing the model time step, while still adequately representing the salient features of the full solution.

This report documents the reference and forecast model development for Point Reyes and vicinity, comprising much of western Marin County, CA. The Point Reyes headland juts out into the Pacific and its lighthouse is a prominent navigation landmark northwest of the entrance to San Francisco Bay. A tide gage within Drake's Bay, in the lee of the headland, provides observations for model validation. While much of the study region lies within a National Seashore area, limiting the population and waterfront infrastructure, there are a number of nearby communities exposed to tsunami impact. Beaches and other natural amenities and the mild climate foster extensive recreational use, and there is a clear need for emergency preparedness. This report addresses the tsunami aspects of the natural hazard spectrum.

[1] Joint Institute for the Study of the Atmosphere and Ocean (JISAO), University of Washington, Seattle, WA
[2]NOAA/Pacific Marine Environmental Laboratory (PMEL), Seattle, WA

1.0 Background and Objectives

1.1. The Setting

Point Reyes, lying to the northwest of the entrance to San Francisco Bay is a prominent navigational landmark. As illustrated in Figure 1 (composed of orthographic images from "MarinMaps" (mmgis.marinmap.org/OrthoGrid/viewer.htm), the headland is the site of a lighthouse and, in Drake's Bay in its lee adjacent to the historic Point Reyes Lifeboat station, is the tide gage bearing the same name. All lie within the Point Reyes National Seashore (PRNS), comprising most of west Marin County, which is essentially unpopulated and in a natural state, with the exception of some agricultural activity that was allowed to continue when the PRNS was established in 1962. As seen in the inset to Figure 1, the San Andreas Fault strongly delineates the eastern boundary of the region though it is submerged in Tomales Bay, in the north, and Bolinas Lagoon in the south. In the neck of land between them are the communities of Olema and Point Reyes Station, which are close to the epicenter of the 1906 San Francisco Earthquake. Several small communities lie on the shores of Tomales Bay (20.4km in length but with a mean depth of only 3.1m, Nieme and Hall, 1996). The connection to Bodega Bay is shallow and constricted. At the southern end, Bolinas (2010 Pop. 1,620) and Stinson Beach (2010 Pop. 632) have greater exposure to damage from tsunami or winter storm waves. Between Stinson Beach and Point Bonita, the southernmost point of Marin County, is Muir Beach, a community of about 310. It is notable, from the tsunami perspective, in that it reported major run-ups during the Unimak-1946 and Alaska-1964 events.

North of Tomales Bay is Bodega Bay whose shores lie both in Marin and Sonoma counties. Apart from the shallow Bodega Harbor, and the communities of Bodega Bay (2010 Pop. 1,077) and Doran Beach extending onto the spit at its mouth, this area too is sparsely populated. The natural beauty of the region, with its mild climate and proximity to the San Francisco area and other urban centers, provides outstanding recreational opportunities, resulting in large numbers of visitors throughout the year. Normally, in selecting the domain of a tsunami forecast model, the location of a tide gage provides the focus but, in this case, a somewhat larger region is included to provide forecast capability to population centers and primary recreational assets. Initially it was hoped that a forecast model could cover the entire region from Bodega Bay to Muir Beach. This proved to be impossible, given the time constraints on model run time imposed by emergency usage, without an unacceptable reduction in spatial resolution. While the C-grid of the Reference Model (RM) does include Tomales Bay and a portion of Bodega Bay, these are excluded from the Forecast Model (FM), which focuses on the south and southwest of Marin County.

The University of Southern California Tsunami Research Center conducted a comprehensive study of potential tsunami inundation, for the entire California coastline. Funded through the California Emergency Management Agency (CalEMA), by the National Tsunami Hazard Program, the study (Barberopoulou et al, 2011) has produced a set of inundation maps for emergency planning purposes accessible online in various forms, including MyHazard (myhazards.calema.ca.gov) which enables users to acquire information specific to their site of interest. The CalEMA inundation results are available in GIS form and those specific to the Point Reyes area are used throughout this report. In

addition to underpinning the modeling effort, the digital elevation model (DEM) for the San Francisco region, provided by the National Geophysical Data Center (NGDC), includes a 3-D oblique view that assists greatly in visualizing the study area. In Figure 2, the CalEMA inundation information is overlaid, together with descriptive labels on an extract from the NGDC image. The full 3-D image is available in the San Francisco DEM Report (Carnigan et al., 2010).

A striking series of aerial photographs (www.californiacoastline.org) show that the study region contains both high cliffs (also seen in Figure 3) that limit potential impact by tsunamis and broad beaches and shallow coastal inlets that are more exposed. Queries to the CalEMA "MyHazards" site for Bolinas and Stinson Beach show flooding and earthquake as other hazards to which they are prone, in addition to tsunami. Available online is a video "Marin Tsunami" (Loeffler and Gesell, 2010), produced for the USGS in cooperation with the Marin County Sheriff – Office of Emergency Services. In addition to providing an overview of the comprehensive level of preparedness for tsunami impact on the communities of Bolinas, Stinson Beach, Dillon Beach/Lawson's Landing, and the popular Limantour Beach within the National Parks area of responsibility, this excellent resource for residents and visitors alike gives insight into the character of the area.

1.2. Natural Hazards

Instances of mild tsunami signals are evident in the tide gage records for Point Reyes (established in 1975), and Marin County sites appears several times in the records compiled by Lander and Lockridge (1989) and its regularly updated online equivalent: NGDC Tsunami Hazard Database (Dunbar, 2007; see www.ngdc.noaa.gov/hazard/). The historical record first mentions Marin County with a wave observed at Sausalito, on the north shore of the Golden Gate, from a Chilean event in 1877. The first time series currently available for analysis is a digitized marigram from Sausalito, recorded during the Sanriku event of 1896 and available in the Alaska/West Coast Tsunami Warning Center (WCATWC) archives. O'Brien (1946) described a 2.6 meter wave (above MLLW) in Drake's Bay during the 1946 Unimak tsunami, with a boat washed onto the highway. While Marin County sites are not explicitly mentioned in connection with the Kamchatka-1952 or Andreanof-1957 events, waves were observed at Bodega and within San Francisco Bay. During the 1960 Chile event, a 1.5 meter run-up was reported at Stinson Beach, and during the 1964 Alaska tsunami waves were observed at several sites within Marin County including Drake's Beach. Time series from several tsunamis are available from the Point Reyes tide gage in recent years, culminating in the major event east of Honshu on March 11, 2011 (also referred to as the Tohuko earthquake.) The latter will be discussed extensively in this report.

Combining events impacting northern California with those that have occurred since the Point Reyes tide gage was upgraded to 1-minute sampling, a total of 27 historical events are available for study. Nineteen of these, listed in Table 1a, are the standards for forecast

Table 1a. Source characterization for historical tsunami events employed in Point Reyes model testing. Those in bold text were used in RM/FM inter-comparison. Sources identified as "ad hoc" may not be identically defined in other Forecast Model reports.

Earthquake / Seismic				Model		
Event	**USGS Date Time (UTC) Epicenter**	**CMT Date Time (UTC) Centroid**	**Magnitude M_w**	**Tsunami Magnitude**	**Subduction Zone**	**Tsunami Source (Reference/Derivation)**
1946 Unimak	01 Apr 12:28:56 52.75ºN 163.50ºW		8.5	8.5	ACSZ	7.5×B23 + 19.7×B24 + 3.7×B25 (López & Okal, 2006)
1952 Kamchatka	04 Nov 16:58:26.0 52.76ºN 160.06ºE		9.0	9.0	KISZ	19.71 × (A4 + Y4 + Z4 + A5 + Y5 + Z5 + A6 + Y6 + Z6) (ad hoc)
1957 Andreanof	09 Mar 14:22:31 51.56ºN 175.39ºW		8.6	8.7	ACSZ	31.4×A15 + 10.6×A16 + 12.2×A17 (Preliminary)
1960 Chile	22 May 19:11:14 38.29ºS 73.05ºW		9.5	9.5	CSSZ	125×(A93 + B93 + Z93 + A94 + B94 + Z94 + A95 + B95) Kanamori & Cipar (1974)
1964 Alaska	28 Mar 03:36:00 61.02ºN 147.65ºW		9.2	8.9	ACSZ	15.4×A34 + 18.3×B34 + 48.3×Z34 +19.4×A35 +15.1×B35 (Tang et al., 2006, 2009)
1994 East Kuril	04 Oct 13:22:58 43.73ºN 147.321ºE	04 Oct 13:23:28.5 43.60ºN 147.63ºE	8.3	8.1	KISZ	9.0×A20 (ad hoc)
1996 Andreanof	10 Jun 04:03:35 51.56ºN 175.39ºW	10 Jun 04:04:03.4 51.10ºN 177.410ºW	7.9	7.8	ACSZ	2.40×A15 + 0.80×B16 (Preliminary)
2001 Peru	23 Jun 20:33:14 16.265ºS 73.641ºW	23 Jun 20:34:23.3 17.28ºS 72.71ºW	8.4	8.2	CSSZ	5.7×A15 + 2.9×B16 + 1.98×A16 (Preliminary)
2003 Hokkaido	25 Sep 19:50:06 41.775ºN 143.904ºE	25 Sep 19:50:38.2 42.21ºN 143.84ºE	8.3	8.3	KISZ	3.95 × (A22 + B22 + A23 + B23) (ad hoc)
2003 Rat Island	17 Nov 06:43:07 51.13ºN 178.74ºE	17 Nov 06:43:31.0 51.14ºN 177.86ºE	7.7	7.8	ACSZ	2.81×B11 (Real-time)
2006 Tonga	03 May 15:26:39 20.13ºS 174.161ºW	03 May 15:27:03.7 20.39ºS 173.47ºW	8.0	8.0	NTSZ	6.6×B29 (ad hoc)
2006 Kuril	15 Nov 11:14:16 46.607ºN 153.230ºE	15 Nov 11:15:08 46.71ºN 154.33ºE	8.3	8.1	KISZ	4.0×A12 + 0.5×B12 + 2.0×A13 + 1.5×B13 (Real-time)
2007 Kuril	13 Jan 04:23:20 46.272ºN 154.455ºE	13 Jan 04:23:48.1 46.17ºN 154.80ºE	8.1	7.9	KISZ	-3.64 × B13 (Real-time)
2007 Solomon	01 Apr 20:39:56 8.481ºS 156.978ºE	01 Apr 20:40:38.9 7.76ºS 156.34ºE	8.1	8.2	NVSZ	12.0×B10 (Preliminary)
2007 Peru	15 Aug 23:40:57 13.354ºS 76.509ºW	15 Aug 23:41:57.9 13.73ºS 77.04ºW	8.0	8.1	CSSZ	0.9×A61 + 1.25× B61 + 5.6×A62 + 6.97×B62 + 3.5×Z62 (Preliminary)
2007 Chile	14 Nov 15:40:50 22.204ºS 69.869ºW	14 Nov 15:41:11.2 22.64ºS 70.62ºW	7.7	7.6	CSSZ	1.65×Z73 (Real-time)
2009 Samoa	29 Sep 17:48:10 15.509ºS 172.034ºW	29 Sep 17:48:26.8 15.13ºS 171.97ºW	8.1	8.1	NTSZ	3.96×A34 + 3.96×B34 (Real-time)
2010 Chile	27 Feb 06:34:14 35.909ºS 72.733ºW	27 Feb 06:35:15.4 35.95ºS 73.15ºW	8.8	8.8	CSSZ	17.24×A88 + 8.82×A90 + 11.84×B88 + 18.39×B89 + 16.75×B90 + 20.78×Z88 + 7.06×Z90 (Real-time)
2011 Honshu	11 Mar 05:46:24 38.297^{0}N 142.372^{0}E	11 Mar 05:47:47.2 38.486^{0}N 142.597^{0}E	9.0	9.0	KISZ	4.66 × B24 + 12.23×B25 + 26.31×A26 + 21.27×B26 + 22.75×A27 + 4.98×B27 (Real-time; Tang et al., 2012)

Table 1b. Supplementary historical tsunami events employed for Point Reyes, CA forecast model testing. Those identified as "ad hoc" and may not be identically implemented in other Forecast Model reports.

Earthquake / Seismic				Tsunami Source (Reference/Derivation)		
Event	**USGS Date Time (UTC) Epicenter**	**CMT Date Time (UTC) Centroid**	**Magnitude M_w**	**Tsunami Magnitude**	**Subduction Zone**	**Tsunami Source**
1896 Sanriku	15 Jun 10:33:00 39.5ºN 144.0ºE		7.6	7.6	KISZ	b25 x 1.413 (ad hoc)
1992 Mendocino	25 Apr 18:06:04 40.368ºN 124.316ºW	25 Apr 18:06:11.8 38.56ºN 123.31ºW	7.2	7.2	ACSZ	a65 x 0.355 **or** b65 x 0.355 (ad hoc)
1995 Chile	30 Jul 05:11:24 23.340ºS 70.294ºW	30 Jul 05:11:56.9 24.17ºS 70.74ºW	8.0	8.0	CSSZ	2.812 x (a75 + b75) (ad hoc)
1995 Kuril	03 Dec 18:01:09 44.663ºN 149.300ºE	03 Dec 18:01:36.1 44.82ºN 150.17ºE	7.9	7.9	KISZ	1.991 x (a17 + z17) (ad hoc)
1996 Irian Jaya	17 Feb 05:59:31 0.891ºS 136.952ºE	17 Feb 06:00:02.8 0.67ºS 136.62ºE	8.2	8.2	NGSZ	2.7984 x (a9 + b9 + a10 + b10) (ad hoc)
2009 PapuaNG	03 Jan 19:43:51 0.414ºS 132.885ºE	03 Jan 19:44:09.0 0.38ºS 132.83ºE	7.6	7.6	NGSZ	0.7046 x (b13 + b14) (ad hoc)
2009 Kuril	15 Jan 17:49:39 46.857ºN 155.154ºE	15 Jan 17:49:48.3 46.97ºN 155.39ºE	7.4	7.4	KISZ	b12 x 0.7063 (ad hoc)
2009 Vanuatu / Santa Cruz	07 Oct 22:03:15 13.052ºS 166.187ºE	07 Oct 22:03:28.9 12.59ºS 166.27ºE	7.6	7.6	NVSZ	1.2×B24 + 0.26×A23 *followed after 15minutes by*
	07 Oct 22:18:26 12.554ºS 166.320ºE	07 Oct 22:19:15.3 11.86ºS 166.01ºE	7.8	7.9	NVSZ	2.6×B23 + 0.9×A23 (Preliminary Wei 2009, Personal Communication)

model testing in the Pacific because their sea floor deformation is reasonably well known, either from the literature or, more recently, derived from direct observation of the wave trains they generated. The remaining eight, listed in Table 1b, have source characteristics that are less well known; they are included to expand the geographical coverage or because of their special relevance to the West Coast. The M_w 7.2 earthquake north of Cape Mendocino on April 25, 1992 was a very mild foretaste of a Cascadia Subduction Zone (CSZ) event but was registered in marigrams at Arena Cove and Point Reyes. Others, due to significant noise in the tide gage, do not produce a clear signal but shed light on Point Reyes as a reference point for coastal impacts. Figure 4 illustrates the distribution of the 27 historical sources. Those highlighted in red were employed for intercomparison of the reference and forecast versions of the model.

Direct seismic impact is another natural hazard to which Point Reyes area is exposed. Its proximity to the rupture zone of the SAF in the San Francisco earthquake of 1906 resulted in significant damage to the town and the destruction of the lighthouse. While the SAF enters the ocean at Bolinas, its strike-slip nature reduces the likelihood of severe tsunami wave generation should ruptures occur in the immediate vicinity. Submarine landslides or collapse of sections of sea cliff are however a potential local source for tsunami damage. Landslides triggered by seismic events caused significant loss of life during the 1929 Newfoundland event and accentuated the 1996 New Guinea tsunami. Landslide-generated tsunami waves are not currently included in the SIFT forecast methodology, nor are those generated meteorologically. However, to the extent that the waves they produce are detected by the DART array, some warning of their presence may be available.

Another local hazard that has been a frequent cause of damage in the Bolinas-Stinson Beach area has been ocean wave action. Originating locally, or as swell from distant storms, such waves in the winters of 1977-78 and 1982-83 caused the loss of several beachfront homes. Another impact of ocean waves, of relevance to tsunami detection and modeling, is in the noise they produce in the tide gage records. Although the Point Reyes tide gage is in the lee of the headland, excessive wave action and resonance can mask weak tsunami signals.

1.3. Tsunami Warning and Risk Assessment

The forecast model development, described here, will permit Point Reyes, CA, to be incorporated into the tsunami forecasting system SIFT, developed at NCTR (NOAA Center for Tsunami Research) and now in operational use at the U.S. Tsunami Warning Centers (TWC's). The system has had considerable success is accurately forecasting the impact of both moderate and severe tsunami events in recent years and in the following section the methodology that permits such forecasts is discussed as prelude to a description of development of the forecast model for Point Reyes. With the model in hand, validated with historical events and with its stability verified by extensive testing against extreme scenarios, real-time forecasts will be available to inform local emergency response. Additionally, the synthetic scenarios investigated during model development, and reported here, provide an initial tsunami risk assessment as described in the Results and Discussion section.

2.0 Forecast Methodology

2.1 The Tsunami Model

In operational use, a tsunami forecast model is used to extend a pre-computed deep-water solution into the shallows, and onshore as inundation if appropriate. The model consists of a set of three nested grids, of increasingly fine resolution that, in a real-time application of the MOST model (Method of Splitting Tsunami: Titov and Synolakis, 1998; Titov and González, 1997), permits forecasts at spatial scales (as little a few tens of meters) relevant to local emergency management. The validity of the MOST model applied in this manner, and the operational effectiveness of the forecast system built around it, has been demonstrated during unplanned tests triggered by several mild to moderate tsunami events in the years since the 2004 Indian Ocean disaster (Wei et al., 2008). Successful hindcasting of observed historic events, even mild ones, during forecast model development lends credence to the ability to accurately forecasting the impact of future events. Such validation of tsunami modeling procedures is documented in other volumes of the series of which this report is but one. Before proceeding to a description of the forecast model development for Point Reyes, it is useful to describe the steps in the overall forecast process.

2.2 The SIFT Forecast System

Operational tsunami forecasts are generated at Tsunami Warning Centers, staffed 24/7 in Alaska and Hawaii, using the SIFT (Short-term Inundation Forecasting for Tsunamis) tool, developed at NCTR. The semi-automated process facilitates the steps by which TWC operators assimilate data from an appropriate subset of the DART® tsunami sensors, "invert" the data to determine the linear combination of pre-computed propagation solutions that best match the observations, then initiate a set of forecast model runs if coastal communities are threatened or, if warranted, cancel the warning.

Steps in the process are as follows:

- When a submarine earthquake occurs the global network of seismometers registers it. Based on the epicenter, the unit sources in the Propagation Database (Gica et al., 2008) that are most likely to be involved in the event, and the DART® array elements (Spillane et al., 2008) best placed to detect the waves passage are identified. TWC watch-standers can trigger DART®s into rapid sampling mode in the event that this did not occur automatically in response to the seismic signal.
- There is now an unavoidable delay while the tsunami waves are in transit to the DART®s; at least a quarter of a cycle of the first wave in the train must be sampled before moving to the "inversion" step.
- When sufficient data have accumulated, at one or more DART®s, the observed time series are compared with the model series from the candidate unit sources. Since the latter are pre-computed (using the MOST code), and the dynamics of tsunami waves in deep water is linear, a least squares approach taking very little time can identify the unit sources, (and the appropriate scale factors for each,) that

best fit the observations. The "inversion" methodology is described by Percival et. al., (2009).

- Drawing again on the Propagation Database, the scale factors are applied to produce a composite basin-wide solution with which to identify the coastal regions most threatened by the radiating waves.
- It is at this point that one or more forecast models are run. The composite propagation solution is employed as the boundary condition to the outermost (A-grid) domain of a nested set of three real-time MOST models that telescope with increasingly fine scale to the community of concern. A-grid results provide boundary conditions to the B-grid, which in turn forces the innermost C-grid. Non-linear processes including inundation are modeled so that, relying on the validation procedures during model development, credible forecasts of the current event are available.
- Each forecast model provides quantitative and graphic forecast products with which to inform the emergency response, or to serve as the basis for canceling or reducing the warnings. Unless the tsunami source is local, the forecast is generally available before the waves arrive but, even when lead-time cannot be provided, the several hour duration of a significant event (in which the first wave may not be the most damaging) give added value to the multi-hour forecasts provided.

Because multiple communities may be potentially at risk, it may be necessary to run simultaneously, or in a prioritized manner, multiple forecast models. Each must be optimized to run efficiently in as little time as possible; the current standard is that an operational forecast model should be capable of simulating 4 hours of real time within about 10 minutes of CPU time on a fast workstation computer.

3.0 Model Development

3.1 Digital Elevation Models

Water depth determines local tsunami wave speed and sub-aerial topography determines the extent to which tsunami waves inundate the land. Thus a prerequisite for credible tsunami modeling is the availability of accurate gridded bathymetric and topographic datasets, termed DEM's (Digital Elevation Models.) Given their expertise in this area, and the number of coastal communities needing tsunami forecast capability, NCTR relies heavily on the National Geophysical Data Center (NGDC) to provide the DEM's needed. In the case of Point Reyes, a sub-region of the San Francisco DEM is employed. The DEM, a composite of multiple data sources merged and converted to a common datum of Mean High Water (MHW), was produced and documented by Carignan et al. (2010). The use of MHW as the "zero level" for forecast results is standard. The MOST model does not include tidal fluctuations and, since a tsunami may arrive at any stage of the tide, it is best to employ a "worst-case" approach by assuming high tide when forecasting inundation. For some Forecast Models grounding of vessels and the strong and the rapidly varying currents often associated with even mild tsunamis are of concern. For Point Reyes, lacking a marina and shoreline infrastructure, low water impacts are less important.

The Point Reyes sub-region of the San Francisco DEM was illustrated in Figure 2; its salient features listed in Table 2 are reproduced from DEM documentation (Carnigan et al., 2010). The NGDC report thoroughly describes the data sources and methods employed in constructing the DEM. With one-third arc second (~10m) resolution, the DEM provides the basis for the B and C-grids for both reference and forecast model usage. NCTR maintains an atlas of lower resolution gridded bathymetries, which can be used for the A-grids, as described later. All of the DEMs employed were verified for consistency with charts, satellite imagery, and other datasets during the course of MOST grid development.

Table 2. The main features of the San Francisco Digital Elevation Model (DEM), which includes Point Reyes, California.

Grid Area	**San Francisco, California**
Coverage Area	123.30º to 121.85º W; 37.32º to 38.48º N
Coordinate System	Geographic decimal degrees
Horizontal Datum	World Geodetic System 1984 (WGS84)
Vertical Datum	**Mean High Water (MHW)**
Vertical Units	Meters
Cell Size	**1/3 arc-second**
Grid Format	ESRI Arc ASCII grid
Version Employed	Update of February 24, 2011

3.2 Tides and Sea Level Variation

The history of tidal observation at Point Reyes dates back only to 1975. The tide station (9415020) is located near the end of the pier projecting into Drake's Bay just west of the historic Lifeboat station. The pilings raise the deck well above sea level and do not impede water movement. The instrumentation was upgraded in 2006 to include a tsunami-capable gage sampling at 1-minute intervals (and, on demand at 15-second intervals); some earlier data was sampled at 6-minute intervals and several historical events are only available as marigrams on microfiche. An ongoing project at NGDC will digitize the more critical images in this archive; a few are available in digitized form in the WCATWC archives.

Station characteristics for 9415020 are provided in Table 3, based on the wealth of online tidal information available at NOAA's CO-OPS (Center for Operational Oceanographic Products and Services) website (tidesandcurrents.noaa.gov). Note the sizeable diurnal range of about 1.7 meters and that, while the long-term rate of change in sea level is low (compared to more seismically active areas), there is substantial seasonal, interannual and short-term variability.

Table 3. Tidal characteristics of the Point Reyes, CA Tide Gage (9415020).

<table>
<tr><th colspan="4">Point Reyes, CA Station#9415020 37^{0}59.7'N, 122^{0}58.6'W</th></tr>
<tr><td colspan="4">Tidal Datum and Range Values (Epoch 1983-2001)</td></tr>
<tr><td>MHHW (Mean Higher High)</td><td>2.964m</td><td rowspan="5">Great Diurnal Range
1.758m</td><td></td></tr>
<tr><td>MHW (Mean High Water)</td><td>2.760m</td><td rowspan="3">Mean Range
1.193m</td></tr>
<tr><td>MSL (Mean Sea Level)</td><td>2.152m</td></tr>
<tr><td>MLW (Mean Low Water)</td><td>1.567m</td></tr>
<tr><td>MLLW (Mean Lower Low)</td><td>1.206m</td><td></td></tr>
<tr><td colspan="4">Sea Level Trends and Cycles</td></tr>
<tr><td>Long Term SL Trend</td><td colspan="3">Increasing 2.10±1.52mm/year</td></tr>
<tr><td>Seasonal Cycle Range</td><td colspan="3">Minimum -89mm(April); Maximum 59mm(September)</td></tr>
<tr><td>Interannual Variation
(from1980)</td><td colspan="3">Minimum -20mm(1989); Maximum +21mm(1998)</td></tr>
<tr><td colspan="4">Extremes to date (June 2011)</td></tr>
<tr><td>Maximum</td><td colspan="3">3.810m on 06 Feb, 1998</td></tr>
<tr><td>Minimum</td><td colspan="3">0.387 on 19 Jan, 1988</td></tr>
</table>

A sample section of the tide gage record, extracted from the CO-OPS website for the period following the Honshu-2011 is included in Figure 18 from Section 4.3. In a several hour section of one-minute data, the signature of an arriving tsunami is generally a burst of higher frequency energy with a sudden onset. However, during the winter months in particular, similar bursts unrelated to tsunami activity are quite common. In January 2011 for example several occurred, one of which is illustrated in Figure 5. The tidal signal has been removed with a Butterworth band-pass filter with cutoff periods at 5 and 120 minutes. This filter will be used through the report is preprocessing tide gage records for comparison with model prediction. The lower panel of Figure 5 is the spectral wave

energy at hourly intervals from NDBC buoy 46026, 18nm west of San Francisco. There is a clear correlation between enhanced swell at this site and the detided residuals in Drake's Bay suggesting that surface waves can excite a coastal response. The amplitude of this noise for the example shown is perhaps 10-20cm and would likely obscure a mild tsunamis signature were one to arrive during such an episode. Deviations (or residuals) from the astronomically predicted tide can be several centimeters and the variability strong. In particular the highest water level reported for the Point Reyes gage is 1.05m above MHW (Feb 6, 1998) so the use of MHW as the zero level of modeled sea level may underestimate the truly worse case. While the simultaneous arrival of the crest of a large tsunami at high tide during a storm surge has low probability, a feature of the simulated events reported below is that sustained oscillations at a resonant period may extend the duration of the threat. This effect is notorious at Crescent City, CA which is frequently the most heavily impacted U.S. west coast location for remote events.

3.3 The CFL Condition and other considerations for grid design

Water depth dependent wave speed, in conjunction with the spacing of the spatial grid representation, place an upper limit on the time step permissible for stable numerical solutions employing an explicit scheme. This is the CFL limit (Courant-Friedrichs-Levy), which requires careful consideration when the grids employed for a reference or forecast model are being designed. Finer-scale spatial grids, or greater water depths, require shorter time steps thereby increasing the amount of computation required to simulate a specific real time interval.

Another feature of the application of gridded numerical solutions to the tsunami wave problem is the shortening that the wave train encounters in moving from deep water onto the shelf. In deep water a grid spacing of 4 arc-seconds (of latitude and longitude, corresponding to ~7km) is normally used to represent propagating wave trains whose wavelength is typically of the order of a few hundred kilometers. The stored results of such propagation model runs are typically decimated by a factor of 4, resulting in a database of ~ 30km spacing (and 1 minute temporal sampling) with which to generate the boundary conditions for the outermost of the nested grids in a model solution. The extraction of the boundary conditions (of wave height and the two horizontal velocity components) is achieved by linear interpolation in space and time. To provide realistic interpolated values the stored fields for these variables must be smoothly varying, and have adequate sampling in space and time to resolve their structure. This necessitates the placement of the offshore boundary of the forecast model domain well offshore. The presence of the Mendocino Escarpment is another incentive to do so, in order that its role in topographic steering of trans-Pacific wave trains is adequately represented.

3.4 Specifics of the model grids

After several rounds of experimentation, the extents and resolutions of the nested grids were chosen, and are illustrated in Figures 7 and 8; details are provided in Tables 4 and 5. The Reference Model (RM) grid extents were set early in the process when the hope was to provide forecast results from Bodega Bay to Muir Beach, but have further value in ensuring adequate representation of waves entering the domain from remote sources. The RM grids are displayed in Figure 7; in the A- and B-grid panels, rectangles show the

nested grid domain within. In the case of the RM grid-C panel, the reduced extent of the equivalent FM grid is indicated. Figure 8 depicts the nested grids of the Forecast Model. The main focus of the FM, and this report, is on the southwestern and southern portion of Marin County. Some mention of the northern portion will be made as appropriate but, with the exception of some results that can be derived from the A-grid, comprehensive forecasts for Bodega Bay will require a dedicated model.

Table 4. Specifics of the Reference (RM) and Forecast model (RM) grids employed for Point Reyes, CA. For the paired values in the resolution and grid points columns, the zonal (East to West) value is listed first, followed by meridional (North to South).

Point Reyes, CA Reference Model (RM)						
Grid	**Zonal Extent**		**Meridional Extent**		**Resolution**	**Grid Points**
A	128.000ºW	121.500ºW	36.000ºN	42.500ºN	30”x30”	781 x 781
B	123.300ºW	122.100ºW	37.475ºN	38.475ºN	4”x3”	1081 x 1201
C	123.150ºW	122.533ºW	37.825ºN	38.350ºN	$^4/_3$”x1”	1666 x 1891

Point Reyes, CA Forecast Model (FM)						
Grid	**Zonal Extent**		**Meridional Extent**		**Resolution**	**Grid Points**
A	125.000ºW	122.000ºW	37.00ºN	39.00ºN	60”x60”	181 x 121
B	123.300ºW	122.100ºW	37.550ºN	38.475ºN	18” x 15”	241 x 233
C	123.130ºW	122.533ºW	37.825ºN	38.100ºN	4” x 3”	538 x 331

Table 5. Grid file names and grid-related parameters. The time steps for the A and B-grids must be integer multiples of the basic time step chosen for the C-grid.

Grid	Filename	Maximum Depth (m)	Minimum CFL (s)	Model Time Step (s)	Water Cells
A	PtReyesCA_RM_A	5002	3.350	1.2 (2x)	436,723
	PtReyesCA_FM_A	4379	7.137	6.0 (3x)	15,977
B	PtReyesCA_RM_B	2166	0.637	0.6 (1x)	664,682
	PtReyesCA_FM_B	2114	3.062	2.0 (1x)	26,598
C	PtReyesCA_RM_C	98.6	0.995	0.6	1,411,698
	PtReyesCA_FM_C	94.7	3.045	2.0	103,086

Both C-grids lie entirely within the NGDC-provided DEM; A and B-grids incorporate bathymetry and topography from other DEM datasets available at NCTR. Some smoothing and editing were necessary to eliminate erroneous points or grid features that tend to cause model instability. For example, “point” islands where an isolated grid cell stands above water are eliminated, as are narrow channels or inlets one grid unit wide; these tend to resonate in the numerical solution. Large depth changes between adjacent grid cells can also cause numerical problems; customized tools (such as “bathcorr”) are available to correct many of these grid defects. An additional constraint on the bathymetry is the SSL (Elena Tolkova, personal communication), which identifies excessive depth changes in the discrete representation.,

Details of the model grids are provided in Tables 4 and 5. The latter lists the maximum depth, the CFL time step requirement that must not be exceeded, and the actual time steps chosen for the reference and forecast model runs. Since in the current version of MOST, employed by SIFT, the numerical solutions in the three grids proceed simultaneously, there is a requirement that the A and B-grid time steps be integer multiples of the (innermost) C-grid time step in addition to satisfying the appropriate CFL requirement. For both reference and forecast models the CFL requirement of the C-grid was the most stringent. The values chosen are shown in the final column of Table 4 and are such that an integer multiple of each time step (15x for the forecast model; 50x for the reference) is identically 30 seconds, the chosen output time interval for both models. When run on an Intel® Xeon® E5670 2.93GHz processor the forecast model produces four hours of simulation in 9.78 minutes, within the desired 10-minute value for this metric.

3.5 Model Run Input and Output Files

In addition to providing the bathymetry file names and the appropriate time step and A, B grid multiples as provided in the tables above, the designer must provide a number of additional parameters in an input file. These include the Manning Friction Coefficient, a depth threshold to determine when a grid point becomes inundated, and the threshold amplitude at the A-grid boundary that will start the model. An upper limit is specified in order to terminate the run if the wave amplitude grows beyond reasonable expectation. Standard values are used: 0.0009 for the friction coefficient and 0.1m for the inundation threshold. The latter causes the inundation calculation to be avoided for insignificant water encroachments that are probably below the uncertainty in the topographic data. Inundation can, optionally, be ignored in the A and B-grids, as is the norm in the (non-nested) MOST model runs that generate the propagation database. When A and/or B-grid inundation is excluded, water depths less than a specified "minimum offshore depth" are treated as land; in effect a "wall" is placed at the corresponding isobath. When invoked, a value of 5m is applied as the threshold, though A and B inundation is normally permitted as a way to gain some knowledge of tsunami impact beyond the scope of the C-grid domain. Other parameter settings allow decimation of the output in space and/or time. As noted earlier, 30-second output has been the target and output at every spatial node is preferred. These choices avoid aliasing in the output fields that may be suggestive of instability (particularly in graphical output), when none in fact exists.

Finally the input file (supplied in Appendix A) provides options that control the output produced. Output of the three variables: wave amplitude, and the zonal (positive to the east) and meridional (positive to the north) velocity components can be written (in netCDF format) for any combination of the A, B, and C-grids. These files can be very large! A separate file, referred to as a "SIFT" file, contains the time series of wave amplitude at each time step at discrete cells of a selected grid. Normally the time series at a "reference" or "warning point", typically the location of a tide gage is selected to permit validation in the case of future or historical events. Also output in the SIFT file is the distribution of the overall minimum and maximum wave amplitude and speed in each grid. By contrast with the complete space-time results of a run, the SIFT file (also netCDF) is very compact and, if more than a single grid point is specified, a broader view of the response is provided.

By default two additional output files are generated: a listing file, which summarizes run specifications, progress, and performance in terms of run time. Also included in this file is information to determine the reason, should a run not start or terminate early. Finally a "restart" file is produced so that a run can be resumed, beginning at the time it ended, either normally or by operator intervention.

The input files described above are specific to the model itself. For an actual run, the program must be pointed toward the files that contain the boundary conditions of wave amplitude (HA), and velocity components (UA, VA), to be imposed at the A-grid boundary. Time varying conditions are generally extracted as a subset of a basin-wide propagation solution (either a single unit source or several, individually scaled and linearly combined) that mimic a particular event. These boundary-forcing files typically consist of 24 hours of values (beginning at the time of the earthquake), sampled at 1-minute intervals and available on a 16 arc-minute grid. Occasionally, for more remote seismic sources (or when delayed arrival of secondary waves due to reflections are a concern, as has been seen at Hawaii,) the time span of the propagation run available for forcing is extended beyond one day.

4.0 Results and Discussion

Before proceeding to an extensive suite of model runs, that explore the threat to Marin County from various source regions, the stability of the model is tested in both low and extreme amplitude situations. The former we refer to as "null source" testing: where the boundary forcing is at such a low level (but not precisely zero of course) that the response is expected to be negligible. These tests can be highly valuable in revealing localized instabilities that may result from undesirable features in the discretized bathymetric representation. Inlets or channels that are only one grid cell wide may "ring" or resonate in a non-physical way in the numerical solution. An instability may not grow large enough to cause the model to fail but, in a run with typical tsunami amplitudes, may be masked by actual wave variability.

Forcing by extreme events should also be tested. In addition to the need to test model stability under such circumstances, there is a parameter in the input file that truncates the run if a prescribed threshold is exceeded. For operational use, the threshold must be set high enough so that an extreme event run is not unnecessarily terminated. Both tests should be done for test sources whose waves enter the model domain from different directions since, although stable for one set of incoming waves, an instability may be encountered for another. The "null" and "extreme" case testing of the forecast and reference models is reported in the following subsections. Further evidence of stability is provided by the extensive set of scenarios, aimed at exploring the dependence of impact to source location, described later in the report, and in independent testing by other members of the NCTR team before the model is released for operational use.

4.1 The "Null" Tests

Three null test cases (see Table 6) were run representing sources in the western Aleutians, the Philippines, and south of Japan. Based on sources from the propagation database (Gica et al., 2008), their amplitudes were scaled down by a factor of 10,000 so as to mimic an M_w=4.8333 / Slip 0.0001m source rather than the M_w=7.5 / Slip 1m standard. A number of grid cells in the B and C grids emerged as potential sources of instability. These were generally minor indentations of the coastline, barely resolved by the grids, or narrow channels. The region contains several inlets (called Esteros) extending far inland that, at a practical level of spatial resolution, proved difficult to accommodate. Among these are the upper reaches of the multiple arms of Drake's Estero and, feeding into Bodega Bay, Estero Americano and Estero de San Antonio. A limited number of grid cells in the outermost (A) grid required correction. Generally these were associated with non-physical features in the topographic database, such as where a track of ship-based soundings were improperly merged with other data sources. After an iterative process of grid correction and retesting using these "null" sources, both of the reference (RM) and forecast model (FM) grids were deemed satisfactory and the testing of realistic events can begin. Figure 9 illustrates a step in the process where a deficiency in the RM grid generated a mild instability (in the EPSZ B19 micro-tsunami scenario – see Table 6) causing the RM time series at the reference point, initially in close agreement with the FM, to develop unrealistic, high frequency oscillations. Though still

Table 6. Synthetic tsunami events employed in Point Reyes, CA model testing. The RM and FM solutions of those shown in bold text were inter-compared extensively.

Scenario Name	Source Zone	Tsunami Source	α [m]
Mega-tsunami Scenario			
KISZ 1-10	**Kamchatka-Yap-Mariana-Izu-Bonin**	**A1-A10, B1-B10**	**25**
KISZ 22-31	Kamchatka-Yap-Mariana-Izu-Bonin	A22-A31, B22-B31	25
KISZ 32-41	Kamchatka-Yap-Mariana-Izu-Bonin	A32-A41, B32-B41	25
KISZ 56-65	Kamchatka-Yap-Mariana-Izu-Bonin	A56-A65, B56-B65	25
ACSZ 6-15	Aleutian-Alaska-Cascadia	A6-A15, B6-B15	25
ACSZ 16-25	Aleutian-Alaska-Cascadia	A16-A25, B16-B25	25
ACSZ 22-31	Aleutian-Alaska-Cascadia	A22-A31, B22-B31	25
ACSZ 50-59	Aleutian-Alaska-Cascadia	A50-A59, B50-B59	25
ACSZ 56-65	**Aleutian-Alaska-Cascadia**	**A56-A65, B56-B65**	**25**
CSSZ 1-10	Central and South America	A1-A10, B1-B10	25
CSSZ 37-46	Central and South America	A37-A46, B37-B46	25
CSSZ 89-98	Central and South America	A89-B98, B89-B98	25
CSSZ 102-111	Central and South America	A102-A111, B102-B111	25
NTSZ 30-39	**New Zealand-Kermadec-Tonga**	**A30-A39, B30-B39**	**25**
NVSZ 28-37	New Britain-Solomons-Vanuatu	A28-A37, B28-B37	25
MOSZ 1-10	ManusOCB	A1-A10, B1-B10	25
NGSZ 3-12	North New Guinea	A3-A12, B3-B12	25
EPSZ 6-15	East Philippines	A6-A15, B6-B15	25
RNSZ 12-21	Ryukus-Kyushu-Nankai	A12-A21, B12-B21	25
Mw 7.5 Scenario			
NTSZ B36	New Zealand-Kermadec-Tonga	B36	1
Micro-tsunami Scenario			
EPSZ B19	East Philippines	B19	0.01
RNSZ B14	Ryukus-Kyushu-Nankai	B14	0.01
ACSZ B6	Aleutian-Alaska-Cascadia	B6	0.01

generally tracking the FM result, and not growing without bound, the feature could behave erratically in simulating real events. Modification of the RM bathymetry eliminated the problem, as seen in the lower panel, and "null" tests involving other sources (RNSZ B14 and ACSZ B6) did not reveal other issues.

4.2 The Extreme Case Tests

The record of tsunami impact on the northern California coast discussed later reveals that sources around the entire periphery of the Pacific can be felt. Indeed the catastrophic Indian Ocean tsunami of 2004 was detectable at Point Reyes as it was throughout the global ocean. A broad suite of 19 extreme events (so-called mega-tsunamis) whose locations are standard for testing of Pacific basin forecast models, are described in Table 6. Their locations are shown in Figure 10. To simulate each mega-tsunami source, ten A-B pairs of unit sources are used, with an evenly distributed slip of 25m. As described by Gica et al. (2008), each unit source represents a 100x50km area of the fault surface with the long axis parallel to the plate boundary. The B-row is shallowest, sloping from a nominal depth of 5km (unless a depth estimate has been provided by the USGS based on the earthquake catalogs), row-A is deeper, followed by rows Z, Y, X, … where appropriate. Thus, the extreme case sources represent 1,000 km long ruptures with a width of 100km; the corresponding magnitude is M_w=9.3.

Discussion of the entire set in greater detail is provided later in the report, once the validity of the Forecast Model has been established. Here we focus on a subset of three synthetic cases, highlighted in Figure 10 and Table 6, to contrast the Forecast Model (FM) with the more highly resolved Reference Model (RM). In Figures 11-13 the RM results (from the subregion spanned by the FM) are shown in the upper panel. The corresponding FM results in the lower panel employ the same scale. Insets are used to show the time series (black for RM, red for FM) of H, U, and V at the reference point (the Point Reyes tide gage). The lagged correlation of H at the reference point.is drawn in the lower inset and illustrates that there is generally only a few minutes lag between the time series with the RM lagging FM. This behavior is repeated in other scenarios illustrated later in the report. It is a general feature of MOST and is due to the tendency of more finely resolved features in the bathymetry slowing the progress of long waves and is discussed further in the context of model validation using observations.

The agreement between the RM and FM results for the three mega-events is good, both for the maximum amplitude and speed distributions, the reference point time series, and the discrete "snapshots" of the amplitude and vector velocity fields. The earliest waves show the best agreement; later in the solution the RM and FM results begin to diverge as multiple reflections with the coastline occur. A qualitative difference between the solutions is often seen along the straight coastline north of Point Reyes Light (see Figures 1 and 2). The straight shoreline, bounded by rocky headlands at the south and north, supports edge waves that appear most noticeably in the RM results almost as a standing wave pattern, but generally do not propagate around the headland and into Drake's Bay.

It is noticeable that, in all three of the cases shown, the RM tends to oscillate longer and have somewhat larger amplitude than does the FM though the two solutions are in close

agreement for the first few tsunami waves. This is likely a physical reality: the more highly resolved bathymetry and coastline of the RM providing greater scope for non-linear features or reflected waves to develop as, for example, near the rocky headland west of Bodega Bay. This observation suggests a caveat to operational use of the FM: while accurate portrayal of the early history of an event is to be expected, the duration of the event and the amplitude of later waves may be under-estimated. Tide gage data will be needed to verify this conjecture, which is pursued later in the report.

The snapshot comparisons in the lower panels of Figures 11-12 are quite reasonable, illustrating that the solutions match not just at the reference point. It is worth noting too that, although the ACSZ 56-65 mega-event represents a massive Cascadia tsunami, the scale of the impact to the Point Reyes area (~ 3m) is not substantially greater than from trans-Pacific locations (KISZ 01-10 off Kamchatka and NTSZ 30-39 near Samoa.) The Crescent City response to the same synthetic Cascadia mega-event exceeds 10m (Arcas and Uslu, 2010). It would appear that the energy propagated along shore to the south, perhaps due to sheltering by Cape Mendocino, is reduced and that perhaps the greatest impact to Marin County may be associated with source regions elsewhere in the Pacific basin.

In Figure 13 the comparison time was intentionally chosen later in the event as a counterexample. While the reference point amplitudes and nearby fields the FM and RM may be in reasonable agreement, the broader wave patterns may have substantial phase differences. The comparisons in these lower panels is restricted to the portion of C-grid area common to both models, There is a suggestion that the near shore velocity fields at the north and south FM boundaries differ somewhat from the RM for which these are internal points.

Before proceeding to validate the model with historical events, one other synthetic event is usual in the testing protocol: a mild source of magnitude 7.5 at a remote location. A single unit source near Samoa (NTSZ-B36) is employed and its representation by the RM and FM are compared in Figure 14. Such an event results in a response of about 4cm in Point Reyes sea level and again there is excellent agreement between both model representations in the earlier portion of the event.

The results presented above, for a variety of synthetic events, suggest that the RM and FM versions of the model are in good agreement. The match is particularly good in the early stages of a wave train; later, as reflections and other interactions with the coastline occur, the solutions may diverge. The next task is to ascertain whether the models reflect observations from actual tsunami events. Given the manner in which the MOST model is forced, at its boundary (with wave amplitudes and currents not available in real observations), it is not possible to validate the model independently. Rather, as described earlier in Section 2.2, the validation will rely on the results of an external model, based perhaps on DART observations or on a description of the tsunami source in the literature. As a result, the success of the model in replicating observations within its domain is in part dependent on the adequacy of the forcing employed to represent the actual external wave field. For historical events preceding the DART array, the unit source representations are based on seismic observations or coastal tide gage data. Past experience suggests that, in the far field at least, the propagation solution is not overly

sensitive to variation in the unit source weights. Nonetheless, imperfections in forecast model predictions of coastal observations will not necessarily indicate a defect in the model itself. Neither are the tide-gage observations, available for comparison with model prediction, perfect. They may include noise from wind wave activity, possibly amplified by harbor resonances.

4.3 Model Validation : The Honshu-2011 Tsunami

In addition to its disastrous impact on the coast of Japan, the Honshu tsunami of March 11, 2011 radiated waves throughout the Pacific Basin. Those arriving at nearby DART's were of unprecedented amplitude and their signal/noise ratios facilitated accurate and early source characterization. Further afield, the waves were detectable at all operational DART's in the basin and, while major damage was mainly confined to Japan, significant signals were obtained at multiple coastal tide gages. Prior to this event, the Kuril-2006 tsunami event was the best available for model validation. For the U.S. West Coast at least, that role has now been taken by Honshu-2011. The adequacy of the composite propagation solution can be assessed by comparison with the BPR signals from the West Coast DART's. An additional BPR record is available for this purpose: the MARS cabled observatory in Monterey Canyon has, since July 2010, had a pair of bottom pressure sensors at a depth of about 870 meters. One is a standard BPR, reporting at the standard DART 15-second recording interval. The other is an experimental sensor – the "Nano" (Paros et al., 2011) sampling at 40Hz with enhanced sensitivity. For this report we employ only data from the standard BPR.

The locations of the West Coast BPR's, reporting during Honshu-2011, are shown in Figure 15. To the left of the locator chart, the actual and propagation model results interpolated to the BPR locations are compared. There is clearly a strong agreement but, even for the earliest waves, there are two points of difference. Firstly the model "waves" arrive about 8 minutes early, a difference that is small compared to the several hours of transit time. Early arrival by the model is typical and is associated with the limited resolution of the basin-wide bathymetry. Finer-scale features in the actual bathymetry slow down the real wave trains. The other feature of the model vs. observation comparison is that the model underestimates the observed signal by about 20% at all locations. In the right-hand panel, the lagged and scaled-up versions of the model time series are seen to be in excellent agreement with observation. Since these results are likely the best obtainable with the current state of the DART array and inversion methodology, less than perfect agreement between forecast model and observations is not necessarily indicative of a major defect in the FM itself.

With that caveat, we proceed with the model validation. The prime location for this purpose is the Point Reyes tide gage itself. However within the forecast system, predictions from elsewhere in the model domain are employed to enhance the "coastal forecast". In its basic form, the "coastal forecast", at selected locations around the basin, is generated by extrapolating offshore values from the propagation solution to the coast using Green's Law. Based on simple assumptions this law indicates that the waves should grow in inverse proportion to the one-fourth power of the depth ratio. The assumption is crude at best and it makes sense that, when a forecast model has been run, the predictions within its domain are likely to be superior to the Green's Law equivalent. For the Point

Reyes model, tide gage observations are available at several points within the domain and, in the case of Honshu-2011 all of these had detectable signals. The auxiliary sites are Bolinas, lying within the C-grid but within the lagoon and with only 6-minute sampling; San Francisco, Alameda, and Richmond within San Francisco Bay and the model B-grid and with 1-minute sampling; Arena Cove, near the northern bound of the FM A-grid and also with 1-minute sampling. The results of the comparison may be seen in Figure 16a,b where the RM (black) and FM (red) versions of the model response are compared to the observations (drawn in green.) The model curves have been lagged to facilitate the comparison but the amplitudes have not been altered. For the first six hours of the event, the agreement is quite gratifying, particularly at Point Reyes itself and at San Francisco. For Arena Cove the agreement is limited more to the early waves; perhaps as a result of resonance associated with Cove geometry, the observed response grows and shifts to a higher frequency than appears in the model signals. The RM solution is a better match in amplitude to the observations from Arena Cove than is the FM whose representation of the geometry is quite coarse.

For Alameda and Richmond, progressing deeper into San Francisco Bay, the match between the models themselves and with the observations, is degraded compared with the better agreement near the entrance. Nonetheless the agreement is quite good and shows promise for an improved "coastal forecast" usage of FM results. Least satisfying, but understandable, is the comparison at Bolinas. The tide gage there lies within the mouth of the lagoon and an adequate representation of the narrow entrance channel is difficult, particularly in the FM. As is common with narrow-mouthed entrances to enclosed regions, there is a tendency for the model to retain water within and clearly (the red curve) the lagoon increasingly does not empty during the "ebb" phase of the tsunami wave train. The RM solution, perhaps as a result of excessive modifications of inaccurate representation of entrance geometry in the DEM, seems to resonate far more than the observational record. It is possible however that, with its 6-minute sampling and placement, the Bolinas tide gage is not well suited to tsunami detection. On a positive note, the timing and amplitude are not grossly dissimilar to the data. The purpose of the FM is more to predict the impact on the seaward side of the Stinson Beach spit and, based on the success at San Francisco, forecasts outside constricted regions of the model domain are likely to be quite useful for warning purposes.

We now step back in order to verify the agreement between the RM and FM solutions throughout the common portion of the C-grid domain. In Figure 17, as was done for the purely synthetic scenarios, the solutions are compared based on their maximum amplitude and speed fields, and the time series and lagged correlation at the Point Reyes tide gage site. The distribution patterns of the maximum fields are comparable and, based on the Point Reyes time series sample, it is not unexpected that the RM should be the greater with the mismatch coming perhaps for the later waves. A point wise (zero lag) correlation distribution (not shown), between RM and FM throughout the FM C-grid domain, indicates that the over 60% of the variance is explained except in constricted areas. The lagged correlation inset confirms a phase difference of only a few minutes between the RM and FM time series at the tide gage. As a further means of comparing the RM and FM solutions, snapshots of the amplitude and velocity fields are also provided in Figure 17. For both the RM (upper panel) and FM (lower panel) a common scale is used. The agreement is particularly close when the comparison time (indicated by

the green line) is close to the first peak's arrival at the tide gage. Two later sample times are shown in Figures 17d,e illustrating that phase differences can increase.

The analysis of the Honshu-2011 in the Point Reyes model is concluded with an examination of the pattern of inundation in Figure 18. For this purpose the full RM C-grid domain is drawn. The model suggests that, had the waves arrived at or above mean high water (MHW), both the Limantour Spit and much of Stinson Beach and the low-lying parts of Bolinas may have been inundated. In fact, as illustrated in the inset based on the observed water level at the Point Reyes tide gage, the waves barely attained MHW. Though the reporting of the impact on the U.S. may have been somewhat muted, given the gravity of the imagery from Japan, it appears that on the U.S/. West Coast the main evidence of the tsunami was in excessive currents, notably at Santa Cruz and Crescent City. As designed, with model sea level set at MHW, the forecast erred on the side of conservatism. In the northern portion of the RM domain (excluded in the FM C-grid) the greatest response was predicted with inundation of the Doran Beach spit and the Dillon Beach/Lawson's Landing area at the north and south ends of Bodega Bay. Although in reality no actual inundation occurred due to the state of the tide, a video clips posted online document strong currents beneath the Lawson's Landing pier, and oscillations of 2-3 feet with 20-minute periodicity are reported for Dillon Beach. Examination of the model time series, both RM and FM, from Bodega Bay (not shown) indicate that the northern and southern portions were rising and falling together, so the large amplitudes responsible for the inundation pattern were not associated with the excitation of an alongshore standing wave mode. Also shown in Figure 18 is the CalEMA Inundation Line, based on an ensemble of synthetic mega events scenarios. The MHW-based model prediction does impact, albeit at a lesser level, the regions the CalEMA study identifies as vulnerable.

4.4 Model Validation with other Standard Historical Events

We now proceed to examine how well the RM and FM solutions compare with observation for several other historical cases highlighted in Table 1 and Figure 6. The RM and FM time series are inter-compared at Point Reyes tide gage, Arena Cove, and San Francisco and validated where possible with observation, and the same representations of maximum amplitude, point wise correlation, and snapshots of the RM and FM fields are drawn.

The results, displayed and described below, represent other DART-detected and well-documented recent events: Chile-2010, Samoa-2009, and Kuril-2006, the latter being the first substantial event for which direct observation of the tsunami wave train was available from multiple deep-water DART sites. These events occurred subsequent to the installation the tide gage at Point Reyes. Two pre-DART cases are examined in this section: Alaska-1964 and Unimak-1946 whose large amplitudes caused severe damage to Hawaii and provided the impetus for the establishment of the TWC's. Source characterization for these events is based on the literature, with the source mechanism estimated from the seismic record.

For Chile-2010 the direct comparison of RM and FM is shown in Figure 19 with satisfactory results both in terms of RM-FM intercomparison and agreement with the

observed time series at three locations displayed in Figure 20. The amplitude series match well throughout the six-hour period shown and there is strong point wise correlation throughout the common domain. Comparisons of observations with predictions based on the dedicated forecast models are to be found in the FM reports for Arena Cove (Spillane, 2010) and San Francisco (Uslu et al., 2010) and in post-event reports online at the NCTR website. Excellent agreement is seen for Point Reyes and San Francisco, though the leading wave at Point Reyes is over-estimated and the timing of some later features at San Francisco is less than perfect. The observational record at Arena Cove is noisier, though the amplitude of the first wave is captured well by both models.

For Samoa-2009, the equivalent set of results is shown in Figures 21 and 22. Despite the considerably more complex structure of the maximum amplitude field, the FM pattern is in good agreement with that from the RM and the time series for the first few hours agree well. Later the FM solution appears to decay faster than the RM. Considering the Point Reyes observations in Figure 22, the RM is in better agreement with the amplitude of later waves. At San Francisco the situation is less clear with the RM perhaps overestimating the observed response, while at Arena Cove neither model (as extracted from the A-grid) reproduces the severe ringing evident in the observations.

Figures 23 and 24 represent the Kuril-2006 event. Agreement between the models is strong both for the early and later portions of the record shown. However, in comparisons with observation, the models underestimate later features in the San Francisco observations and, at Arena Cove, the FM response decays far too rapidly. At both locations outside the C-grid, the predicted maxima are less than 50% of what was observed. To summarize these three events, with weaker impacts than Honshu-2011, the accuracy of a revised "coastal forecast" based on the A- and B-grids may be reduced. It remains to be demonstrated whether they are significantly better than those based on Green's Law.

The Unimak-1946 and Alaska-1964 events were widely felt along the U.S. west coast, though the greatest impact was to the Hawaiian Islands. Reported run-ups associated with Unimak-1946 were 240cm at Arena Cove, 130cm at Bolinas and 256cm at Muir Beach; run-up at San Francisco and Alameda were 26 and 20cm respectively. During the Alaska-1964 event a run-up of 240cm was reported for Drake's Bay (Point Reyes) with 274cm at Muir Beach and 113cm at San Francisco. Arena Cove and Bodega experienced run-up of 183 and 76cm. were 2.40 and 1.83 meters respectively. The model representations of these major pre-DART events are illustrated in Figures 25-28. In 1946 only the tide gage record for San Francisco is available but shows good agreement with the model-based values. The model time series for Arena Cove are in good agreement but substantially underestimate the reported run-up there, as do the maximum FM amplitudes of 58cm near Bolinas and 96cm at Muir Beach. For the Alaska-1964 event too, only the San Francisco tide gage record is readily available, showing good agreement between model and data. At Point Reyes the model intercomparison is good but while the FM and RM representations of the leading wave match closely, the FM decays more rapidly for later waves. Maximum amplitudes from the sites of reported run-up are 217cm at Drake's Beach, 173cm at Muir Beach and 116cm at San Francisco. These and the values of 140cm at Arena Cove and 129cm near Bodega are far better with observation than was the case for the Unimak event. Other measures of the intercomparison between FM and

RM: the maximum amplitude and correlation, and the amplitude and velocity fields at a selected comparison time, are good for both events.

4.5 Further Historical Simulations

The above analysis has documented good agreement between the forecast model and the slower running reference version. This permits us to simulate the balance of the historical cases in Table 1, where impacts to the study area have been reported (and the remaining mega-tsunami scenarios) with the forecast model alone. These runs are intended to further validate the stability of the FM but also provide some information on the exposure of the region to tsunamis generated at various points on the periphery of the Pacific.

The quality of the historical events highlighted above is likely to be the result of good characterizations of the source, based on DART observations in the case of recent tsunamis or extensive post-event analysis in the case of the historical examples. In the absence of direct and timely observations, the successes of the forecast models are likely to be much reduced. An extreme case in point is the Sanriku-1896 event, a so-called "tsunami-earthquake" (Dudley and Lee, 1998), causing devastating losses in Japan despite its modest magnitude and scant warning in the form of ground motion. A digitized marigram from Sausalito (across the Golden Gate from San Francisco) is available from the WCATWC archives and is drawn in the lower panel of Figure 29. While the timing is reasonably represented, the amplitude considerably underestimates the reported run-up of 10cm at Sausalito and 20cm at San Francisco. Reports are not available from nearby locations outside the bay, the closest being 150cm at Santa Cruz.

For the Andreanof-1957 event reported run-up of 29cm at Bodega, 26cm at San Francisco and 18cm at Alameda are in reasonable agreement with the model results (35cm, 46cm, and 23cm respectively). No observed time series is available for comparison for this event, nor for East Kuril-1994. For the later only a 4cm run-up, reported at Alameda is available for validation; the maximum model amplitude for Alameda at 2.5cm is in good agreement. For the remaining events in Table 1, Part A time series are available for more thorough validation and are displayed in Figures 30-NN without extensive comment; run-up values where available are added as annotations to the graphics.

Kamchatka-1952 with M_w 8.6 is available as a marigram from San Francisco (Figure 30.) It's amplitude there is well represented by the model, suggesting that a run-up of three meters or more may have occurred at Point Reyes and elsewhere in Marin County. For the Chile-1960 M_w 9.5 event, whose San Francisco marigram was also obtained from the WCATWC archive, the character of the observed response is quite different from the model representation. As seen in Figure 31, the model exceeds the observed amplitude response by a factor of 2-3, and lacks the higher frequency components evident in the observations some hours into the event. The model wave arrived about 20 minutes early. At Alameda, also within San Francisco Bay, the maximum amplitude of the model, at 68cm, is about twice the reported run-up of 31cm. At Stinson Beach the model exaggeration is less severe: 217cm compared to the observed 152cm, but is again large (68cm compared to the observed 25cm) near Bodega.

Figure 32 presents the validation results for the Andreanof-1996 event. At Point Reyes the agreement is quite good and at Alameda the weak model waves seem to capture some of the features of the observed series. At Arena Cove however the signal is far to weak to be visible against the high noise background. For the Peru-2001 (Figure 33) and Hokkaido-2003 (Figure 34) events the validation is quite satisfactory, but for the winter Rat Island-2003 event, as seen in Figure 35, there is considerable noise at the validation sites, limiting the visibility of signals as weak as the model predicts. This event is however notable in that, aided by direct observations of BPR, from pre-cursors to the DART array, useful forecasts were provided to inform the Hawaii emergency response. The Tonga-2006 event proved useful for validation of the Point Reyes model, with a strong response, shown in Figure 36, that agrees well with the observations.

The year 2007 brought several events with which to validate the model, beginning with the normal thrust seaward of the Kuril Trench on January 2007. As seen in Figure 37, the model correctly captured the leading trough and amplitude seen at Point Reyes and San Francisco, though at Arena Cove the background noise limits the usefulness of the observations. The Solomon-2007 event (Figure 38) is reasonably satisfactory, though the signal in both the model and the observations is weak. In August an event off Peru (Figure 39) appears to match well the observations at Point Reyes but, at Arena Cove and San Francisco, while the model seems to capture the amplitude and timing of the early waves, the later portion of the event is less satisfactory. The final event to be treated, from the standard suite of Table 1, Part A is the weak winter Chile-2007 event. Not surprisingly, since the forecast amplitudes are very small off California, there is not a lot to be learned from this event displayed in Figure 40.

Several additional events, listed in Table 1, Part B are available for analysis. Of these, the Sanriku-1894 event has been presented earlier, and the Cape Mendocino tsunami of 1992 as the sole, albeit weak, representative of a Cascadia event is described later in the next Section. The remainder, generally weak in terms of their impact and most occurring in winter where the noise background limits the S/N ratio, are not reported other than to state that all ran without difficulty or evidence of instability.

To summarize the analysis of historical events, given above and in subsection 4.6, it would appear that the Arena Cove FM is capable of producing accurate forecasts for this open coast site on the U.S. west coast. Though the actual waves may be difficult to observe accurately at the tide gage during winter storms, the objective of producing credible forecasts of sizeable tsunami impacts appears to have been met.

4.6 The Mendocino Earthquake of April 25, 1992

Of special interest to northern California is the Mendocino earthquake of April 25, 1992. This has the distinction of being the most recent substantial thrust event on the Cascadia subduction zone. While strike-slip events are commonplace offshore in this region, as shown in the upper right panel of Figure 41, it is thrust faults that have the potential to generate significant vertical displacements of the sea floor that cause large tsunamis. The epicenter of the 1992 event was on land to the southeast of the plate triple-junction off Cape Mendocino. Uplift of the order of a meter of a 25km stretch of the nearshore, between Cape Mendocino and Punta Gorda to the south was evident in a die-off of

intertidal organisms, reported by Carver et al., (1994). Presumably extending offshore too, this deformation is not well represented well by either of the southernmost unit sources (ACSZ-A/B65) now available in the propagation database (see Figure 6 where the epicenter is marked by the seismic "beach ball".) A custom source, available from NCTR but not part of the propagation database, is used to model the event for comparison with two digitized marigrams, plotted in the lower panels of Figure 41. These were obtained from the WCATWC archives. The model performs reasonably in representing the leading wave, though the model series had to delayed by 30 minutes to achieve alignment. This time offset, greater both in actual time units and as a percentage of travel time, than those typically necessary to adjust trans-basin predictions, may be the result of the coarse representation of the near shore bathymetry. Another possible explanation is that this event, described by Gonzâlez et al. (1995), may have generated a train of coastal-trapped edge waves. Traveling slower than normal tsunami waves taking a deep-water route, the edge waves may have resulted in a delayed arrival and an extended duration for the event. This possibility, and the suggestion that the ACSZ source line ought to be extended at least one unit further south, make this an event worth further study. The reference and forecast models for Point Reyes, and others existing or planned for the west coast (Point Reyes, Eureka, Crescent City, etc.), have a major role in ongoing risk assessment studies for Cascadia.

4.7 Simulation of the remaining Synthetic Mega-events

We conclude this section with a summary of other model runs that were made in order to verify its stability, but which provide useful information on the exposure of Point Reyes to potentially hazardous future events within the Pacific. As noted earlier, the sparse instrumental record of actual events needs to be augmented with credible scenarios to permit risk assessment. While not pretending to be a full-blown risk assessment for the Point Reyes and southwest Marin County area, the full set of mega-tsunamis modeled during stability testing can provide some early estimates.

Results for the set of 19 mega-tsunamis, based on the FM are presented in Figure 42. Each source is a composite of 10 unit sources from the A and B rows with an evenly distributed slip representing an M_w 9.3 event. A color-coded square, drawn at the geometric center of each synthetic source, is used to represent the impact at Point Reyes resulting from that source. The measure of impact employed in Figure 42 is the maximum amplitude of the predicted time series at the reference point. There is not any simple relationship apparent between source orientation, location, or great circle distance to Point Reyes; focusing associated with seafloor features can more than compensate for the decay associated with geometric spreading. It is notable that the greatest impact at Point Reyes comes from trans-basin sources, rather than from those representing Cascadia. The latter apparently beam most of their energy directly onshore of offshore into the open ocean; arrows normal to the plate boundary are used in Figure 42 as an approximate indicator of main bean direction.

Further results from the suite of mega-event scenarios are presented in Table 7. Seven sites within the C and B-grids of the FM are represented; the first being Point Reyes tide gage that was illustrated graphically in Figure 42. Limatour Beach is a well-visited recreational site within the PRNS; Stinson Beach, adjacent to Bolinas, and Muir Beach

Table 7. Mega-tsunami scenario impacts, represented by flooding (km^2 in the sub-region 123.1:122.5W, 37.8:38.1N) and maximum amplitude (cm) at several sites within the model domain (identified in the footnote). The maxima are highlighted and ranked.

Scenario (km)	**Flooding** Area		**Impact Sites** PTR[1]	LIM[2]	STN[3]	MUR[4]	DOR[5]	LAW[6]	SFO[7]	**Amp. Rank**
AC 56-65 (688)	5.18	7	159	152	160	182	201	**224**	115	13
AC 50-59 (1278)	4.72	11	202	106	217	**373**	194	193	203	4
CS 1-10 (2994)	1.18	18	**99**	69	64	72	48	52	37	18
AC 22-31 (3277)	6.34	4	239	221	288	227	251	**333**	150	6
AC 16-25 (3731)	4.97	8	266	121	234	**275**	162	194	102	8
AC 6-15 (4731)	2.55	17	134	87	117	**136**	118	120	81	17
KI 1-10 (5856)	4.93	10	**354**	152	184	245	144	189	90	6
CS 37-46 (6070)	0	19	**42**	36	38	35	37	38	25	19
KI 22-31 (7724)	4.24	12	**251**	129	170	231	212	182	74	11
NT 30-39 (8054)	7.00	2	**402**	226	263	277	239	309	127	3
KI 32-41 (8368)	6.39	3	318	169	288	**502**	361	440	159	2
RN 12-21 (8808)	3.27	15	**209**	84	115	162	110	121	57	14
KI 56-65 (9429)	3.94	13	166	96	145	**233**	171	204	87	12
NV 28-37 (9553)	4.96	9	**258**	131	149	149	173	202	88	10
MO 1-10 (9943)	**7.71**	1	460	295	324	**513**	240	277	200	1
CS89-98 (10063)	3.48	14	**140**	134	102	78	102	136	43	16
NG 3-12 (10801)	3.15	16	**162**	107	143	145	133	131	104	15
EP 6-15 (10932)	6.31	5	246	160	264	**296**	211	235	137	7
CS102-11(11010)	3.27	6	**265**	132	156	193	157	172	77	9
	Overall Max		**402**	**295**	**324**	**513**	**361**	**440**	**203**	

C-Grid: 1-Point ReyesTG, 2-Limantour Beach, 3-Stinson Beach, 4-Muir Beach,
B-Grid: 5-Doran Spit, 6-Lawson's Landing, 7-San Francisco TG.

are coastal communities between Point Reyes and the southern limit of the FM C-grid at Point Bonita. Doran Beach and Lawson's Landing represent communities within Bodega Bay, which is only represented in the FM B-grid. San Francisco, also in the B-grid, is included owing to the wealth of tsunami records available there. While Point Reyes has the most instances (10) of having the greatest amplitude among the selected sites, for the mega-events treated here, Muir Beach with 7 and the two overall greatest impacts, is clearly threatened; these results are consonant with the large run-up reported at Muir Beach in the historical record. Lawson's Landing too, with the remaining two cases (one representing the southern end of Cascadia, the other the mid-Aleutians, is clearly at risk and given the inundation that might have resulted had the Honshu-2011 waves arrived under adverse tidal condition (Figure 18) and statements by emergency responders in the "Marin Tsunami" video, Bodega Bay warrants a dedicated forecast model, though lacking an instrumented reference point. Given the linear geometry and orientation of Bodega and Tomales Bays Version 4 of MOST, which is not limited to north-south and east-west grid lines, should be well suited.

Finally the set of 19 mega-tsunami scenarios evaluated here is an approximate match to the set employed in the CalEMA study that established an inundation line for California. In Figure 43, an ensemble of the inundation predictions by the Point Reyes FM is compared with the CalEMA result. The FM C-grid cells inundated by one or more of the meta-tsunami scenarios are colored red; the CalEMA inundation line is drawn in blue. (The flooded area, in square kilometers, associated with each scenario is included in Table 7.) As underlying topography Figure 43 uses the RM grid to better indicate coastal indentations. The FM provides a reasonable match in most of the threatened areas, particularly the Limantour Spit and Beach areas and Stinson Beach. In some areas, such as Muir Beach, the reduced resolution of the FM limits the penetration of flooding there. No attempt has been made to adequately represent Tomales Bay in the Forecast Model. Its shallowness and the constrictions at its mouth cannot be adequately represented at the spatial resolution necessitated by the run-time constraints for emergency usage.

5.0 Conclusions

To conclude, good agreement between observations and model predictions for a subset of historical events, including the recent Honshu-2011 tsunami, has been established and the stability of the model for numerous synthetic events has been demonstrated. In particular the reliability of the forecast model, designed to run rapidly in a real time emergency conditions, has been proven by the favorable comparison with reference model predictions, particularly during the early hours of an event. The model will be included in the SIFT system employed operationally at the Tsunami Warning Centers, and will permit the Point Reyes beaches and the communities of Bolinas, Stinson Beach, and Muir Beach to be added to the coastal communities for which forecast capability is available. Additionally it will provide a tool of use in risk assessment studies.

In addition to the scenarios run by the author, and reported here, further tests have been made by other members of the group at NCTR, and will continue to be made by staff at the Warning Centers and others, perhaps in training situations. Among the many related tools developed at NCTR is ComMIT (Community Model Interface for Tsunami, nctr.pmel.noaa.gov/ComMIT/), which provides a highly intuitive graphical environment in which to exercise and explore forecast models for any combination of propagation database unit sources. Were any of these avenues to reveal a problem with the model, its origin (most likely in some quirk of the bathymetric files) would be located and corrected then the revised version re-installed for operational use. The development of the forecast system will be a dynamic process, with new models added (and old ones revisited) from the current list of U.S interests and globally. In the coming years it is expected that further capabilities (for example landslides) will be added as algorithms and methodologies mature.

6. Acknowledgments

Many members of the NCTR GROUP provided valuable assistance in the production of this report. In particular Diego Arcas edited the first draft for content and style. CalEMA and other California entities distribute GIS online dataset used in the graphics. The modeling could not proceed without the detailed DEM produced at NGDC by the painstaking combination of numerous bathymetric and topographic surveys. Digitized marigrams for a number of historic events were acquired from the WCATWC archives. This publication is [partially] funded by the Joint Institute for the Study of the Atmosphere and Ocean (JISAO) under NOAA Cooperative Agreements NA17RJ1232 and NA10OAR4320148, Contribution No. XXXX. It is PMEL Contribution No. NNNN

7. References

Arcas, D. and B. Uslu (2009): PMEL Tsunami Forecast Series: Vol. 2. A Tsunami Forecast Model for Crescent City, California

Barberopoulou, A., J. C. Borrero, B. Uslu, M. R. Legg and C. E. Synolakis (2011): A Second Generation of Tsunami Inundation Maps for the State of California. *Pure and Appl. Geophys. DOI: 10.1007/s00024-011-0293-3*

Carignan, K.S., L.A. Taylor, B.W. Eakins, R.J. Caldwell, D.Z. Friday, P.R. Grothe and E. Lim (2010): Digital Elevation Models of Central California and San Francisco Bay: Procedures, Data Sources and Analysis. www.ngdc.noaa.gov/dem/report/download/1220

Carver, G.A., A.S. Jayko, D.W. Valentine and W.H. Li (1994): Coastal uplift associated with the 1992 Cape Mendocino earthquake, northern California. *Geology 22(3), 195-198.*

Dudley, W.C. and Min Lee (1998): Tsunami! University of Hawai'i Press, 362pp.

Dunbar, P. (2007): Increasing public awareness of natural hazards via the Internet. *Nat. Hazards 42(3) 529-536, DOI: 10.1007/s11069-006-9072-3*

Gica, E., M. Spillane, V.V. Titov, C.D. Chamberlin, and J.C. Newman (2008): Development of the forecast propagation database for NOAA's Short-term Inundation Forecast for Tsunamis (SIFT). NOAA Tech. Memo. OAR PMEL-139, NTIS: PB2008-109391, 89 pp.

González, F.I., K. Satake, E.F. Boss and H.O. Mofjeld (1995): Edge wave and non-trapped modes of the 25 April 1992 Cape Mendocino tsunami. *Pure and Appl. Geophys. 144, 409-426, DOI: 10.1007/BF00874375*

Kanamori, H. and J.J Ciper (1974): Focal process of the great Chilean earthquake, May 22, 1960. *Phys Earth Planet. In., 9,128-136.*

Lander, J.F., and P.A. Lockridge (1989): United States Tsunamis, 1690 to 1988, Publ. 41–2. National Geophysical Data Center, Boulder, CO, 265 pp.

Loeffler, Kurt, and Gesell, Justine, editors/cinematographers, 2010, Marin Tsunami: U.S. Geological Survey General Information Product 95 (video). URL: pubs.usgs.gov/gip/95/index.html

López, A.M., and E.A. Okal (2006): A seismological reassessment of the source of the 1946 Aleutian "tsunami" earthquake. *Geophys. J. Int., 165(3), 835–849*, doi: 10.1111/j.1365-246x.2006.02899.x.

Niemi, T.M. and N.T. Hall (1996): Historical Changes in the Tidal Marsh of Tomales

Bay and Olema Creek, Marin County,California. *J. Coastal Res., 12(1): 90-102.*

O'Brien, M.P. (1946): Preliminary Report on Seismic Sea Waves from Aleutian Earthquake of April 1, 1946, *Tech. Rep. HE 116207*, Wave Project, Fluid Mechanics Lab., U. Cal. (Berkeley).

Paros, J., E. Bernard, J. Delaney, C. Meinig, M. Spillane, P. Migliacio, L. Tang, W. Chadwick, T. Schaad, and S. Stalin (2011): Breakthrough underwater technology holds promise for improved local tsunami warnings. Oceans '11 Paper

Percival, D.B., D. Arcas, D.W. Denbo, M.C. Eble, E. Gica, H.O. Mofjeld, M.C. Spillane, L. Tang, and V.V. Titov (2009): Extracting tsunami source parameters via inversion of DART® buoy data. NOAA Tech. Memo. OAR PMEL-144, 22 pp.

Spillane, M.C., E. Gica, V.V. Titov, and H.O. Mofjeld (2008): Tsunameter network design for the U.S. DART® arrays in the Pacific and Atlantic Oceans. NOAA Tech. Memo. OAR PMEL-143, 165 pp.

Spillane, M.C. (2011): Development of a Tsunami Forecast Model for Arena Cove, California. NOAA OAR Special Report, PMEL Tsunami Forecast Series: Vol. , pp.

Tang, L., C. Chamberlin, E. Tolkova, M. Spillane, V.V. Titov, E.N. Bernard, and H.O. Mofjeld (2006): Assessment of potential tsunami impact for Pearl Harbor, Hawaii. NOAA Tech. Memo. OAR PMEL-131, NTIS: PB2007-100617, 36 pp.

Tang, L., V.V. Titov, and C.D. Chamberlin (2009): Development, testing, and applications of site-specific tsunami inundation models for real-time forecasting. *J. Geophys. Res.*, *114*, C12025, doi: 10.1029/2009JC005476.

Titov, V., and F.I. González (1997): Implementation and testing of the Method of Splitting Tsunami (MOST) model. NOAA Tech. Memo. ERL PMEL-112, NTIS: PB98-122773, NOAA/Pacific Marine Environmental Laboratory, Seattle, WA, 11 pp.

Titov, V.V., and C.E. Synolakis (1998): Numerical modeling of tidal wave run-up. *J. Waterw. Port Coast. Ocean Eng.*, *124*(4), 157–171.

Titov, V.V., F.I. González, E.N. Bernard, M.C. Eblé, H.O. Mofjeld, J.C. Newman, and A.J. Venturato (2005): Real-time tsunami forecasting: Challenges and solutions. Nat. Hazards, 35(1), Special Issue, U.S. National Tsunami Hazard Mitigation Program, 41–58.

Uslu, B., D. Arcas, V.V. Titov, and A.J. Venturato (2010): A Tsunami Forecast Model for San Francisco, California. NOAA OAR Special Report, PMEL Tsunami Forecast Series: Vol. 3, 88 pp.

Wei, Y., E. Bernard, L. Tang, R. Weiss, V. Titov, C. Moore, M. Spillane, M. Hopkins,

and U. Kânoğlu (2008): Real-time experimental forecast of the Peruvian tsunami of August 2007 for U.S. coastlines. *Geophys. Res. Lett.*, *35*, L04609, doi: 10.1029/2007GL032250.

FIGURES

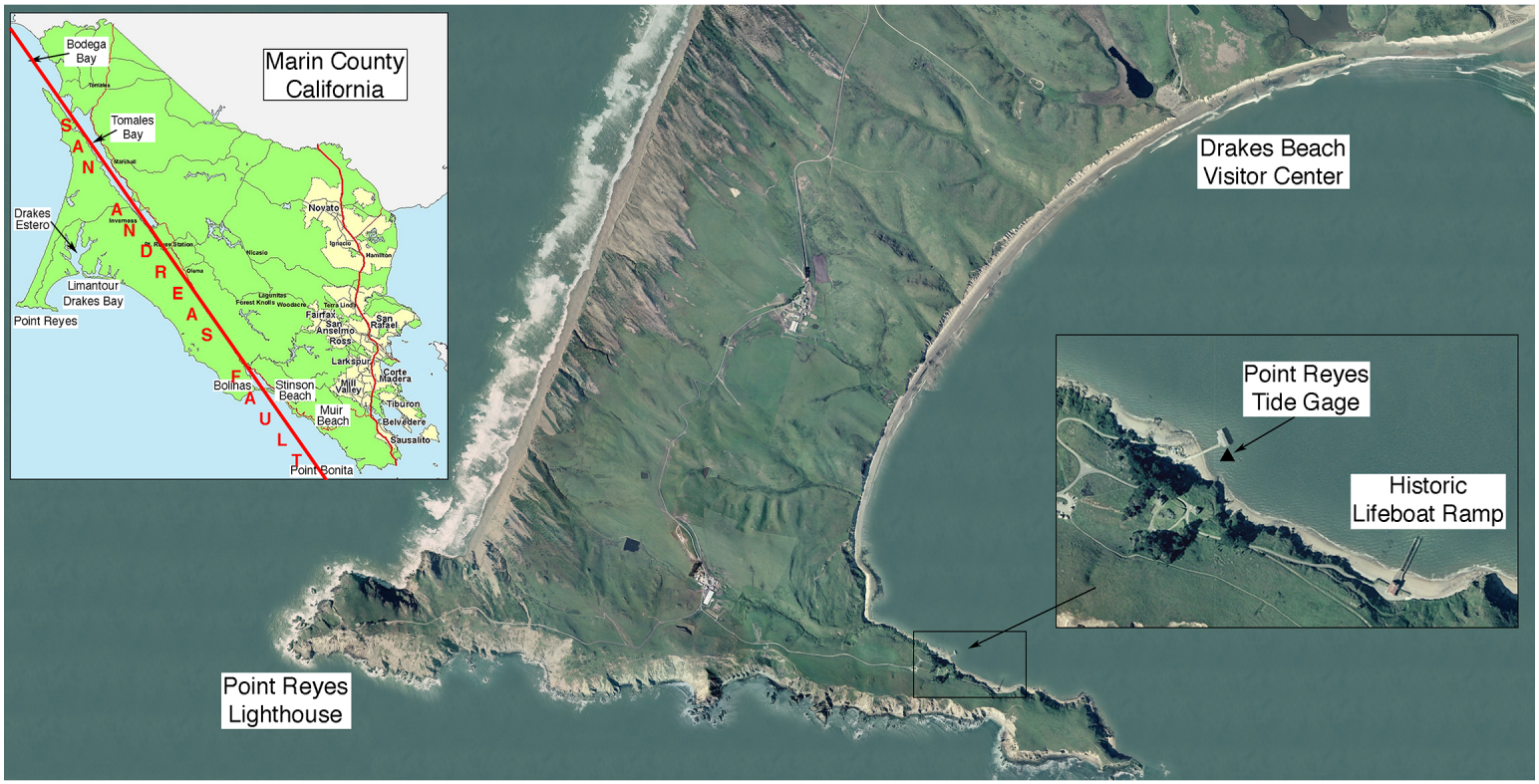

Figure 1. The Point Reyes area of west and south Marin County, CA.

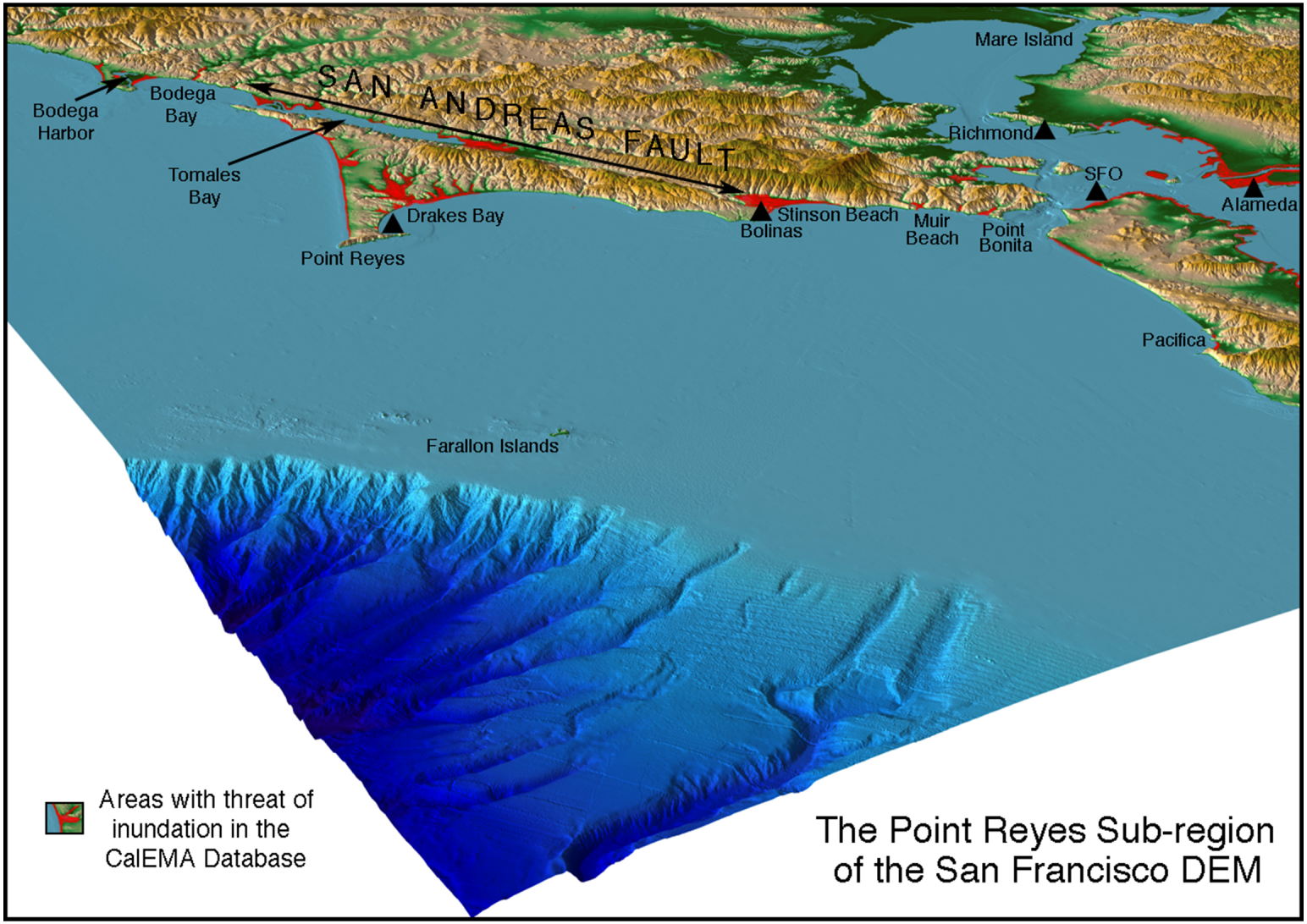

Figure 2. Extract from the oblique 3-D view of the San Francisco DEM provided by NGDC. The focus is Point Reyes; areas of potential inundation identified by CalEMA are highlighted in red.

Figure 3. View of the Point Reyes headland and Drake's Bay in its lee.

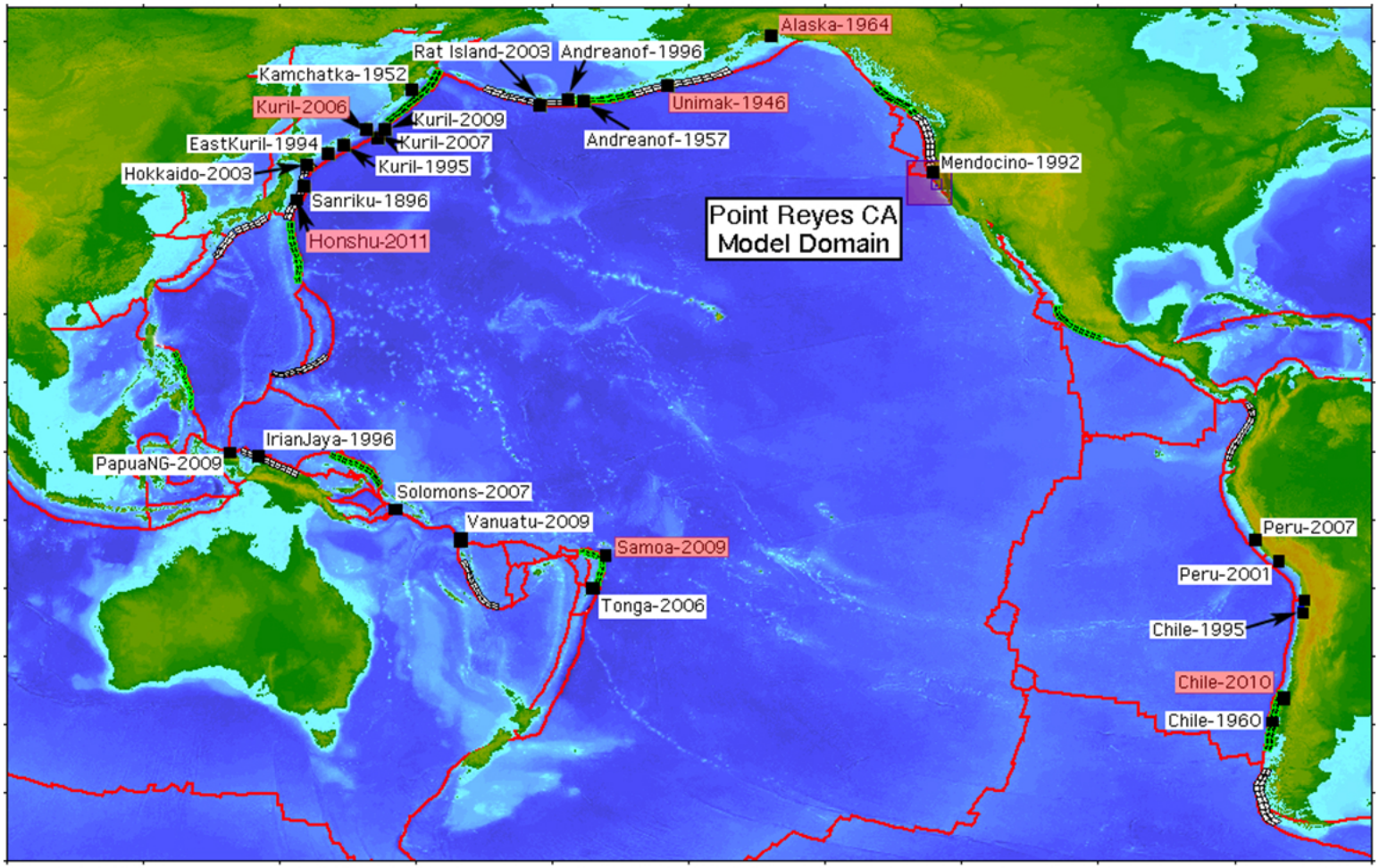

Figure 4. Distribution of the historical tsunami sources employed for the development of the Point Reyes forecast model. Those highlighted in red are more extensively investigated using the reference model.

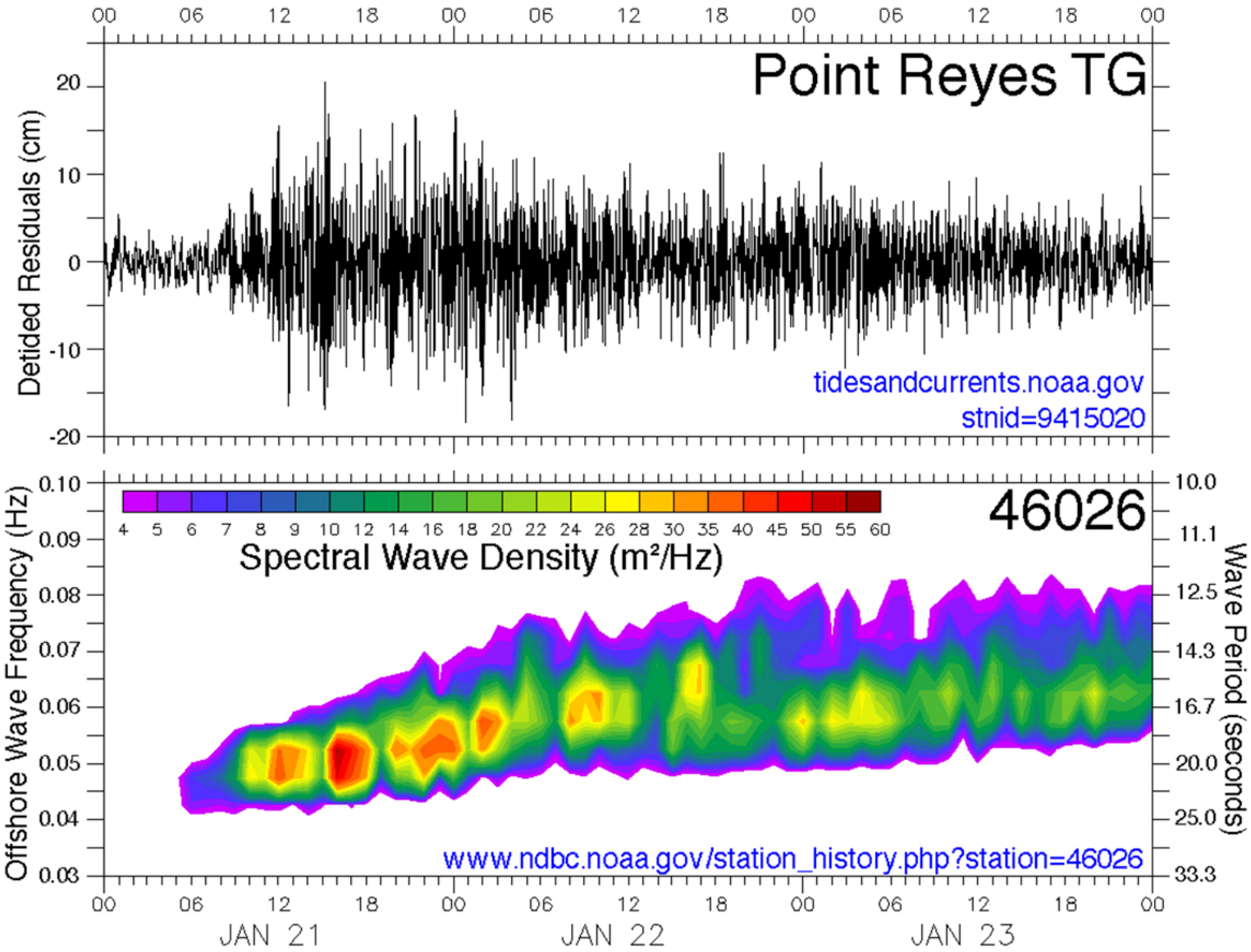

Figure 5. A sample time interval from the Point Reyes tsunami-capable tide gage, unrelated to tsunami activity. The evolving surface wave spectrum is shown in the lower panel.

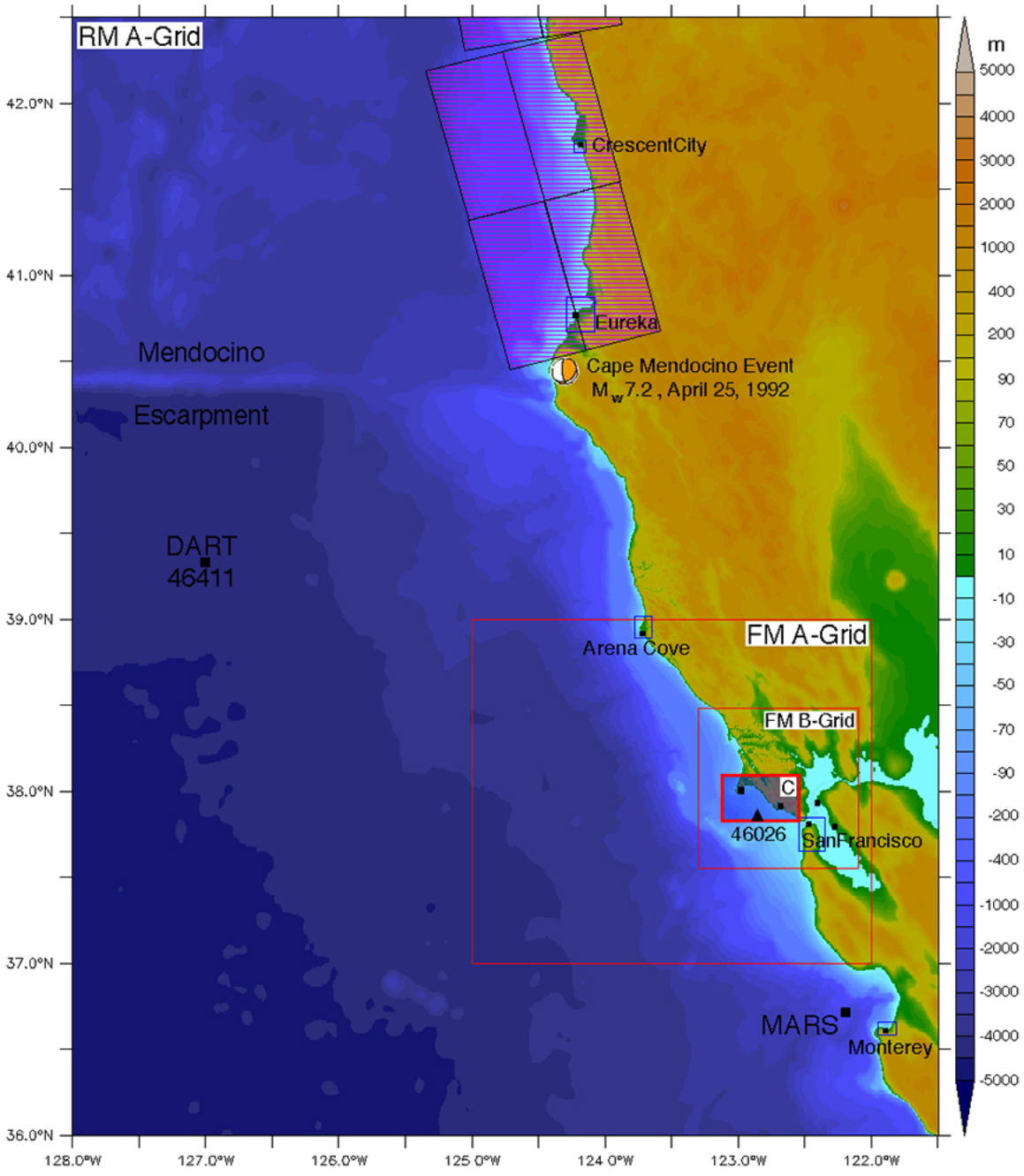

Figure 6. The setting of Point Reyes and its nested FM grids. The C-grids of other west coast forecast models are marked, as are various sites with data available for this study. The closest unit sources of the propagation database lie north of Cape Mendocino, and the epicenter of the most recent Cascadia thrust event is marked.

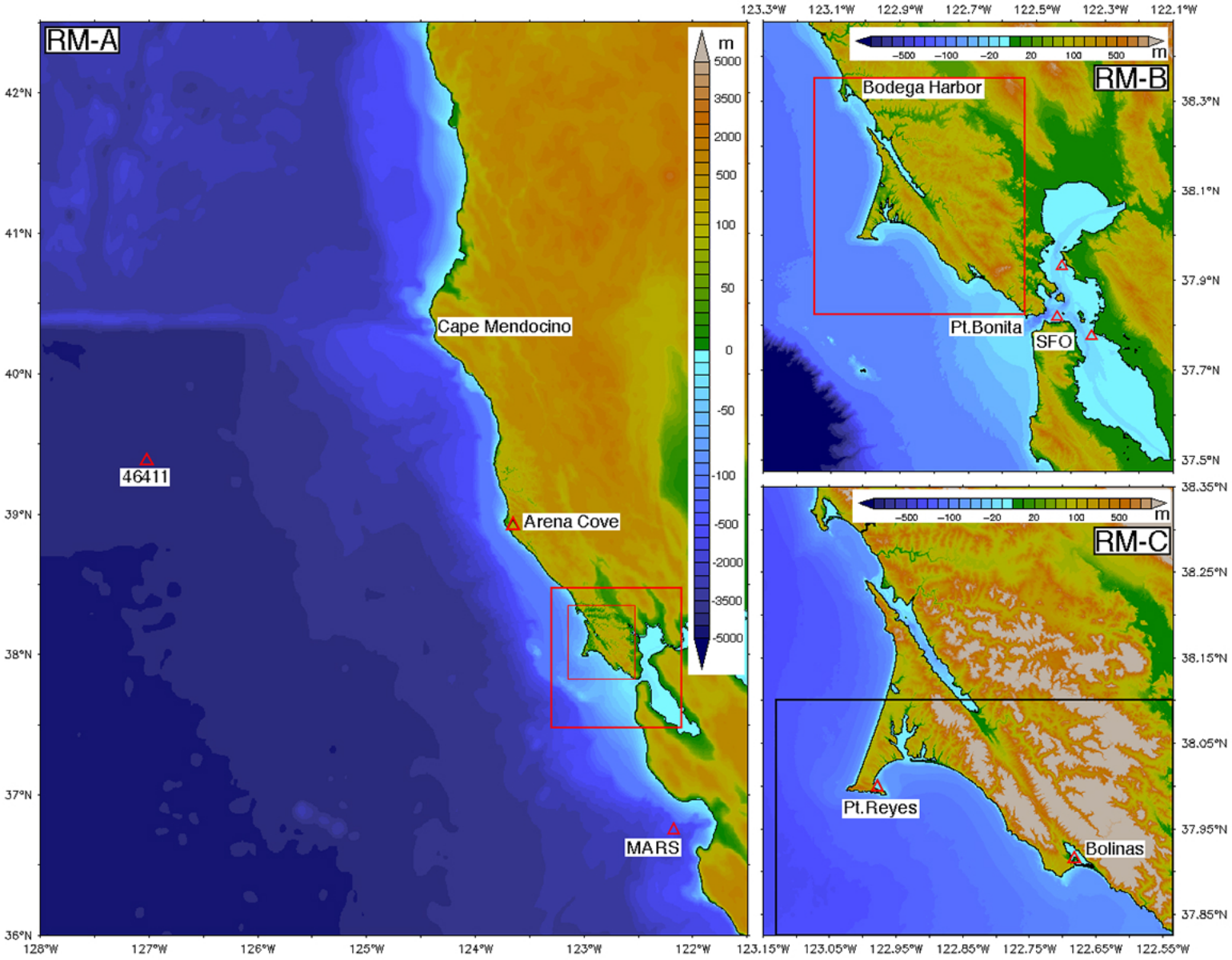

Figure 7. Nested grid representation for the Reference Model (RM).

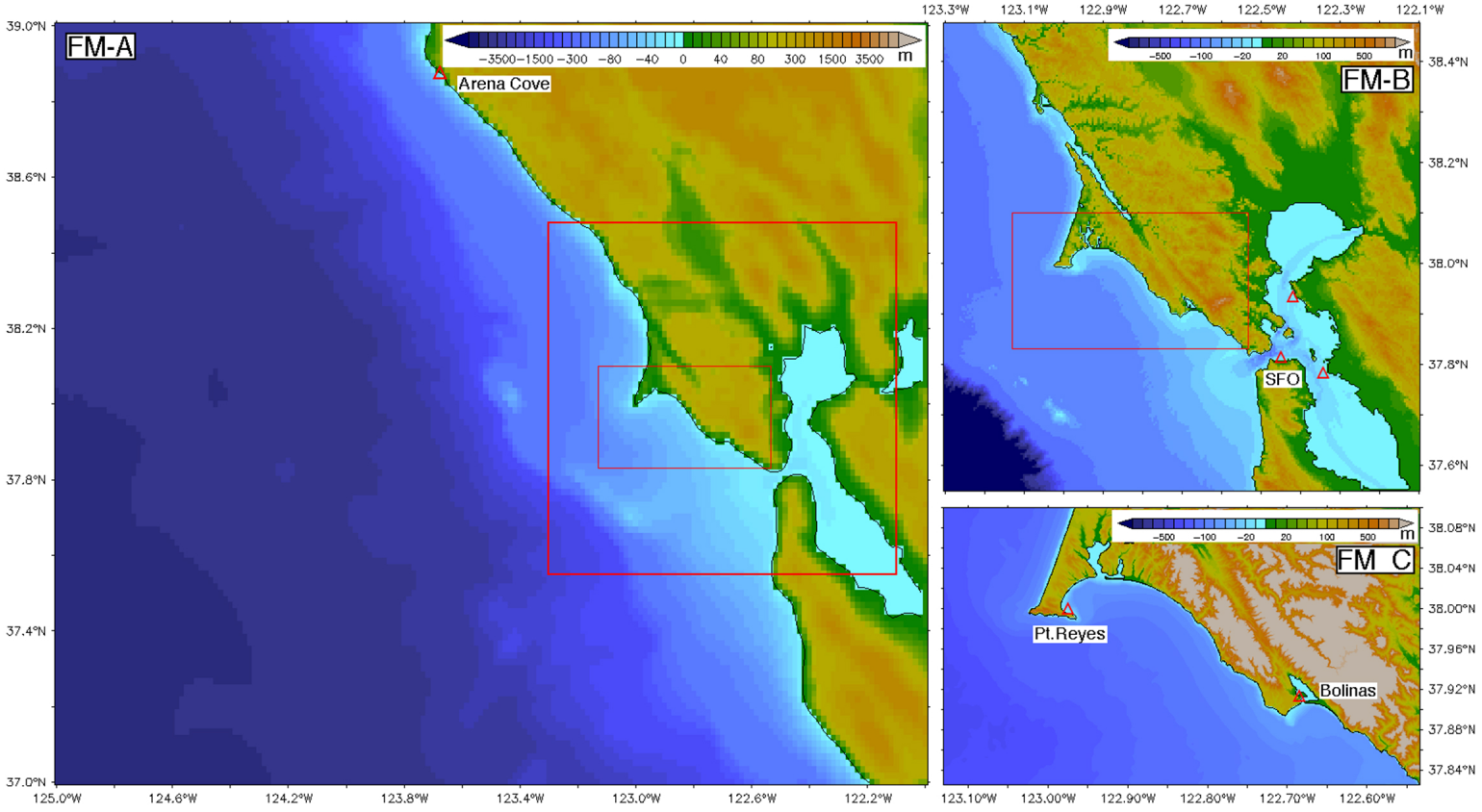

Figure 8. Nested grid representation for the Forecast Model (FM).

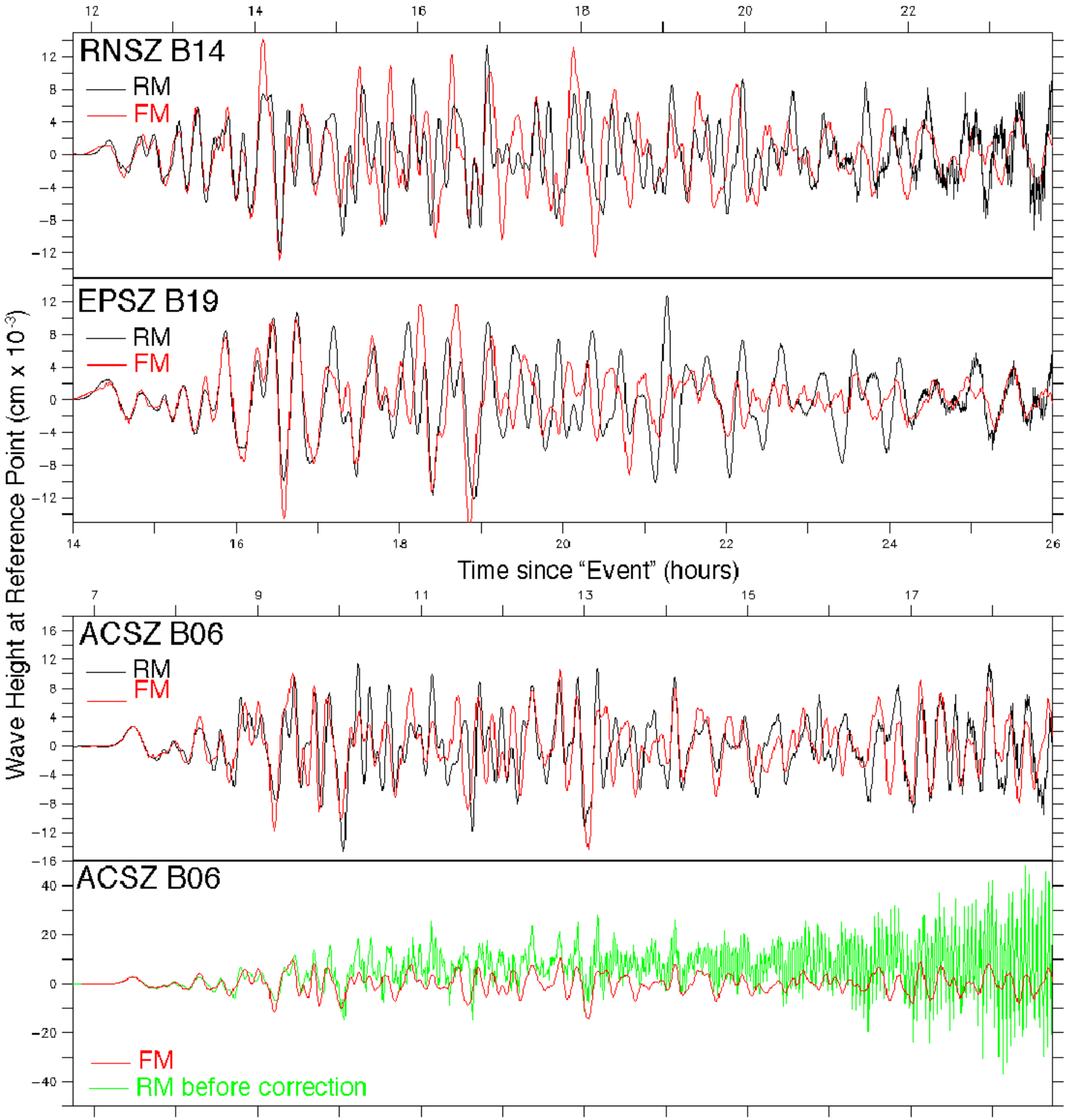

Figure 9. Comparison of the RM and FM time series at the reference point for three "Null" sources in the Western Pacific. The lowest panel illustrates the appearance of model instability before the RM C-grid bathymetry was finalized.

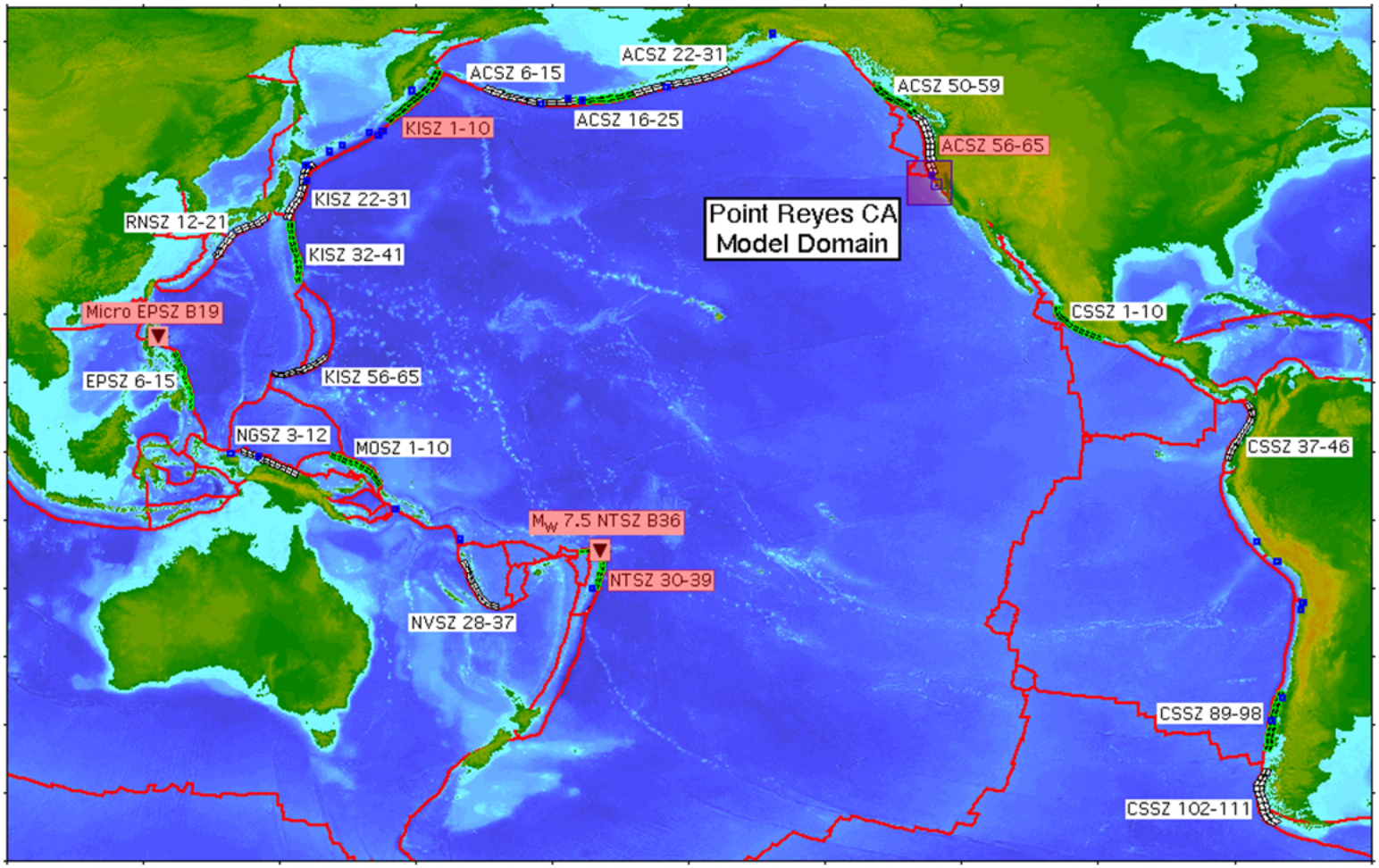

Figure 10. Locations of synthetic tsunami scenarios employed in model development.

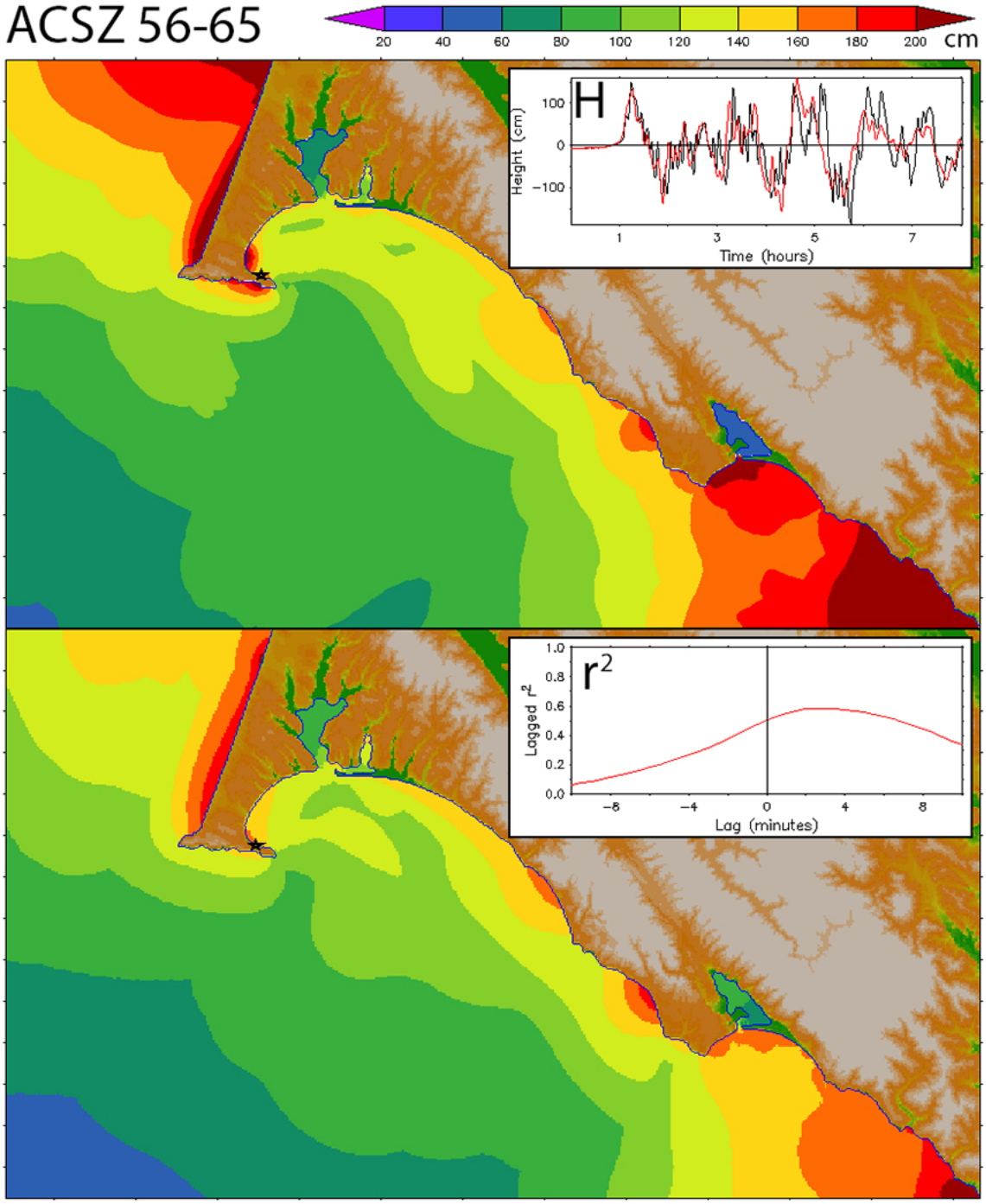

Figure 11. Comparison of Reference (RM) and Forecast (FM) model results for the ACSZ 56-65 synthetic mega-event, representing the Cascadia Subduction Zone. a) Maximum amplitude from the RM (upper panel), the FM (lower panel), time series at the Point Reyes tide gage (upper panel inset: black for RM, red for FM). The lagged correlation at the TG (lower inset) shows that there is only a few minutes difference in the model arrival times.

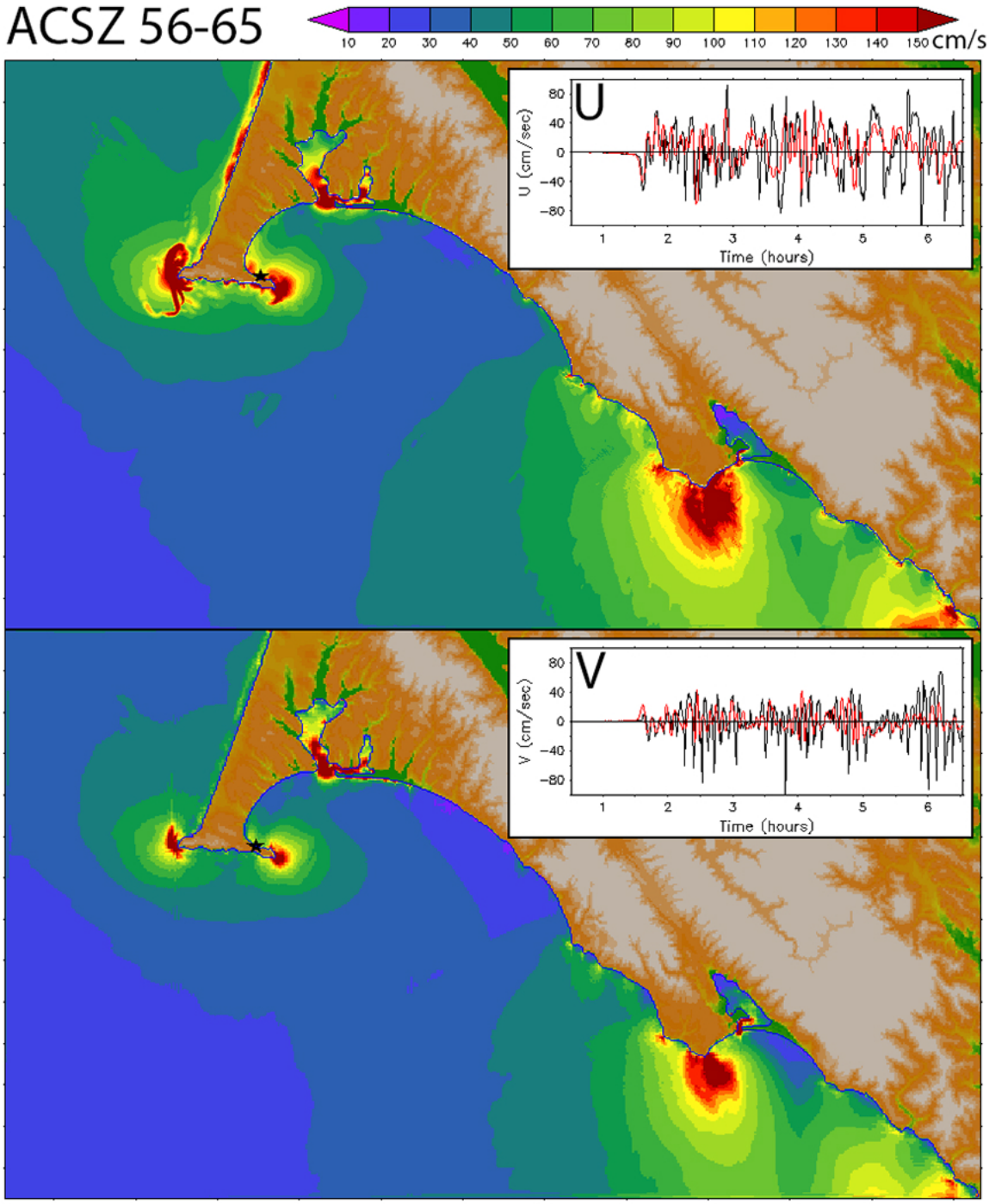

Figure 11 continued. . b) Comparison of maximum speed from the Reference Model (upper panel) and Forecast Model (lower panel). Inset panels compare the time series of the velocity components at the TG.

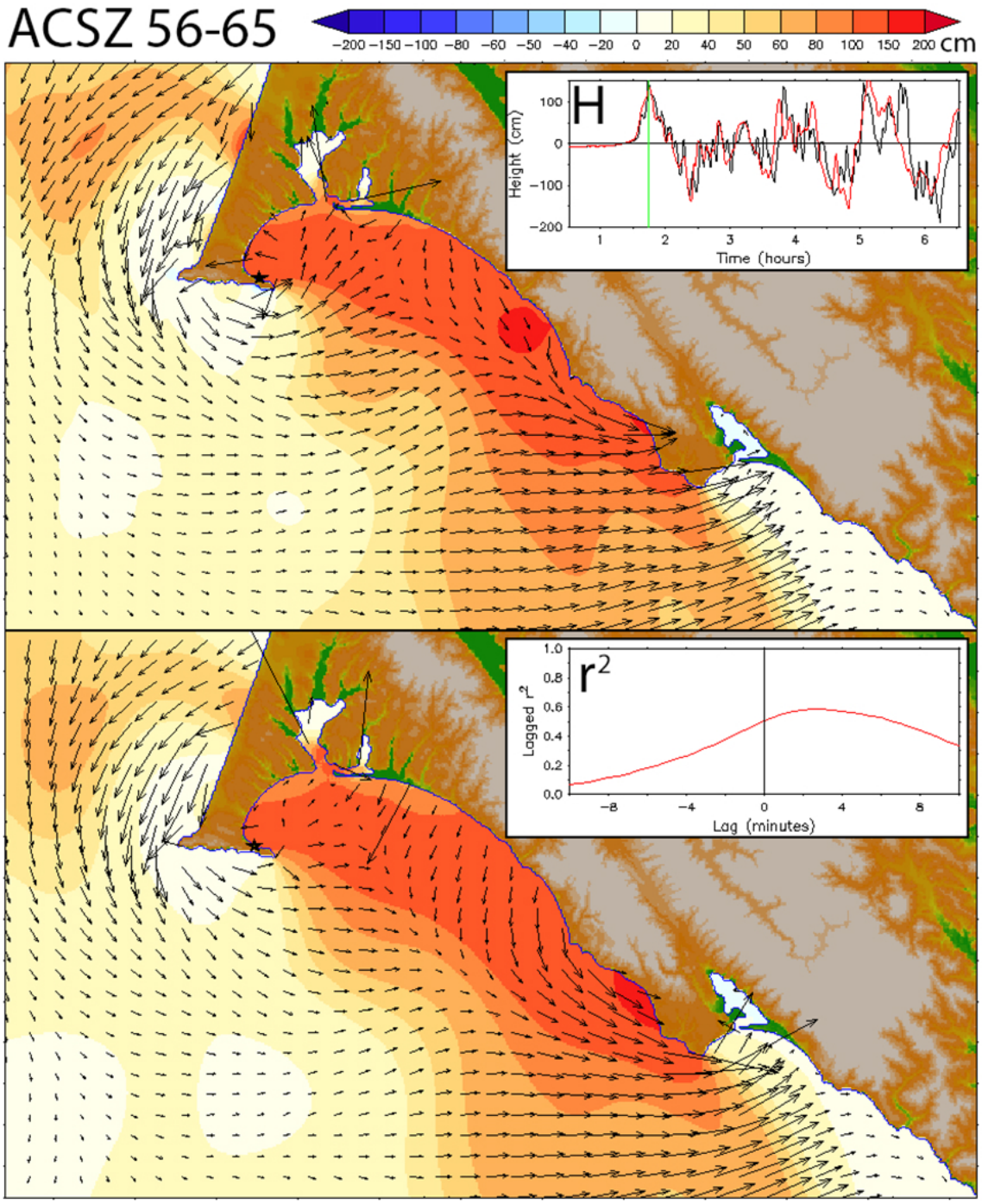

Figure 11 continued. c) Comparison of the amplitude and vector current fields at the time indicated by the green line in the upper inset panel.

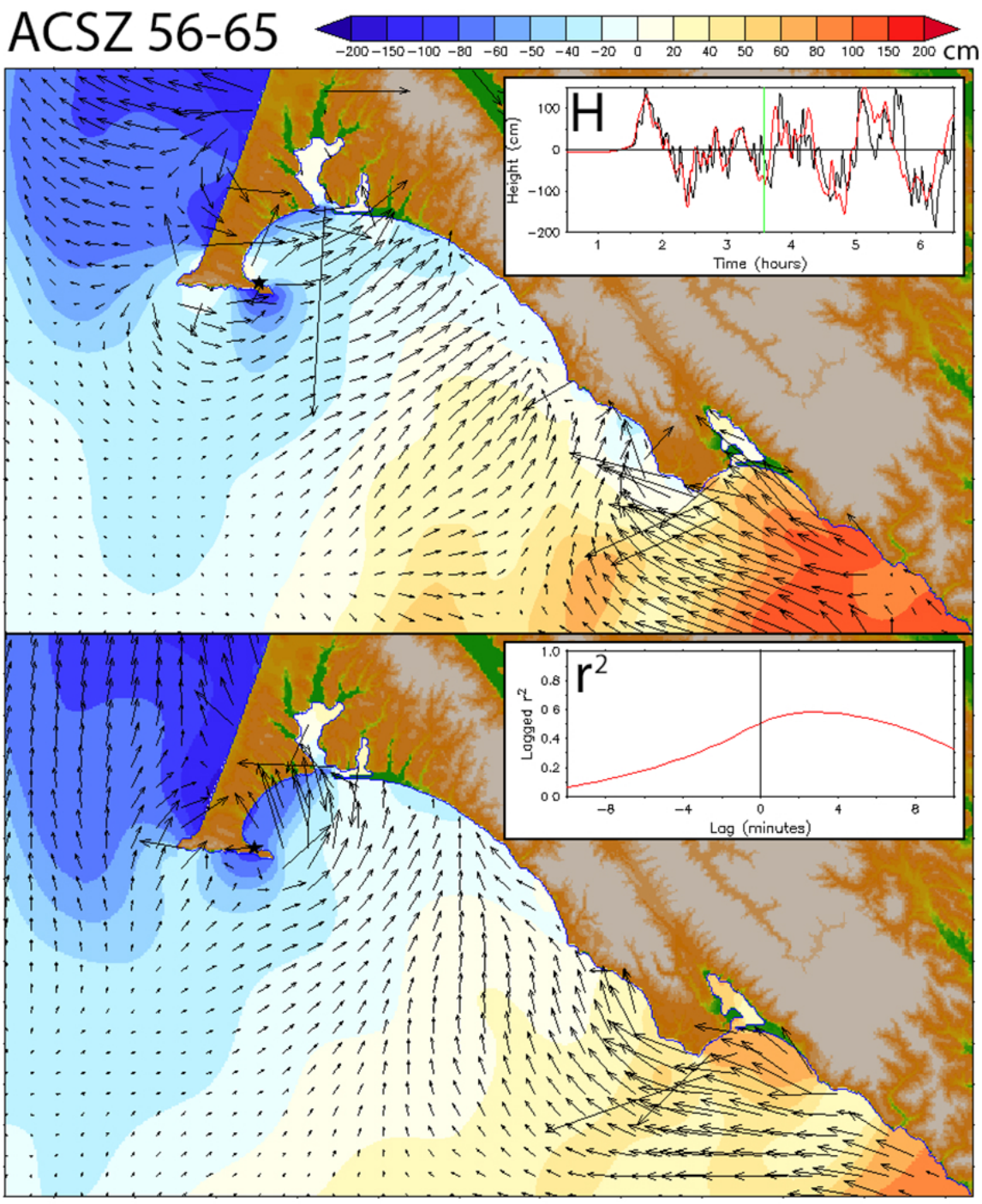

Figure 11 continued. d) As for c) but at a later time in the model runs.

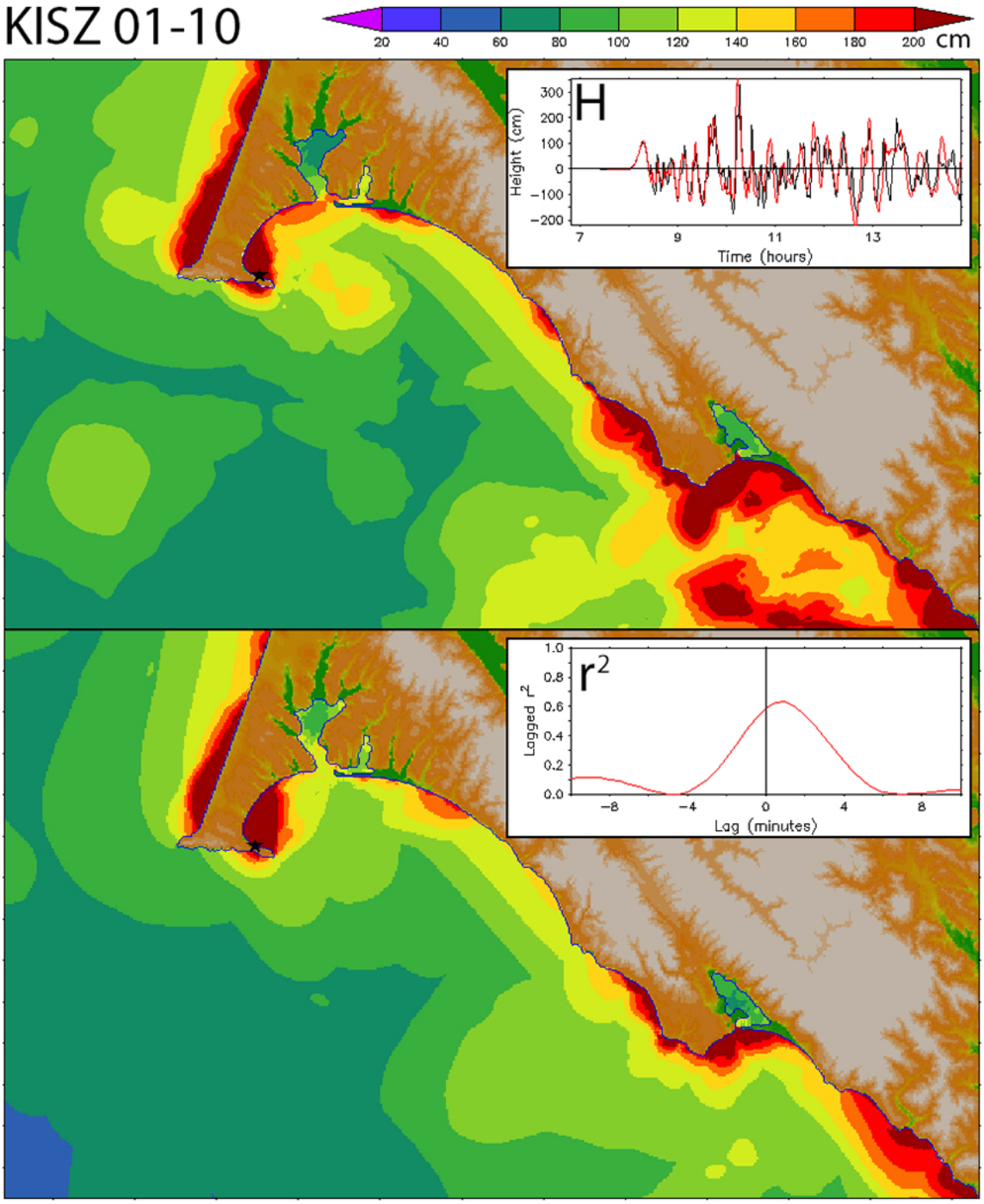

Figure 12. As in Figure 11, but for the KISZ 01-10 scenario representing Kamchatka.
a) Maximum amplitude for RM (upper panel) and FM (lower panel).

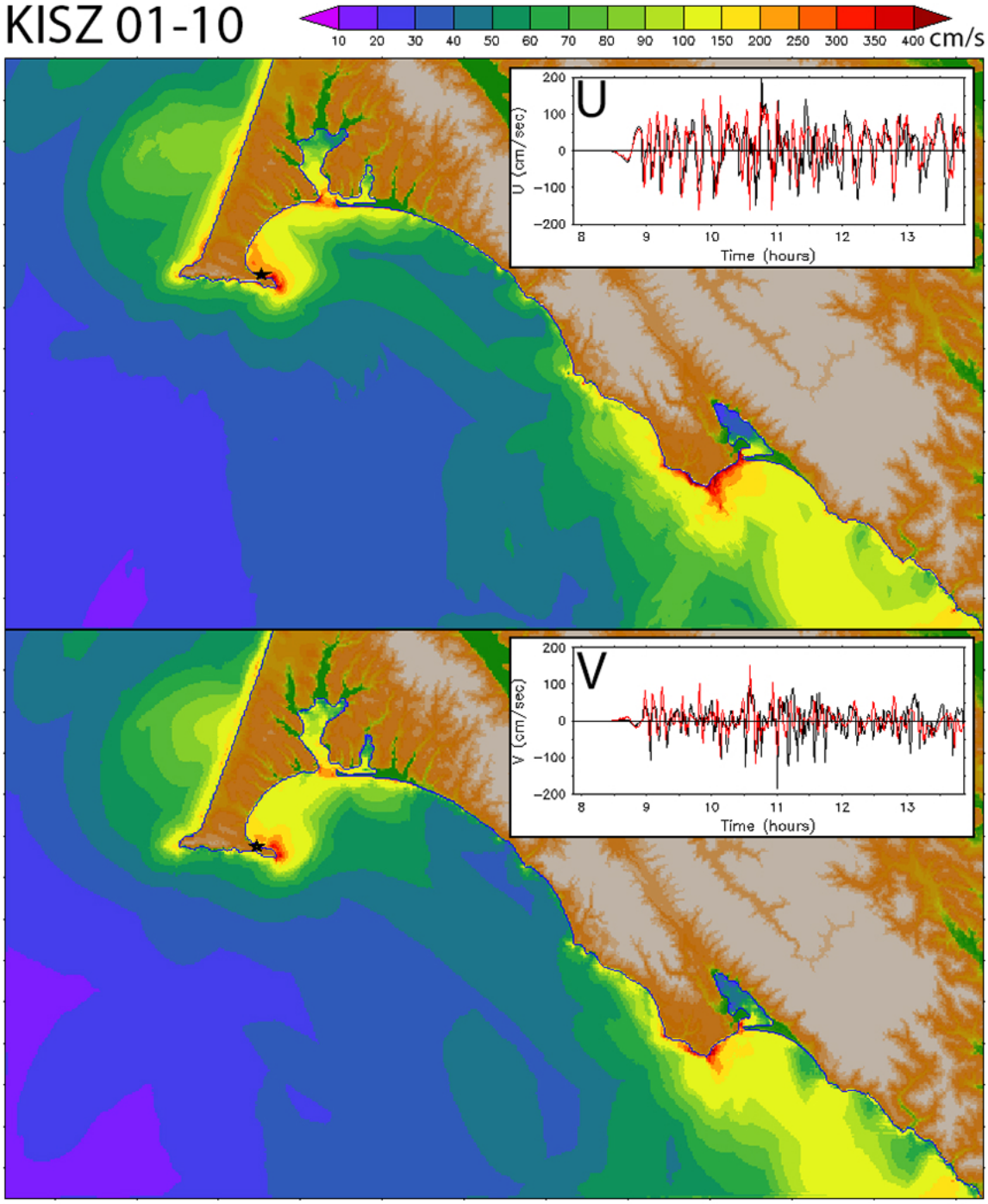

Figure 12 continued. As in Figure 11b, but for the KISZ 01-10 scenario representing Kamchatka.

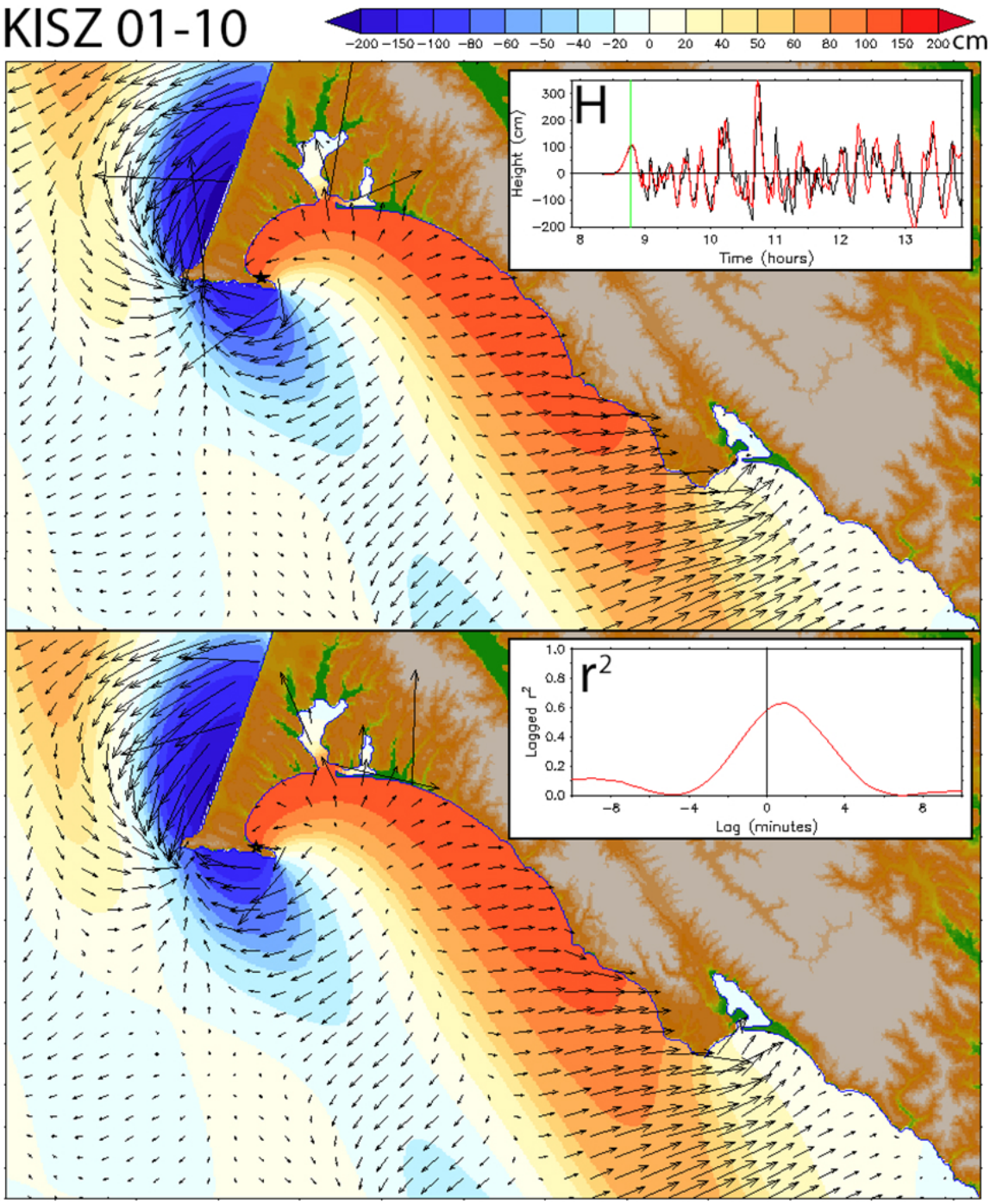

Figure 12 continued. As in Figure 11c, but for the KISZ 01-10 scenario representing Kamchatka.

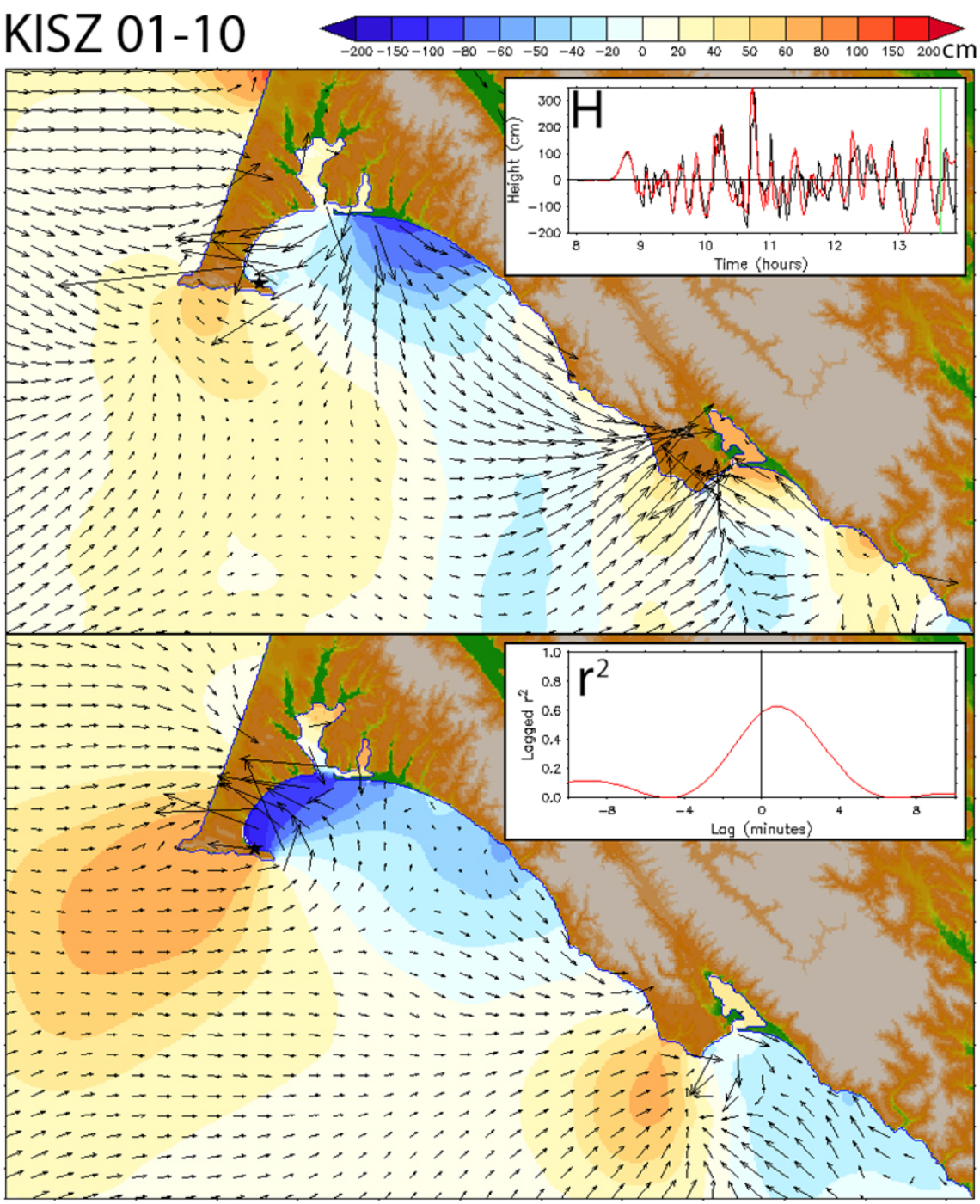

Figure 12d. As in Figure 11d, but for the KISZ 01-10 scenario representing Kamchatka.

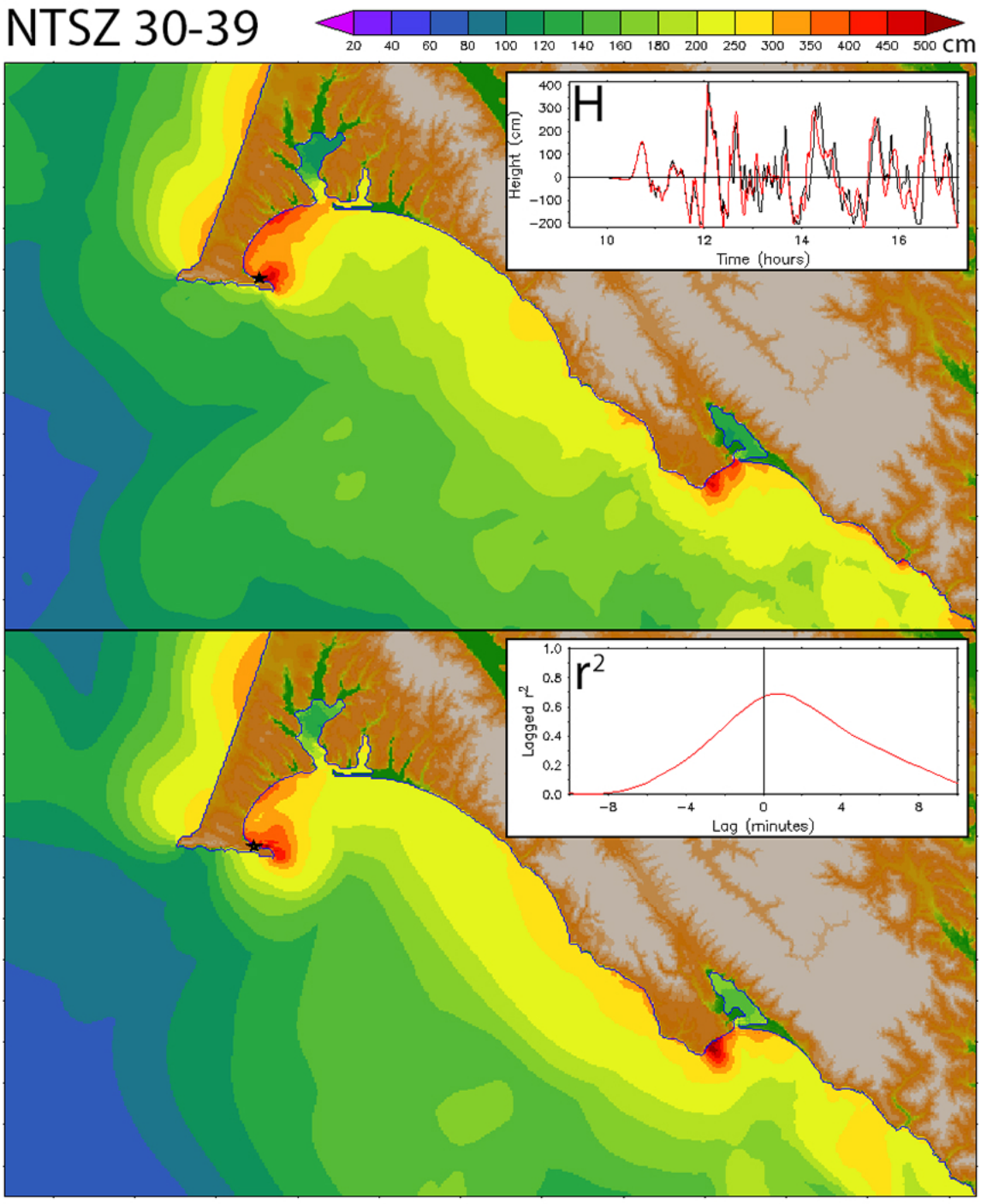

Figure 13. As in Figure 11, but for the NTSZ 30-39 scenario representing Samoa.
a) Maximum amplitude for RM (upper panel) and FM (lower panel).

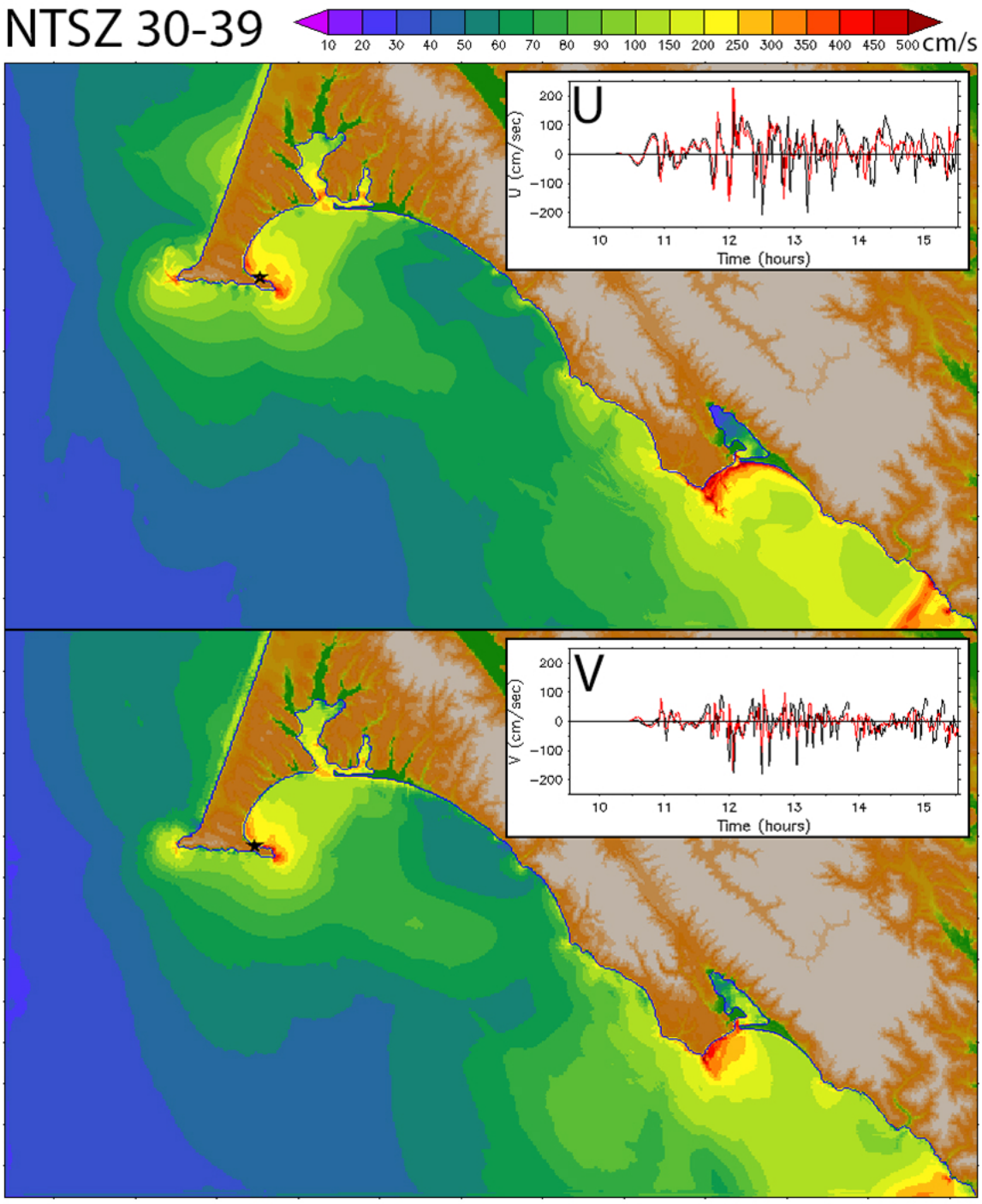

Figure 13 continued. As in Figure 11b, but for the NTSZ 30-39 scenario representing Samoa.

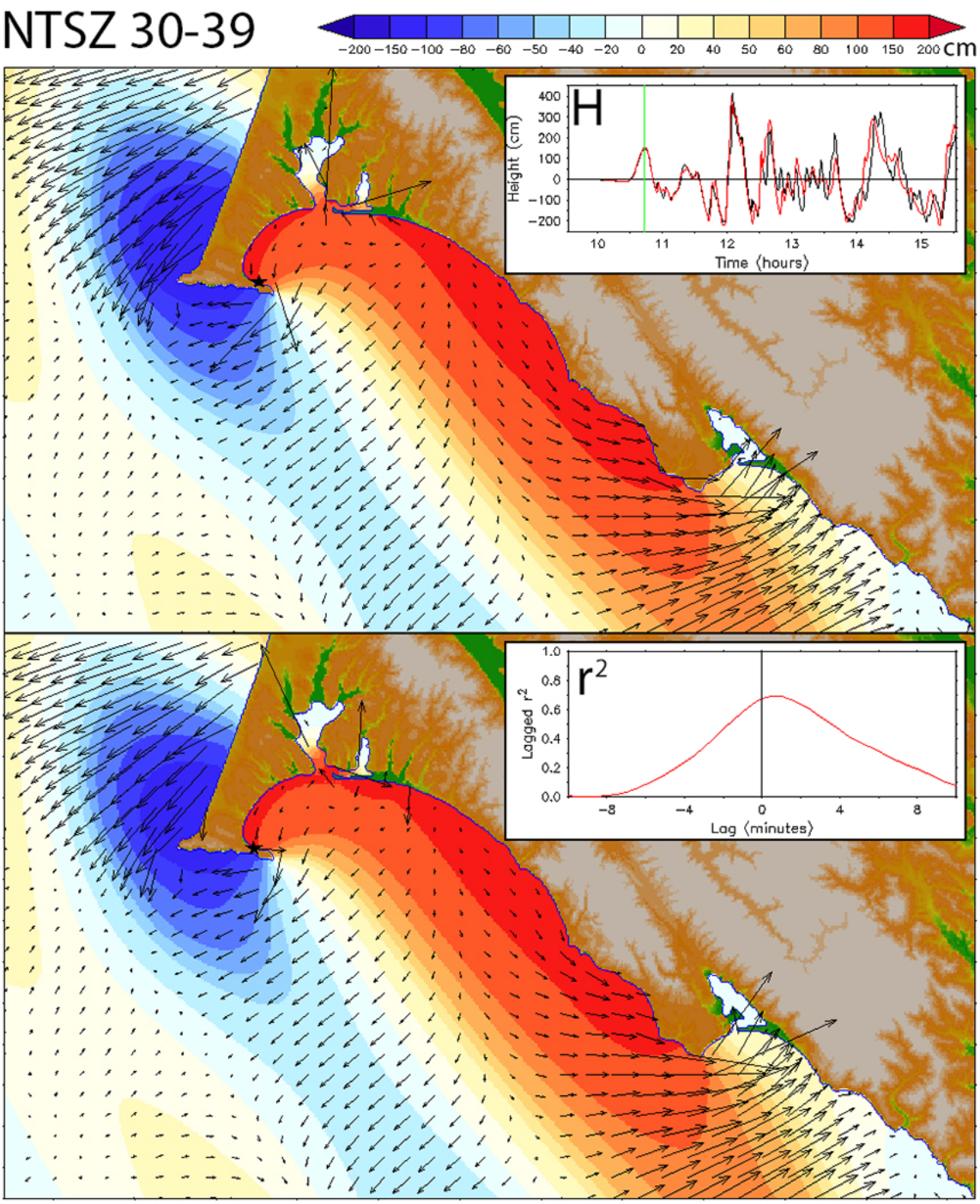

Figure 13c. As in Figure 11c, but for the NTSZ 30-39 scenario representing Samoa.

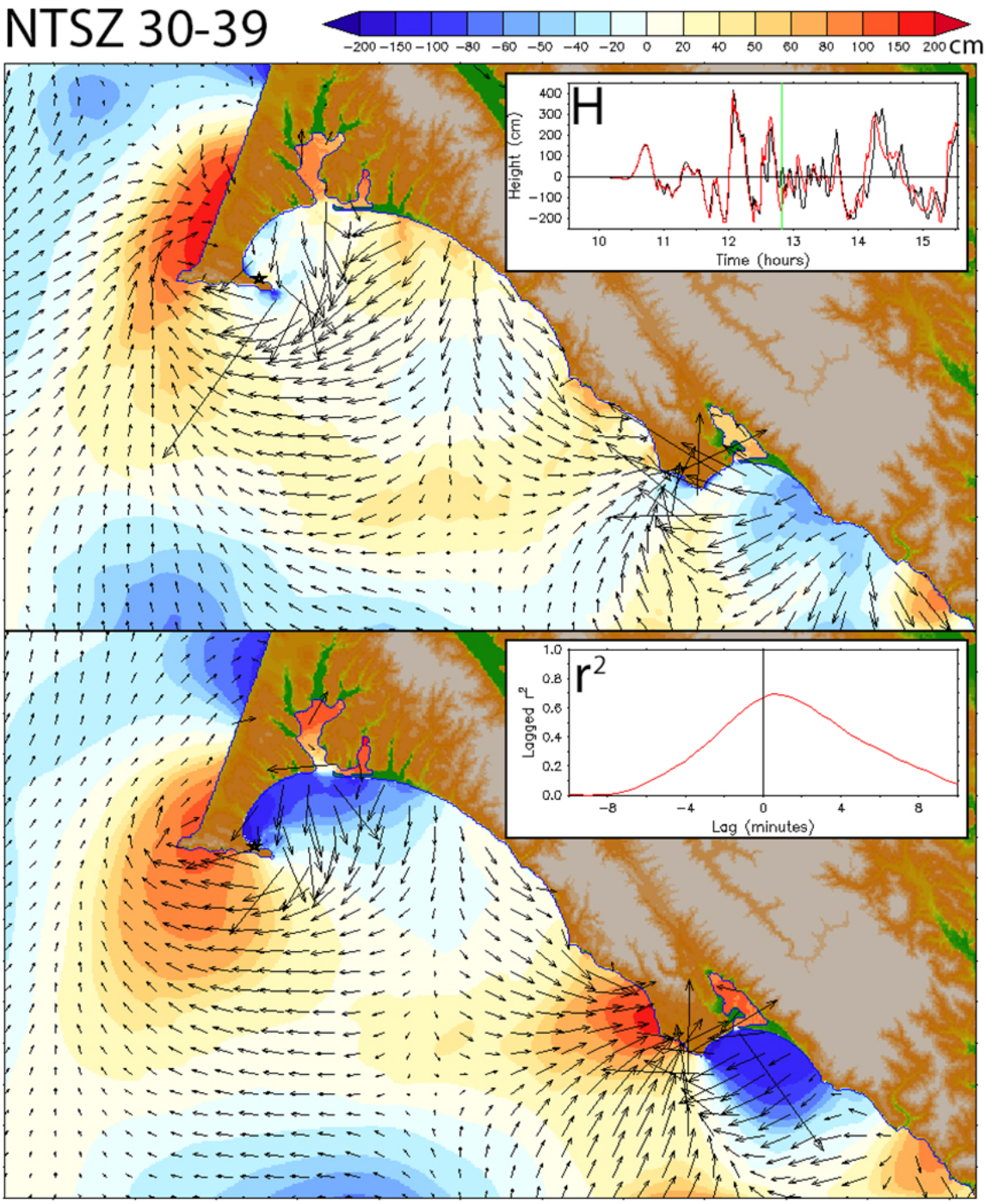

Figure 13d. As in Figure 11d, but for the NTSZ 30-39 scenario representing Samoa.

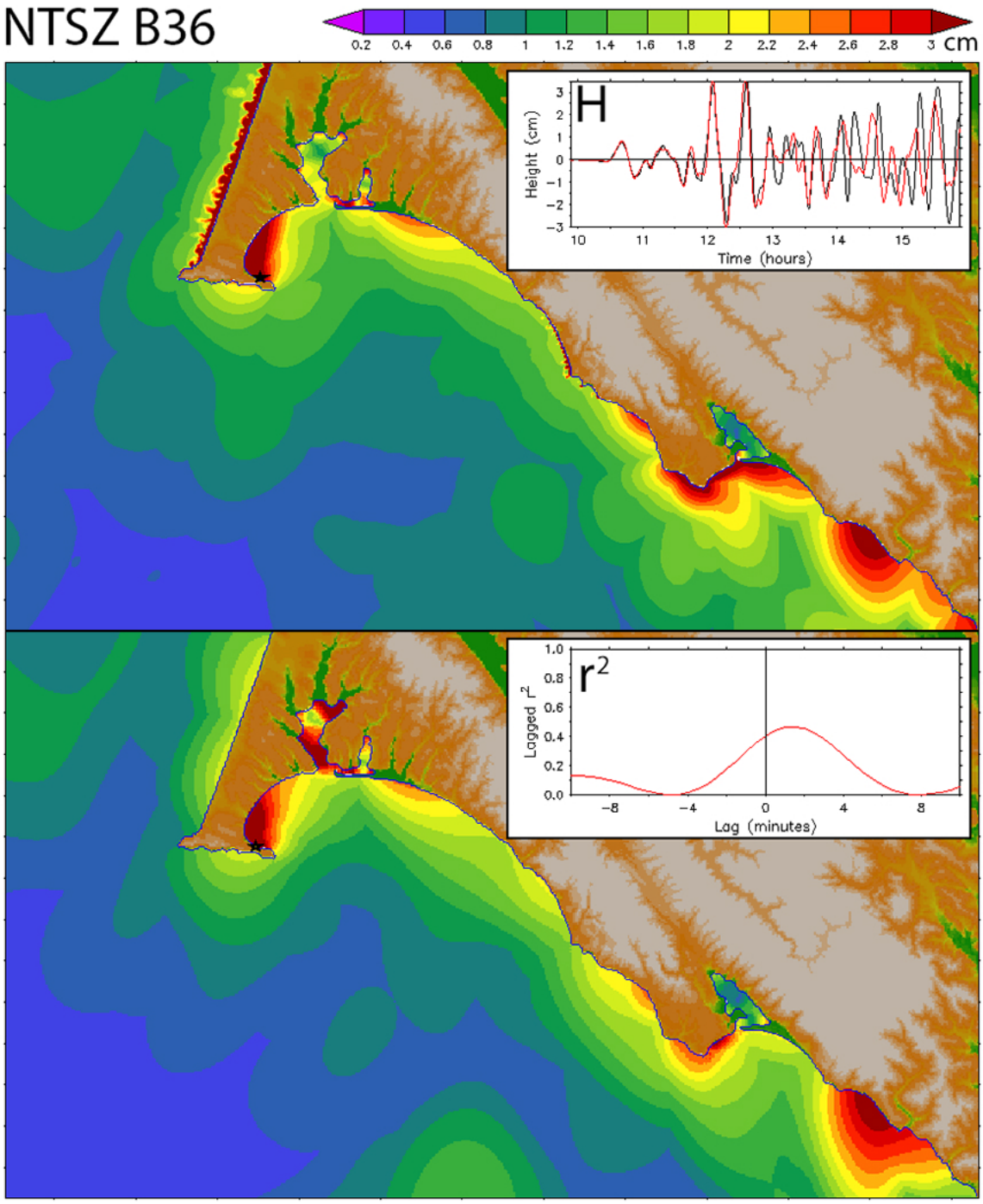

Figure 14. As in Figure 11, but for a synthetic moderate event at NTSZ B36 near Samoa. a) Maximum amplitude for RM (upper panel) and FM (lower panel).

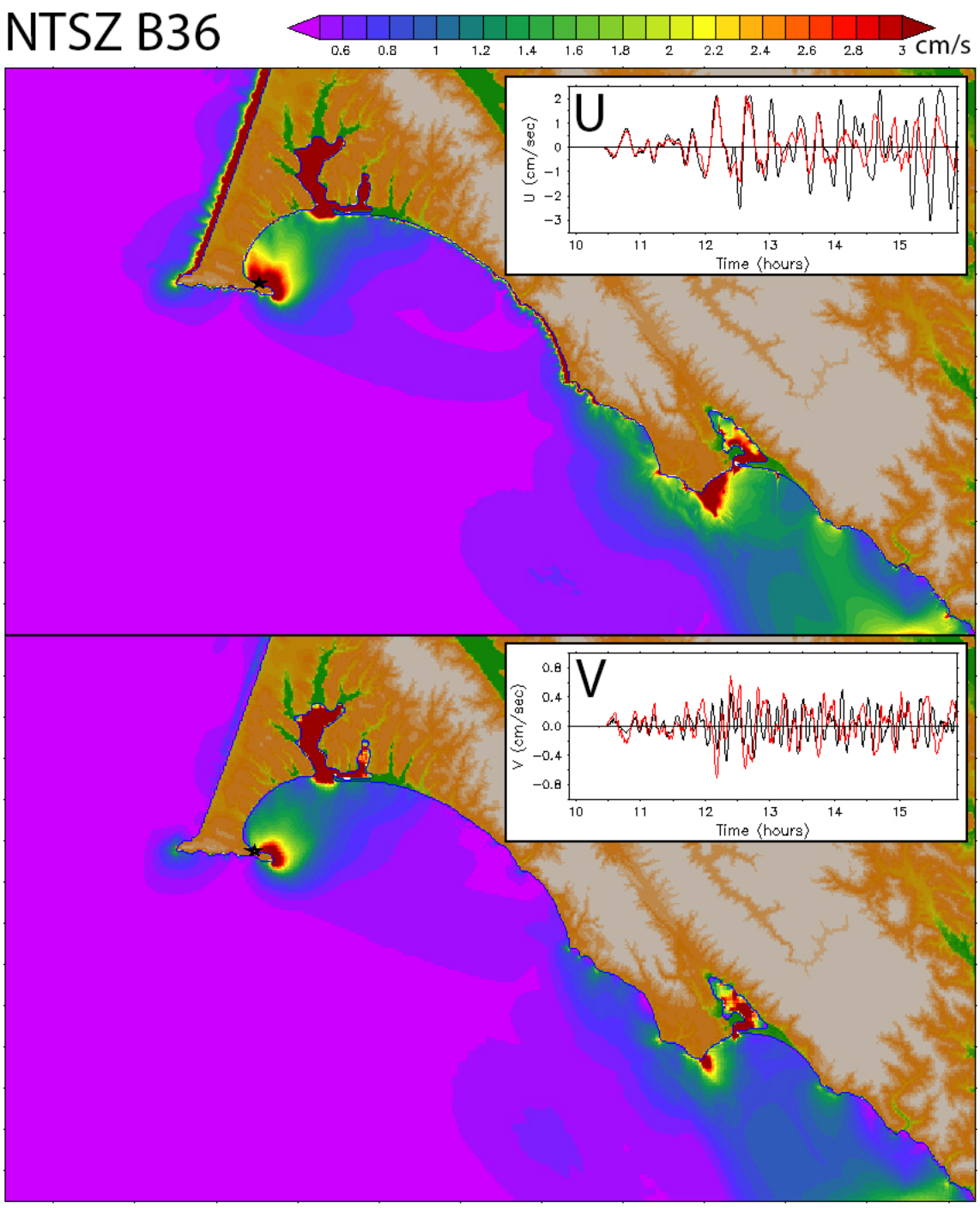

Figure 14b. As in Figure 11b, but for a synthetic moderate event at NTSZ B36 near Samoa.

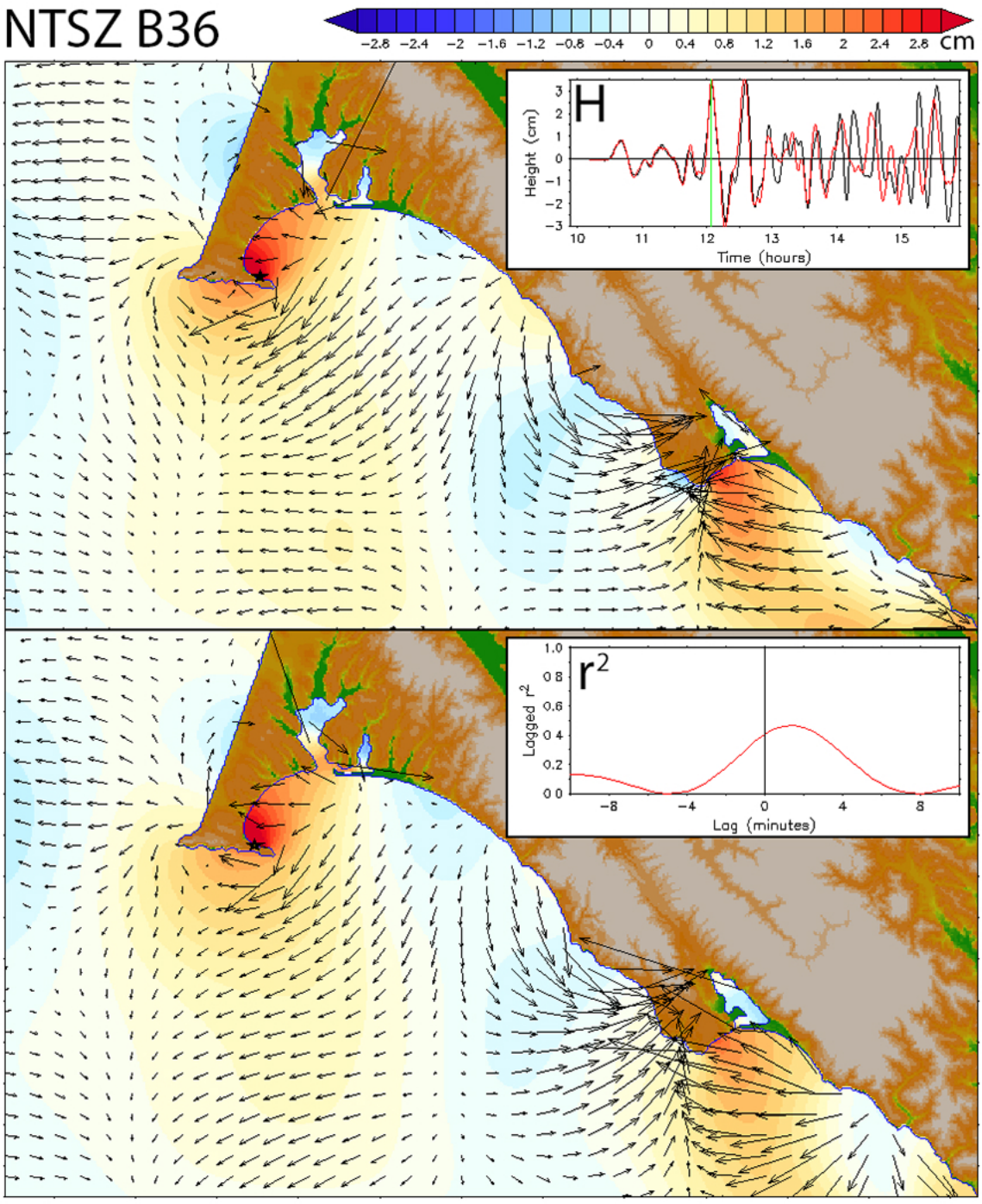

Figure 14c. As in Figure 11c, but for a synthetic moderate event at NTSZ B36 near Samoa.

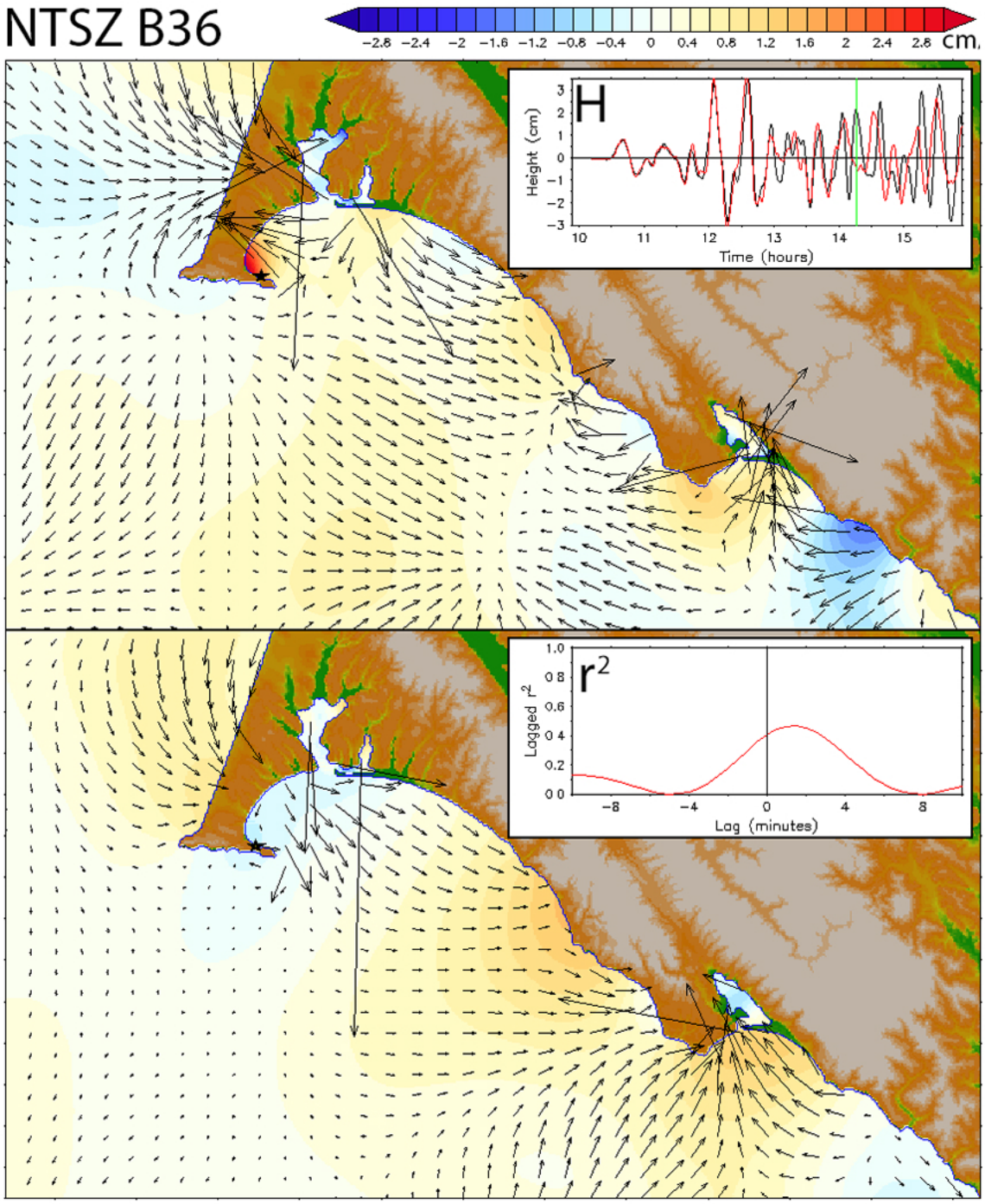

Figure 14d. As in Figure 11d, but for a synthetic moderate event at NTSZ B36 near Samoa.

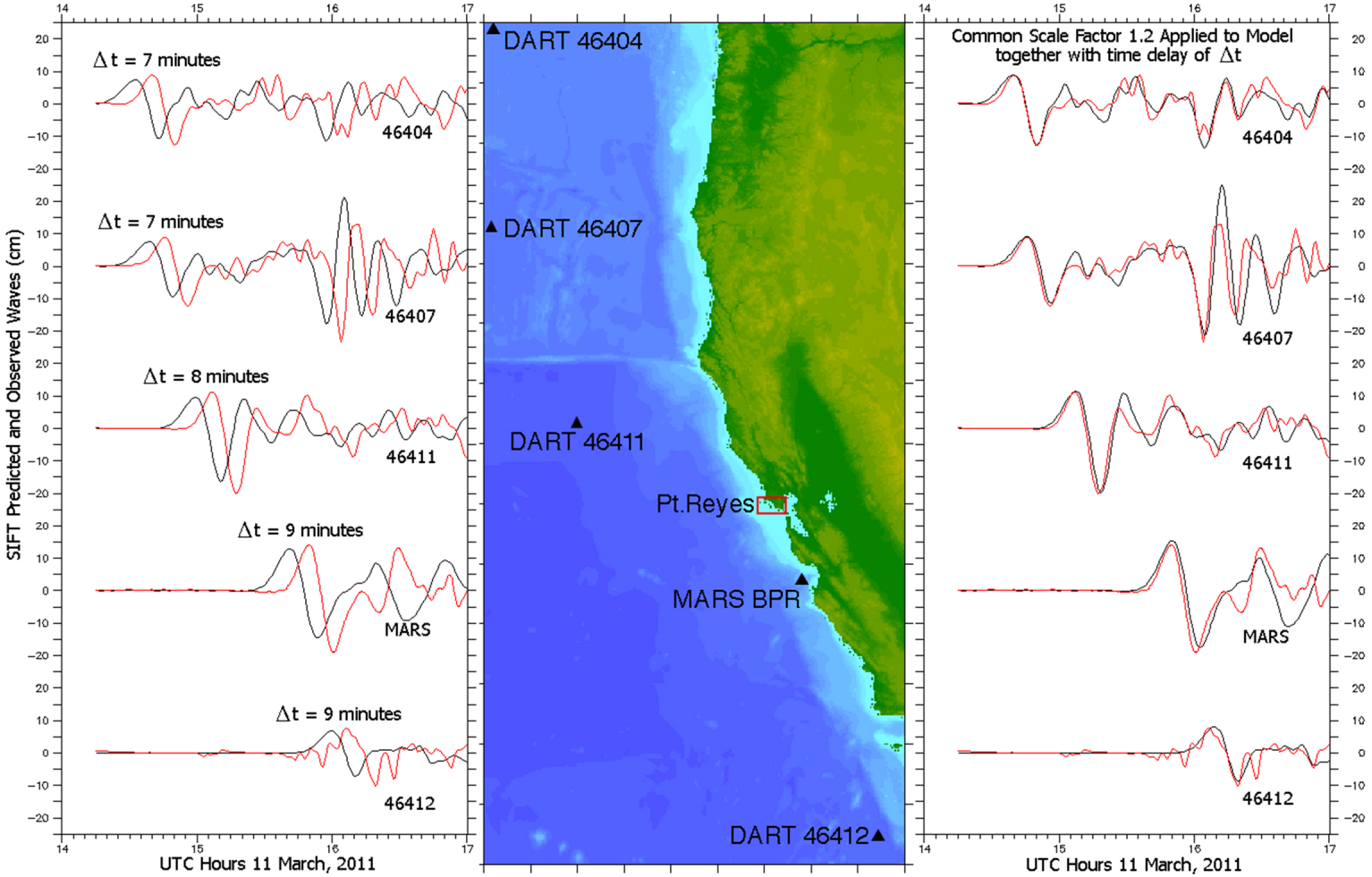

Figure 15. Observed time series from DART and MARS bottom pressure sensors during the Honshu-2011 event, compared with the model representation based on the propagation database (see Table 1). Model time series in the right hand panel have been lagged, and a common scale factor of 1.2 applied.

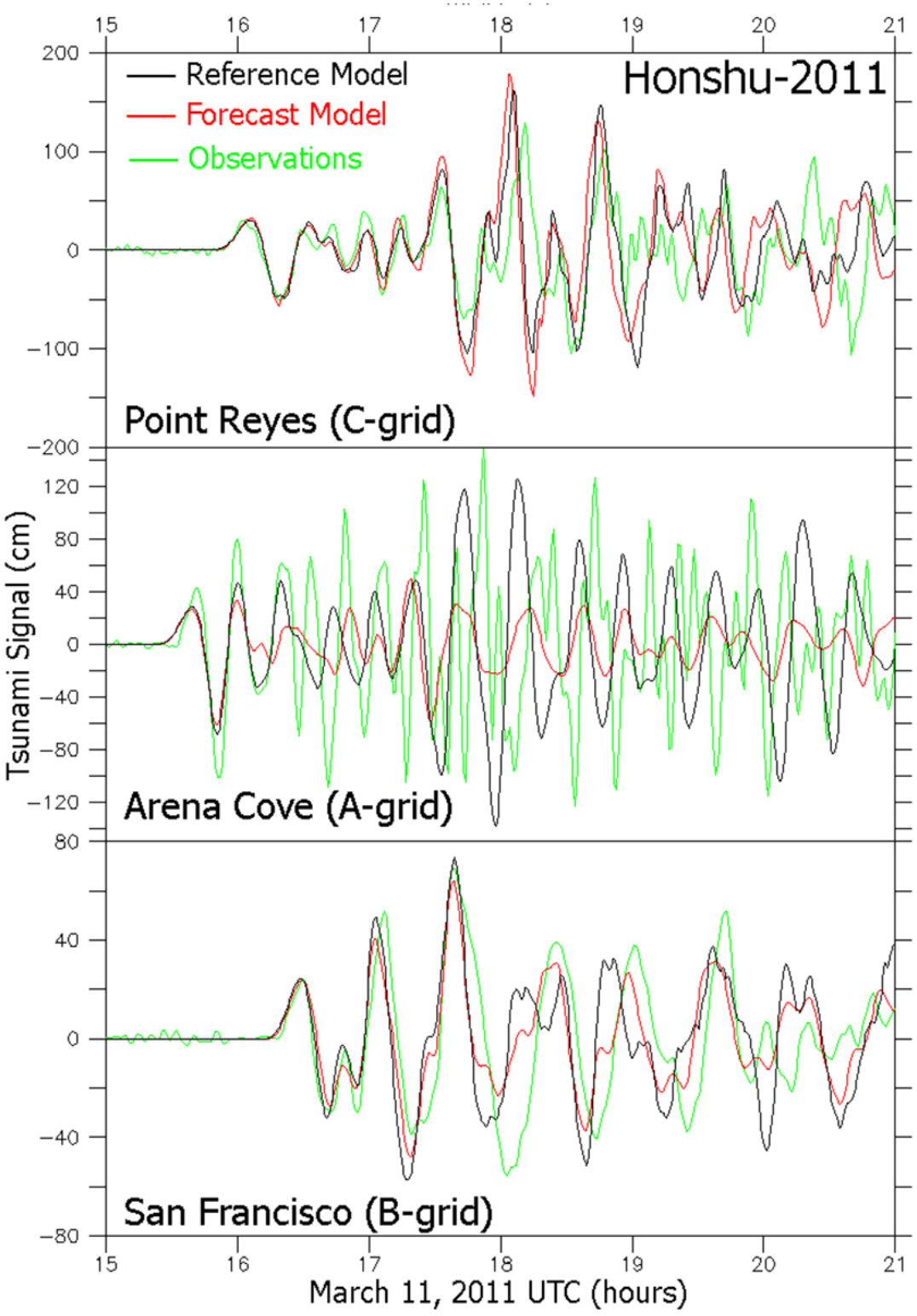

Figure 16. Comparison with RM and FM-predicted time series at selected locations where tide gage data are available: a) Point Reyes, Arena Cove, and San Francisco.

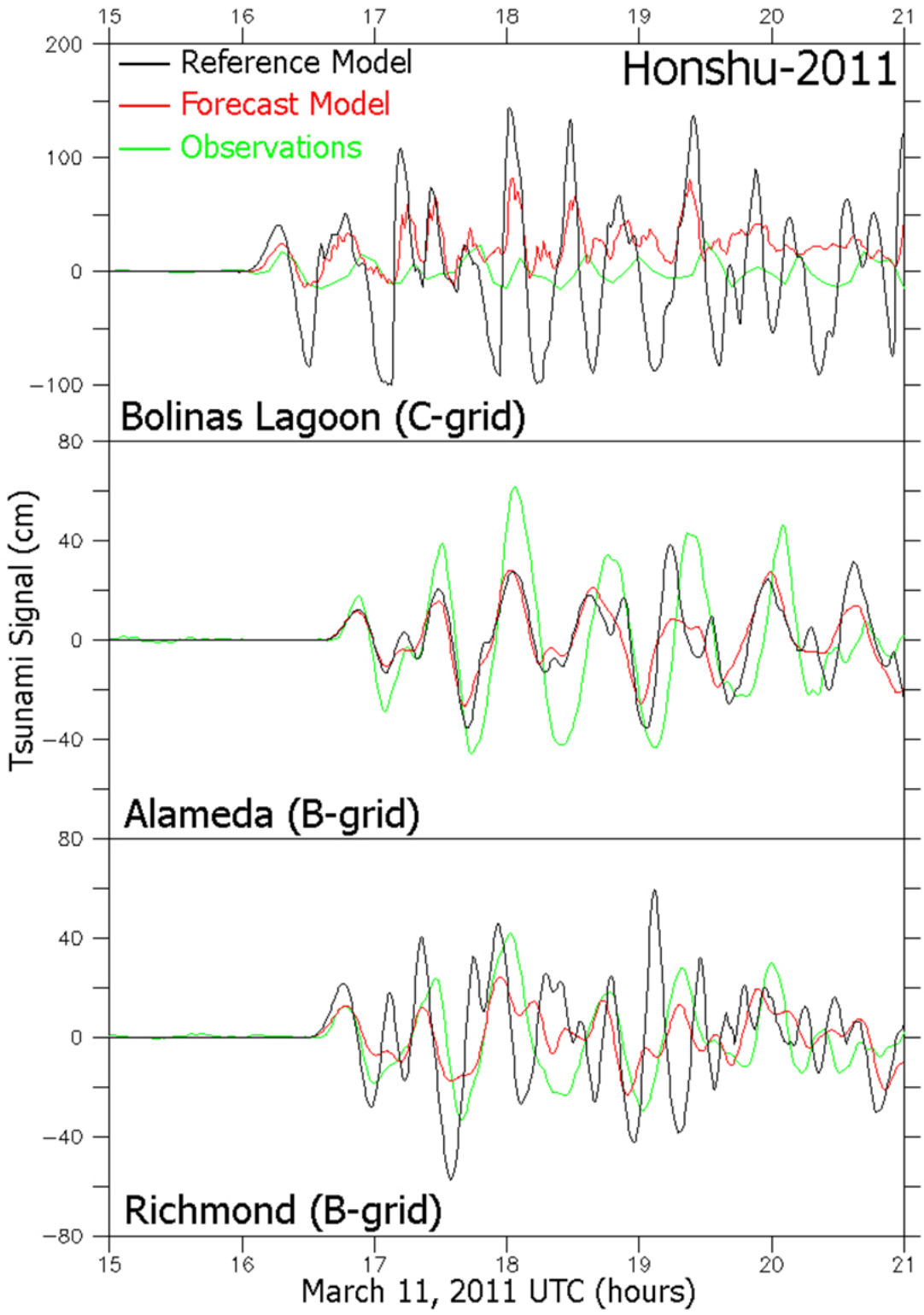

Figure 16 continued. b) Bolinas (6-minute data), Alameda, and Richmond.

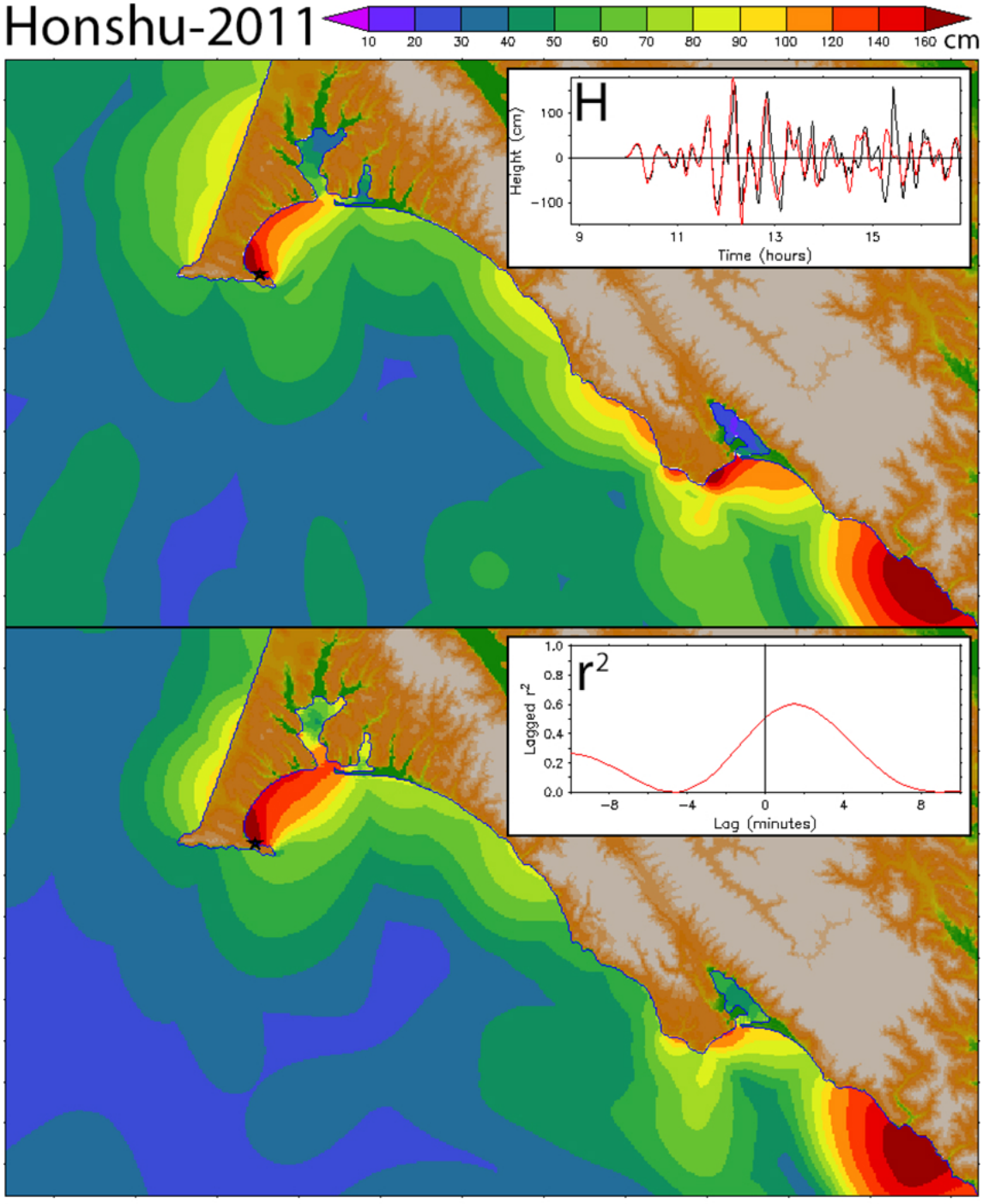

Figure 17. Intercomparison of RM and FM predictions for the Honshu-2011 event.
a) Maximum amplitude for the RM (upper panel) and FM (lower panel).

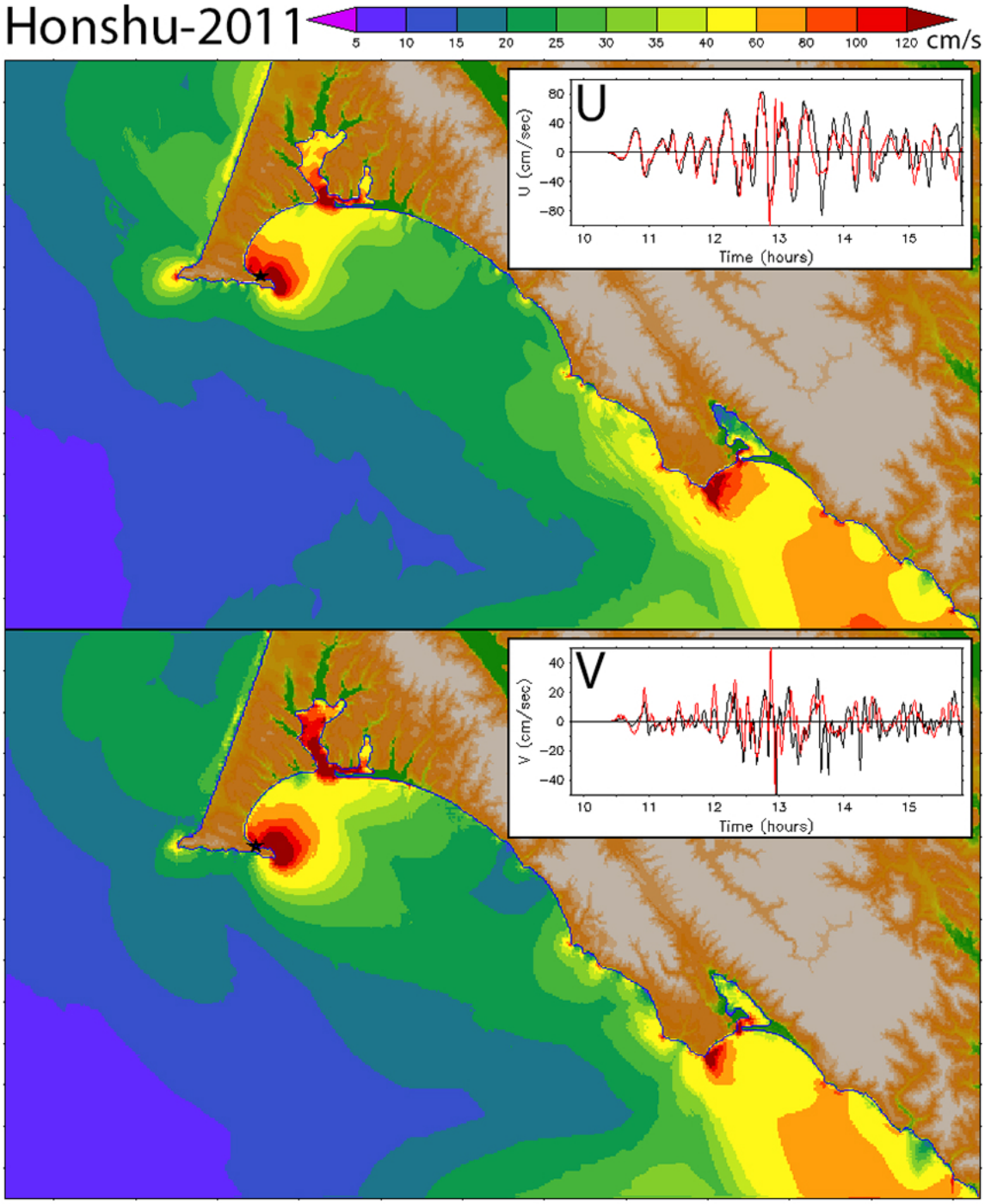

Figure 17 continued. Intercomparison of RM and FM predictions for the Honshu-2011 event. b) Maximum speed distribution in the style of Figure 11b.

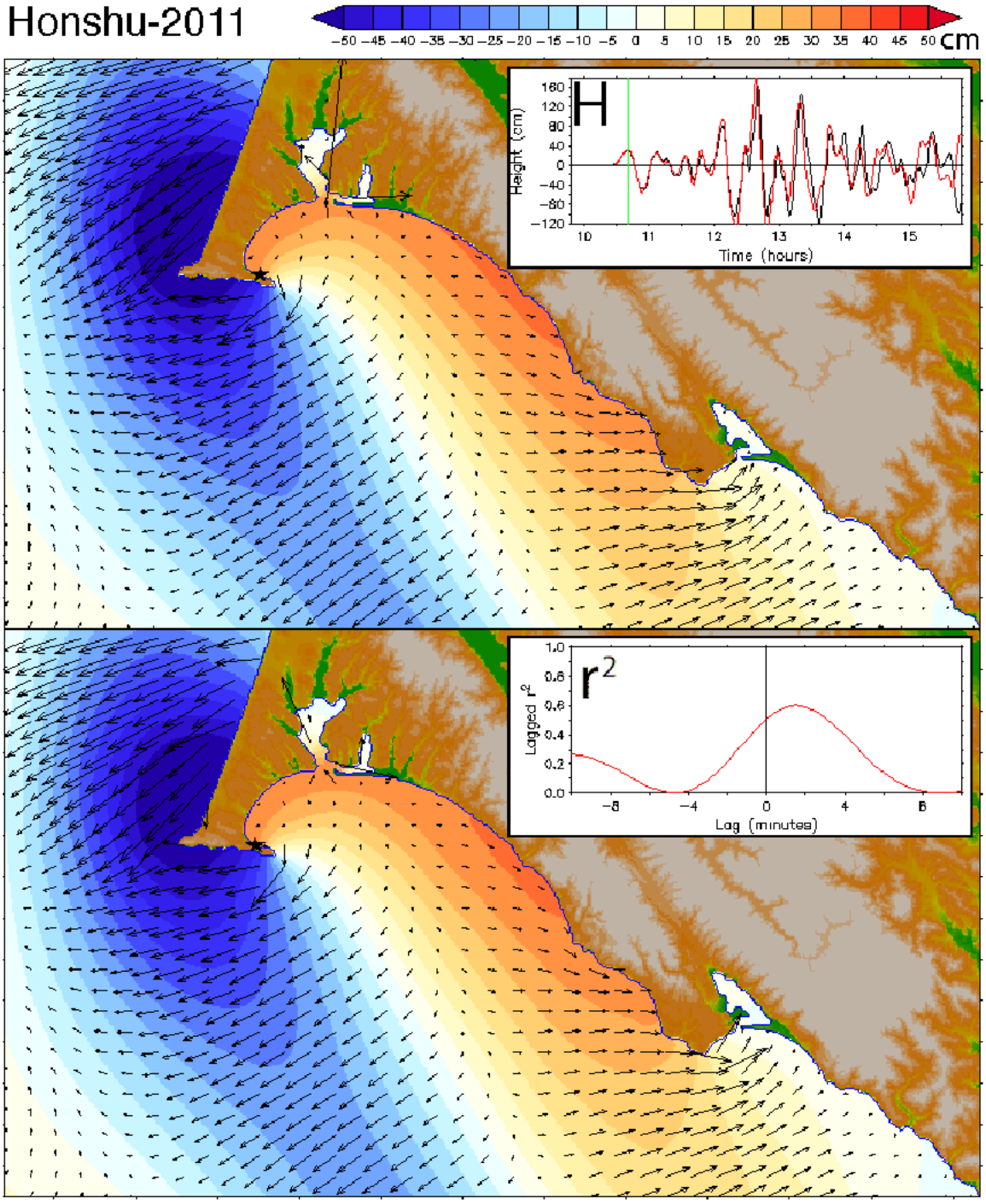

Figure 17 continued. Intercomparison of RM and FM predictions for the Honshu-2011 event. c) snapshot of amplitude and velocity at the discrete time, marked in the upper panel inset. RM and FM C-grid results are in the upper and lower panels.

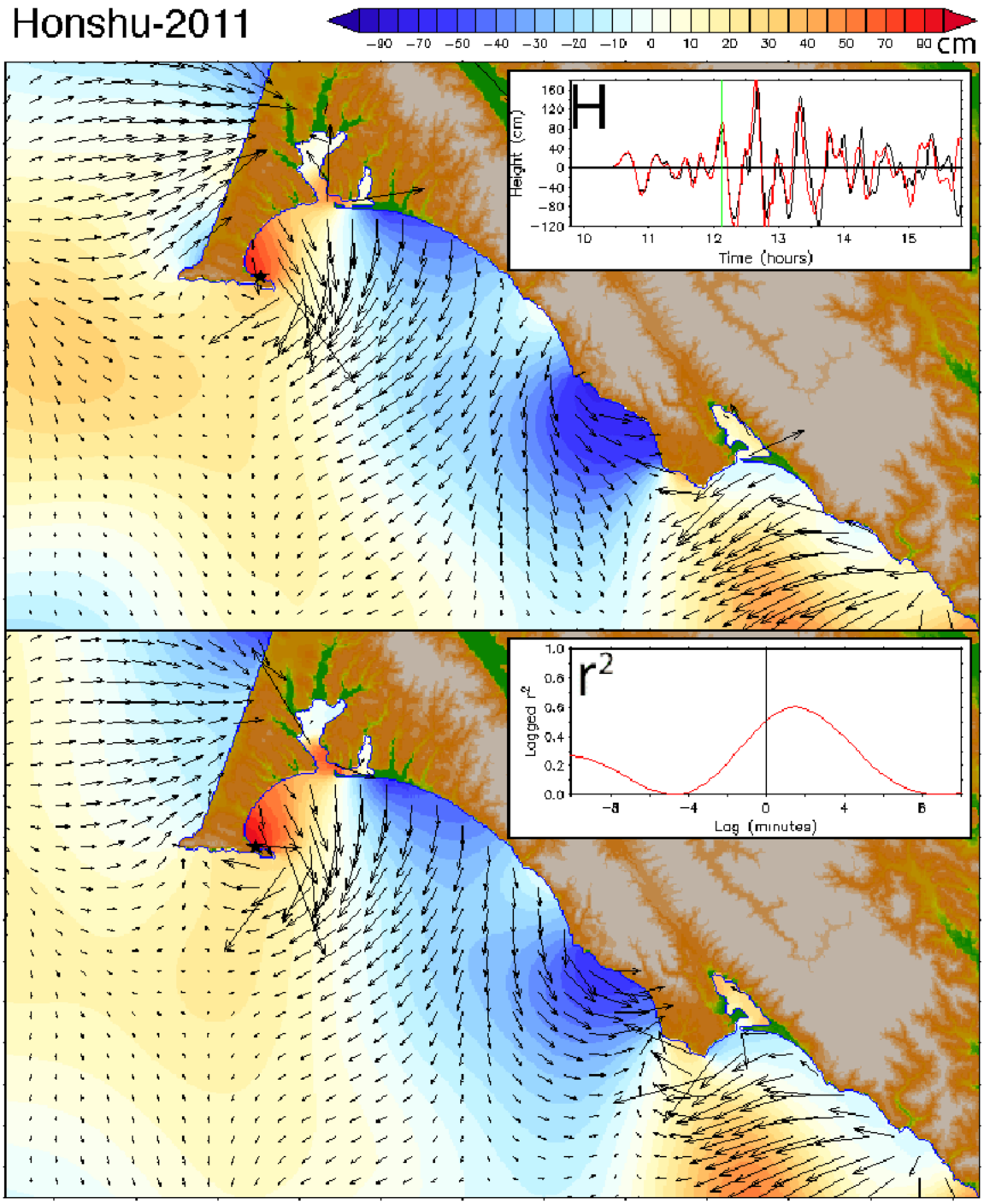

Figure 17 continued. Intercomparison of RM and FM predictions for the Honshu-2011 event. d) as in Figure 17c but at the later time indicated in the upper panel inset.

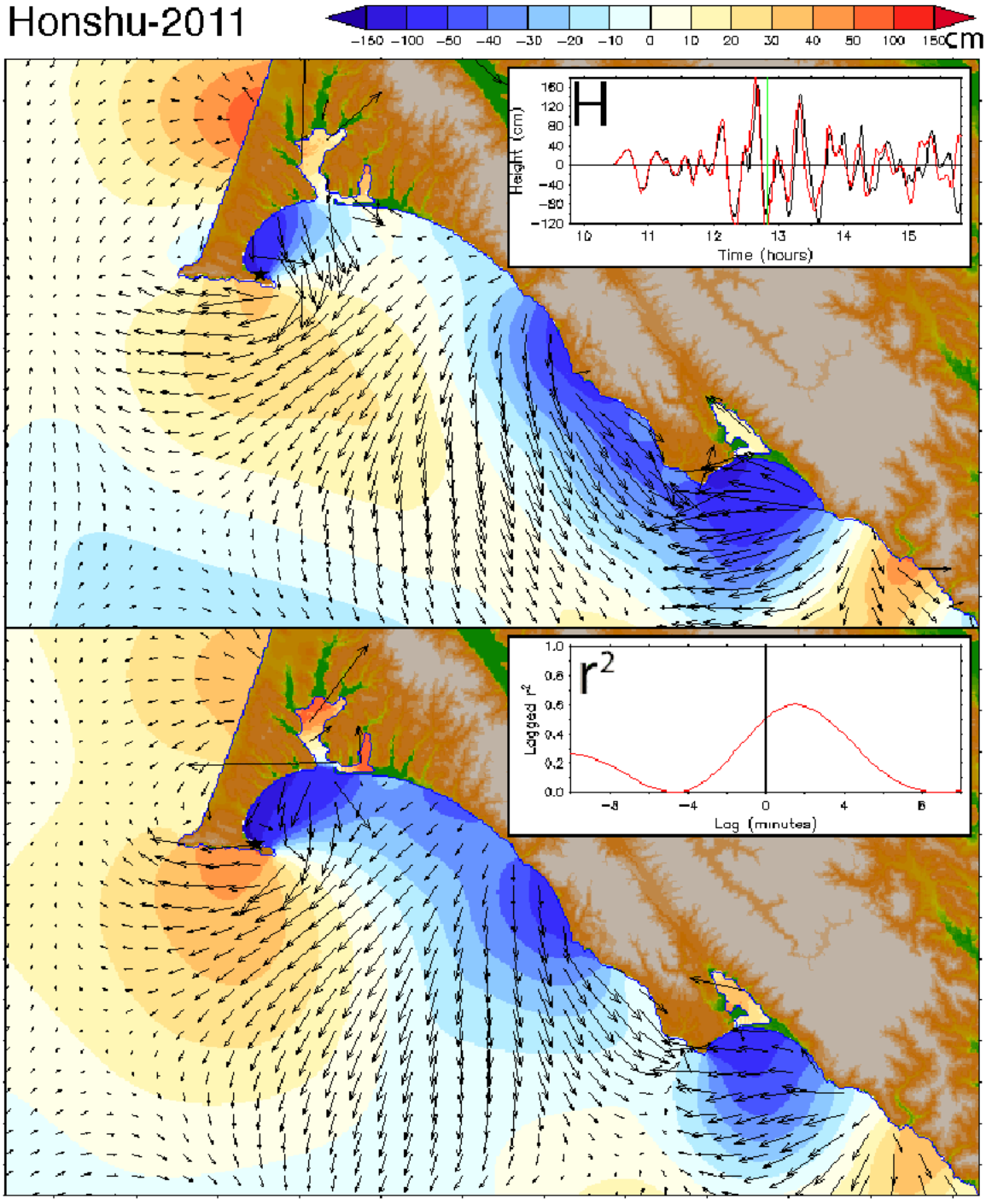

Figure 17 continued. Intercomparison of RM and FM predictions for the Honshu-2011 event. e) as in Figure 17c but at the later time indicated in the upper inset panel.

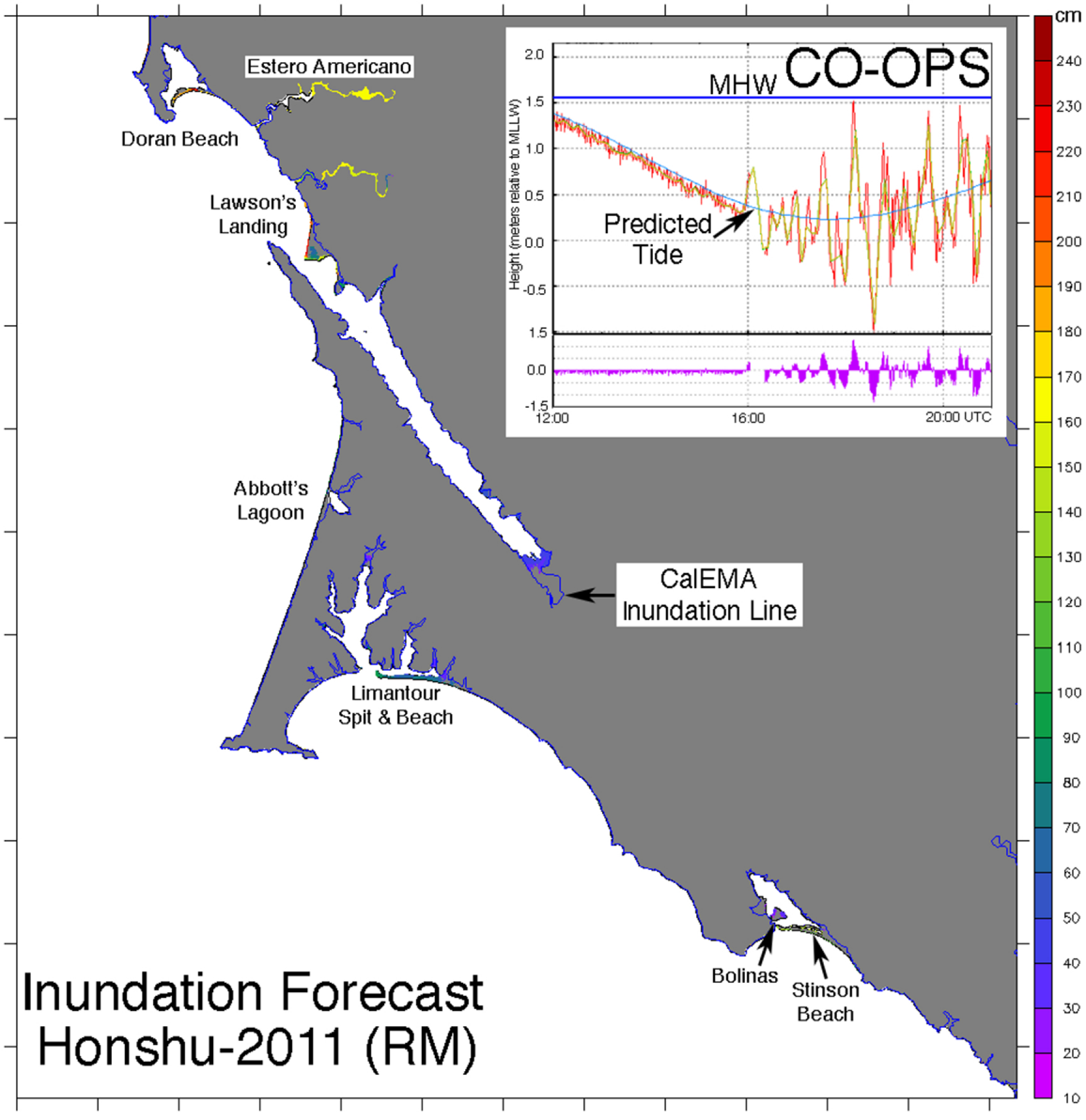

Figure 18. Inundation forecast for the Honshu-2011 event in the RM C-grid, compared with the CalEMA inundation line. The inset in the upper right shows tide gage data from Point Reyes. Actual tides were well below MHW so the inundation forecast was overly conservative.

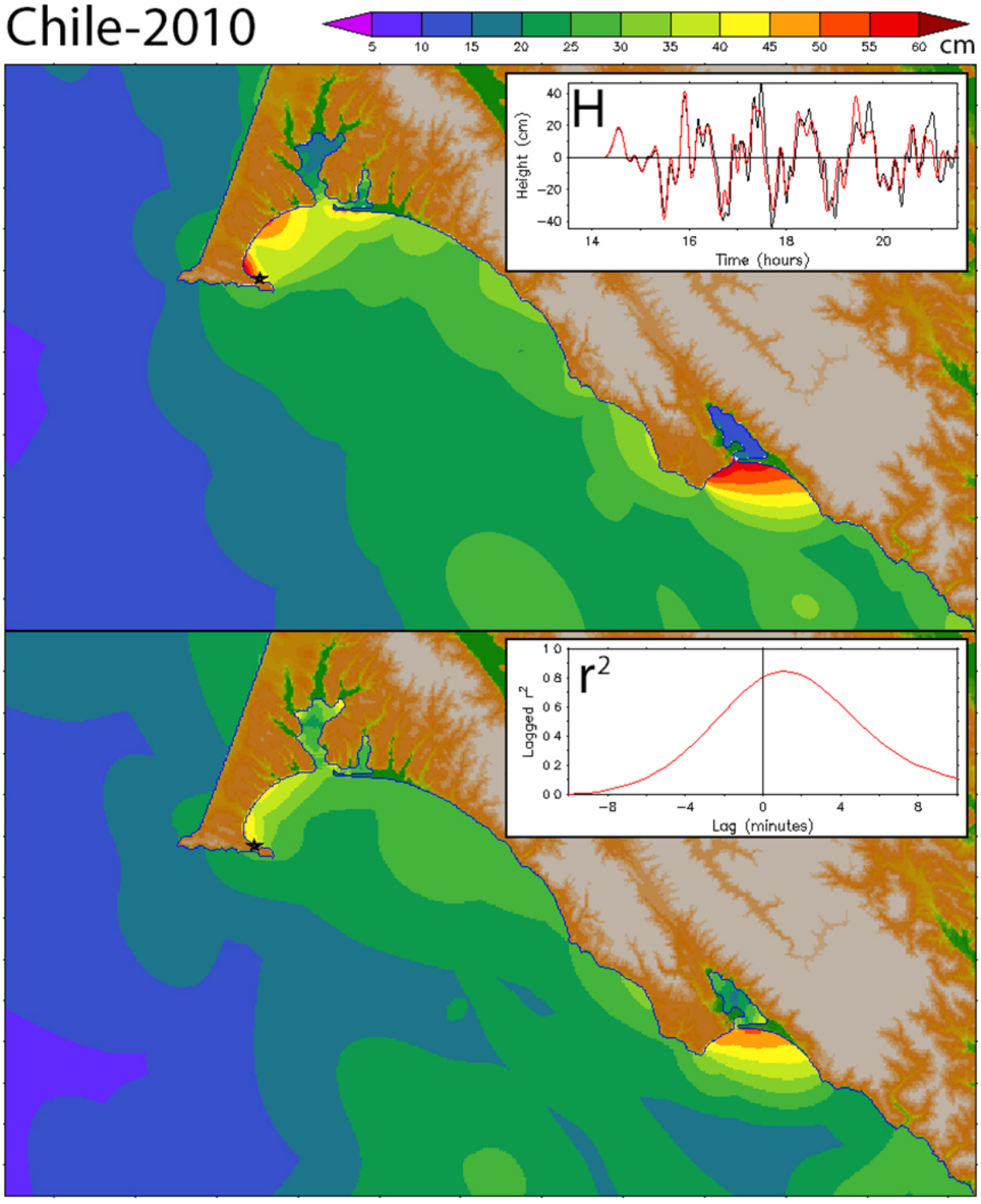

Figure 19. Reference and Forecast Model comparison for the Chile-2010 event.
a) Maximum amplitude for the RM (upper panel) and FM (lower panel).

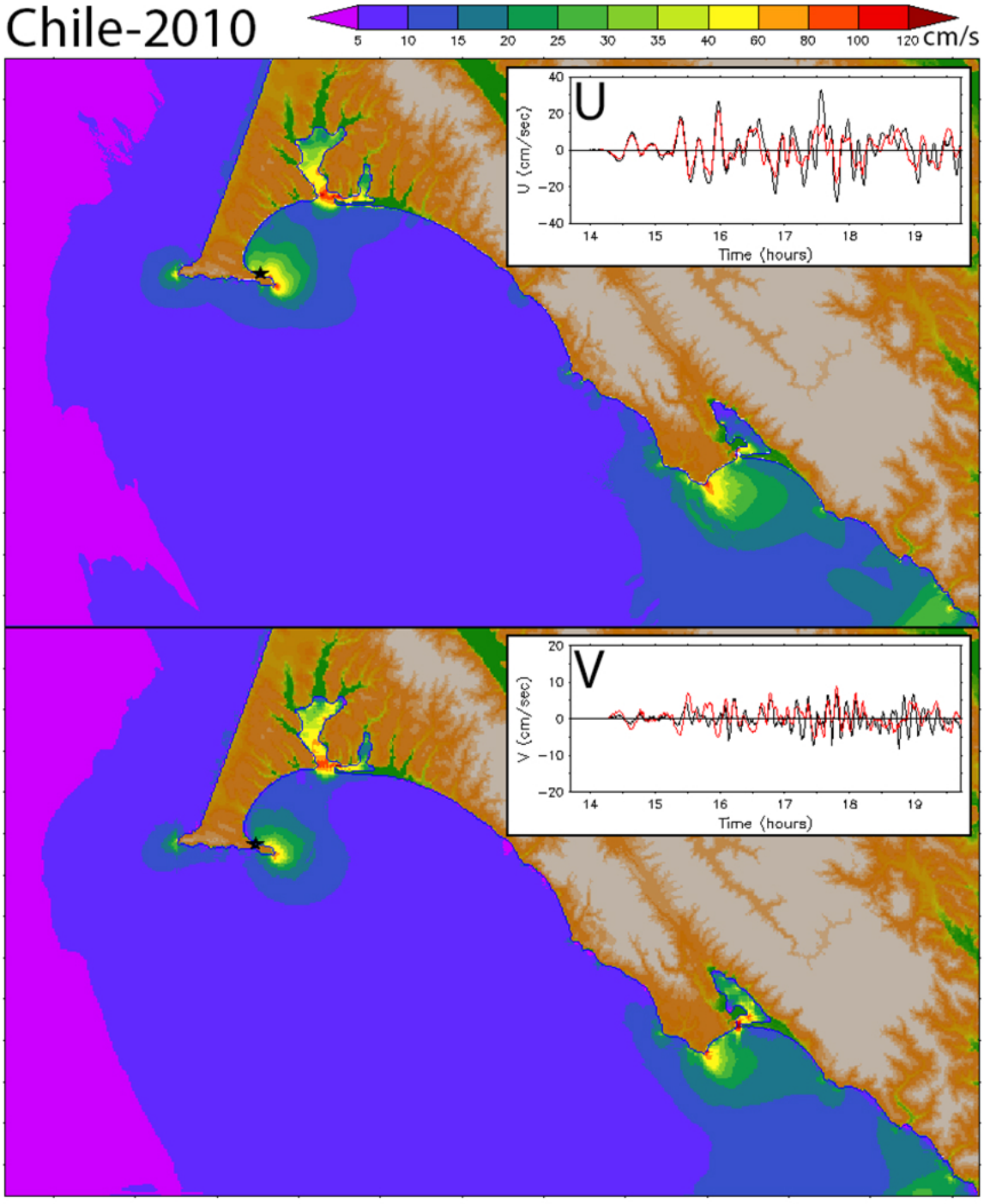

Figure 19 continued. Reference and Forecast Model comparison for the Chile-2010 event.
b) Maximum speed distribution for RM (upper panel) and FM (lower panel).

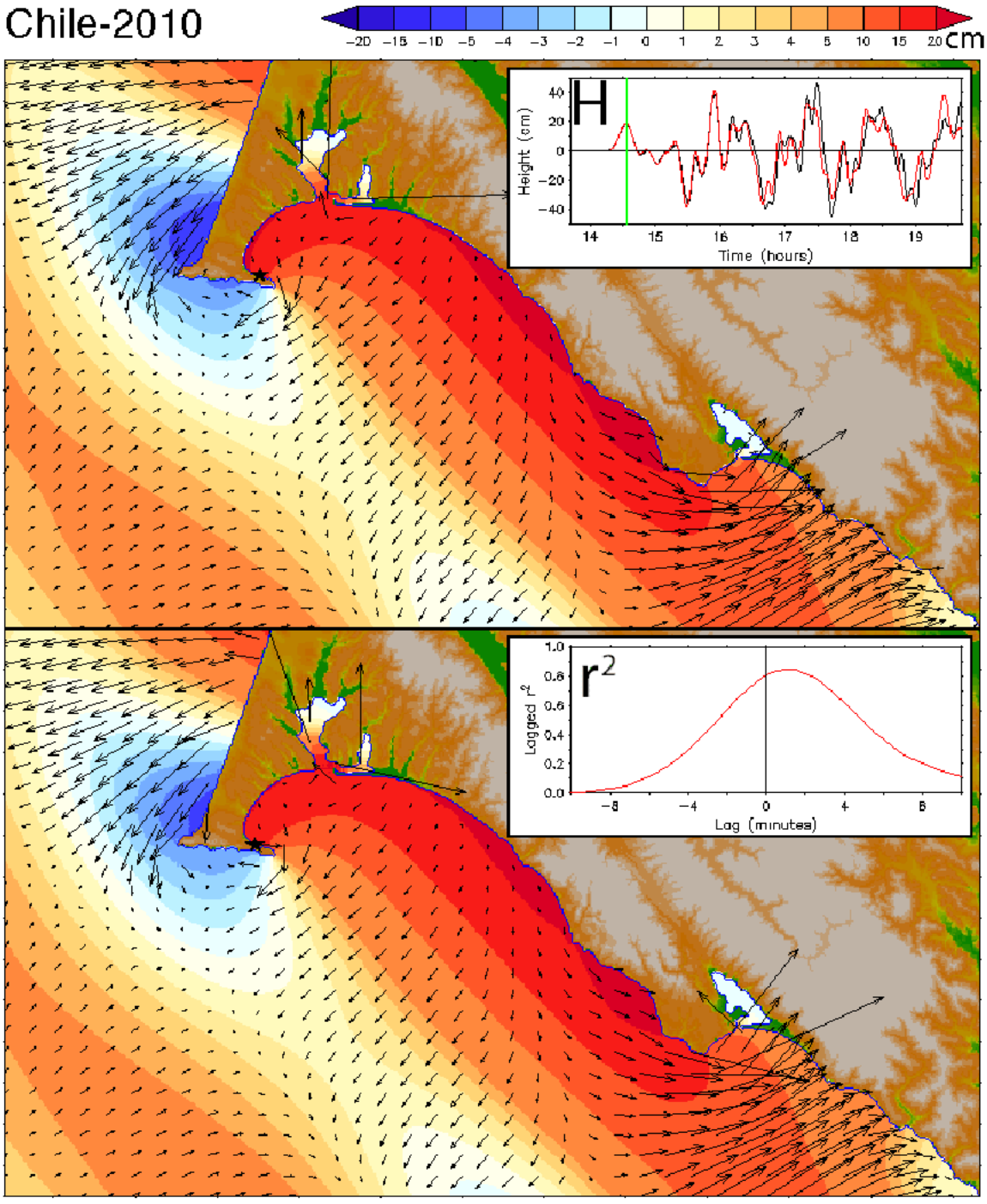

Figure 19 continued. Reference and Forecast Model comparison for the Chile-2010 event.
c) snapshot of amplitude and current at the indicated time.

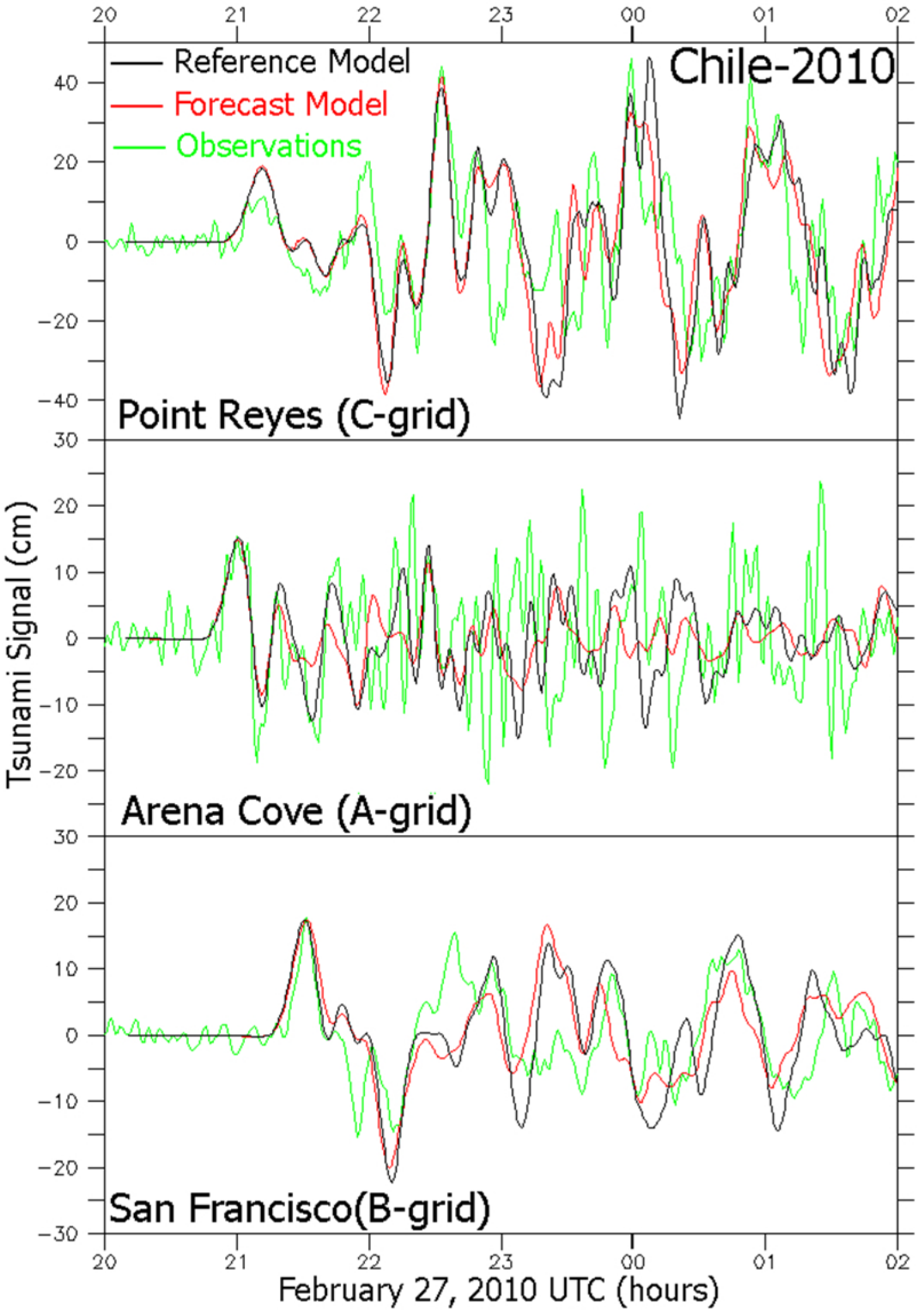

Figure 20. Model and observed time series comparison for the Chile-2010 event.

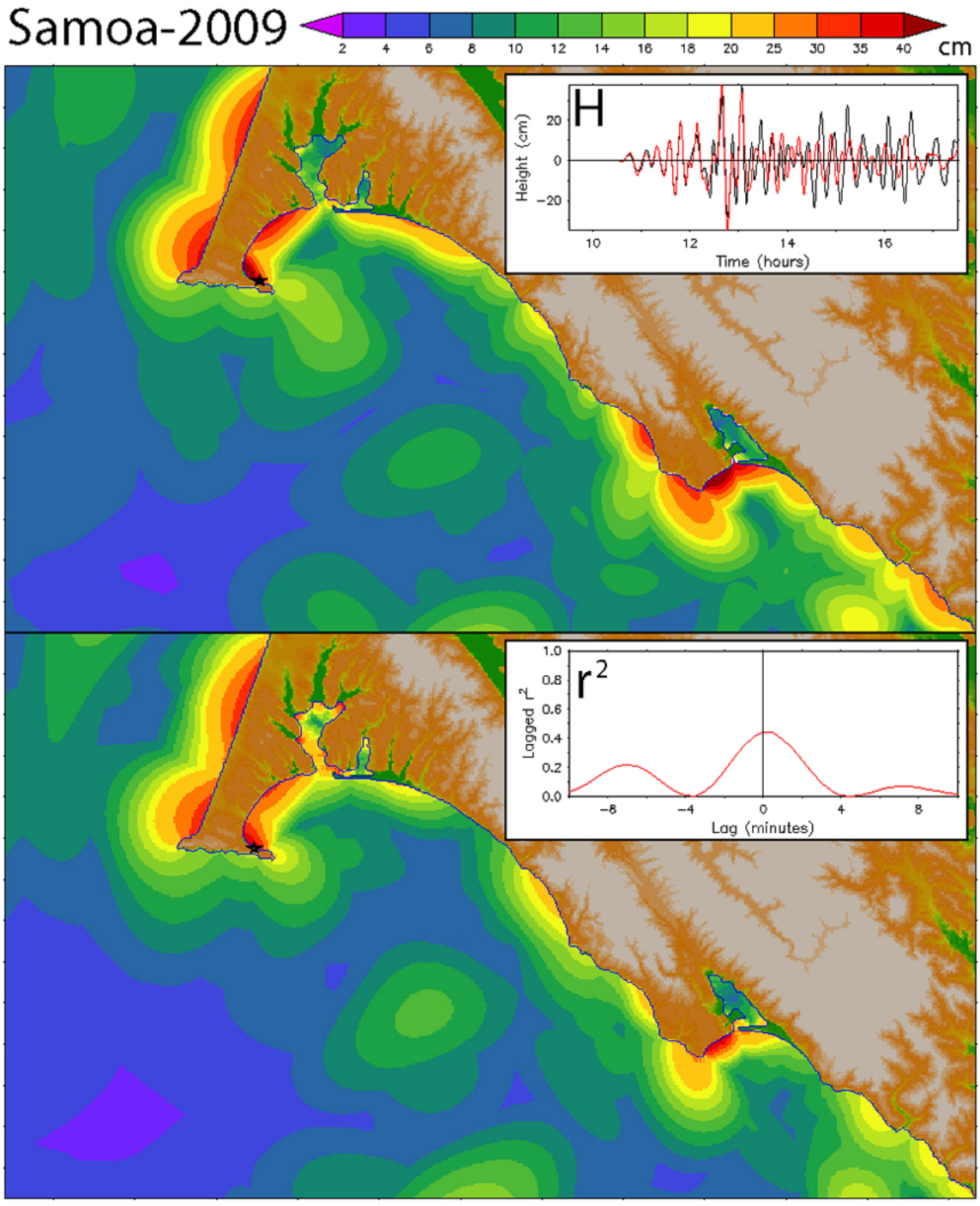

Figure 21. RM and FM comparison, as in Figure 19 but for the Samoa-2009 event. a) Maximum amplitude for the RM (upper panel) and FM (lower panel).

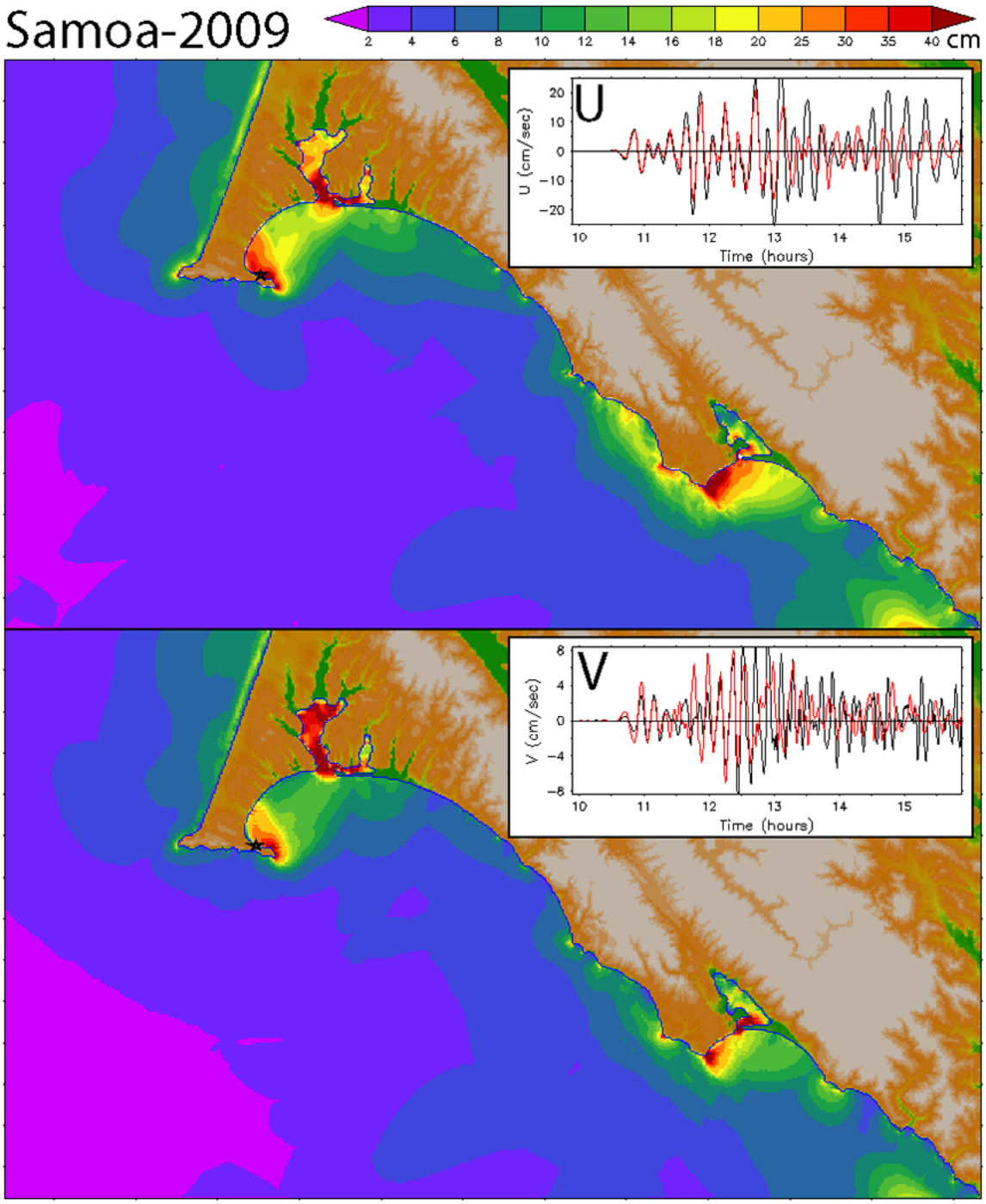

Figure 21continued. RM and FM comparison, as in Figure 19 but for the Samoa-2009 event. b) Maximum speed for the RM (upper panel) and FM (lower panel).

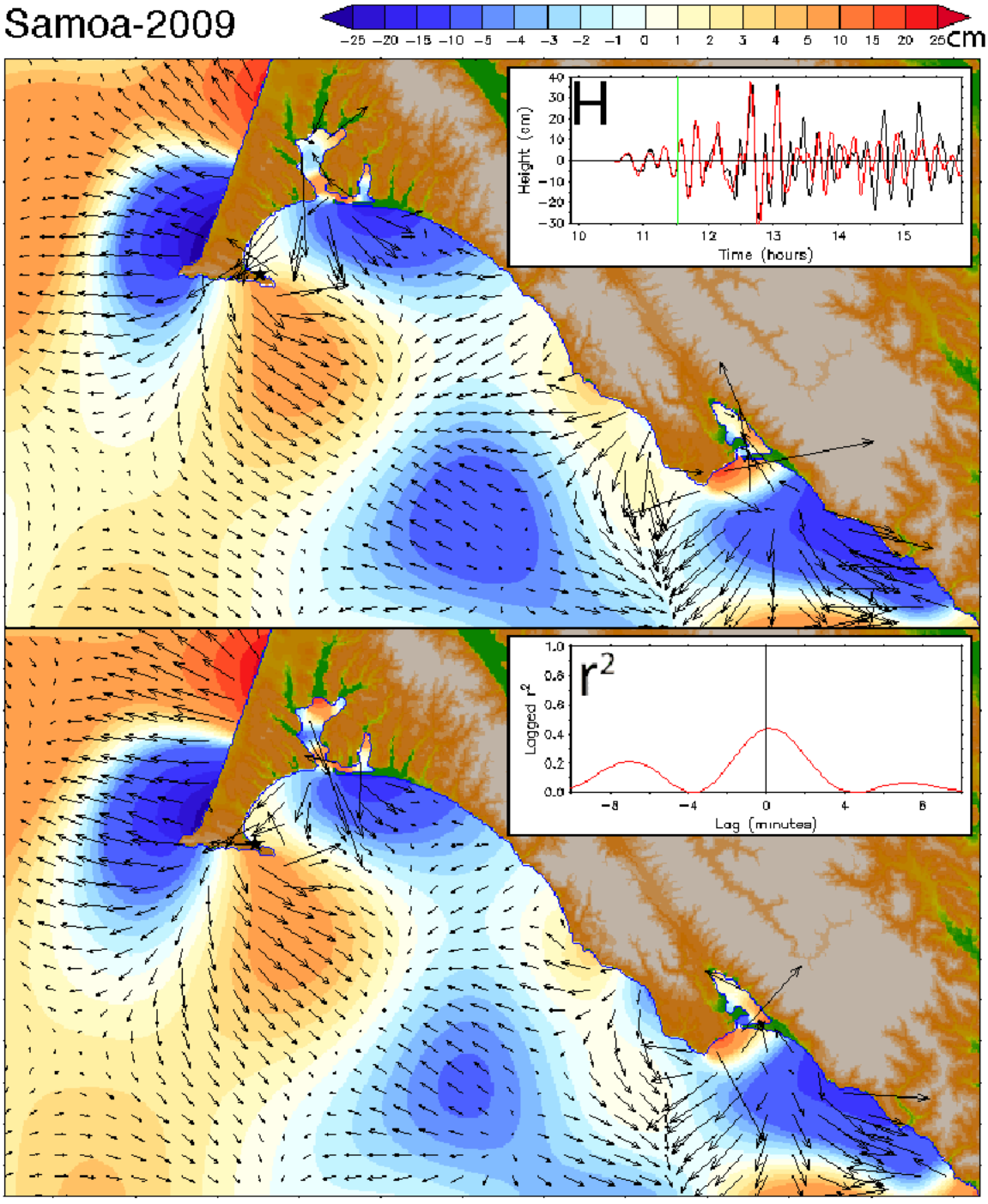

Figure 21 continued. RM and FM comparison, as in Figure 19 but for the Samoa-2009 event. c) snapshot of amplitude and current at the indicated time.

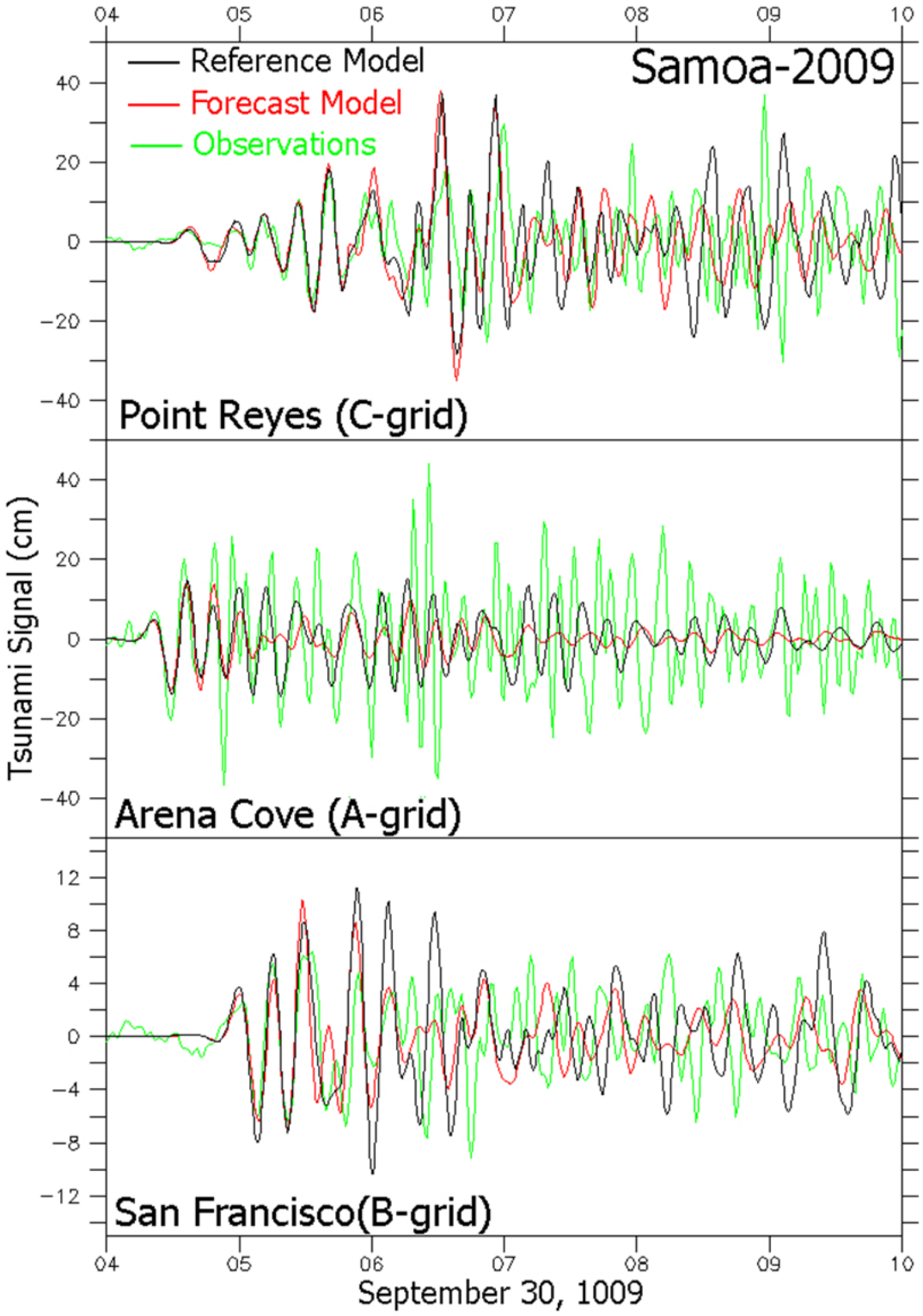

Figure 22. Model and observed time series comparison for the Samoa-2009 event.

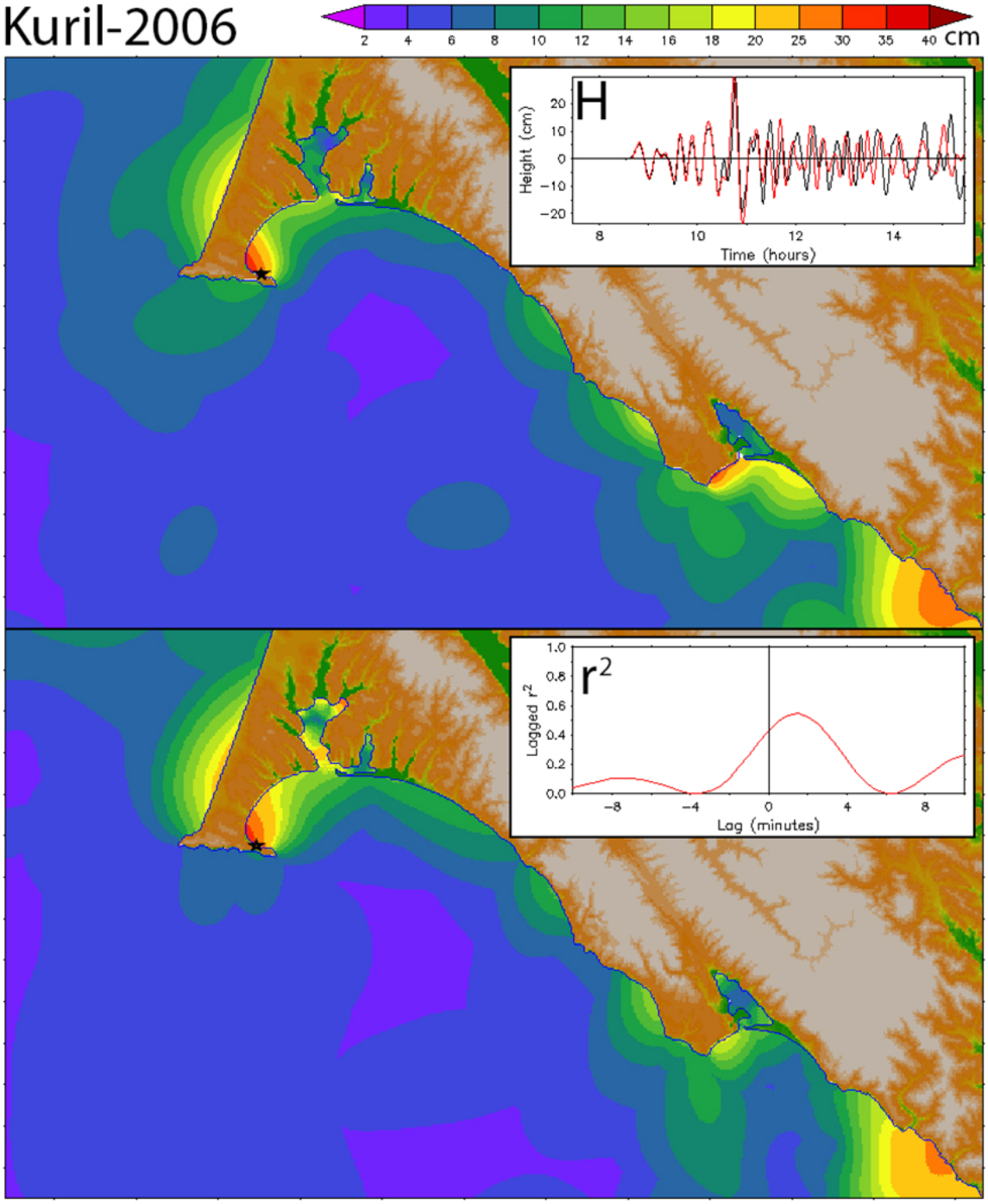

Figure 23. RM and FM comparison, as in Figure 19 but for the Kuril-2006 event.
a) Maximum amplitude for the RM (upper panel) and FM (lower panel).

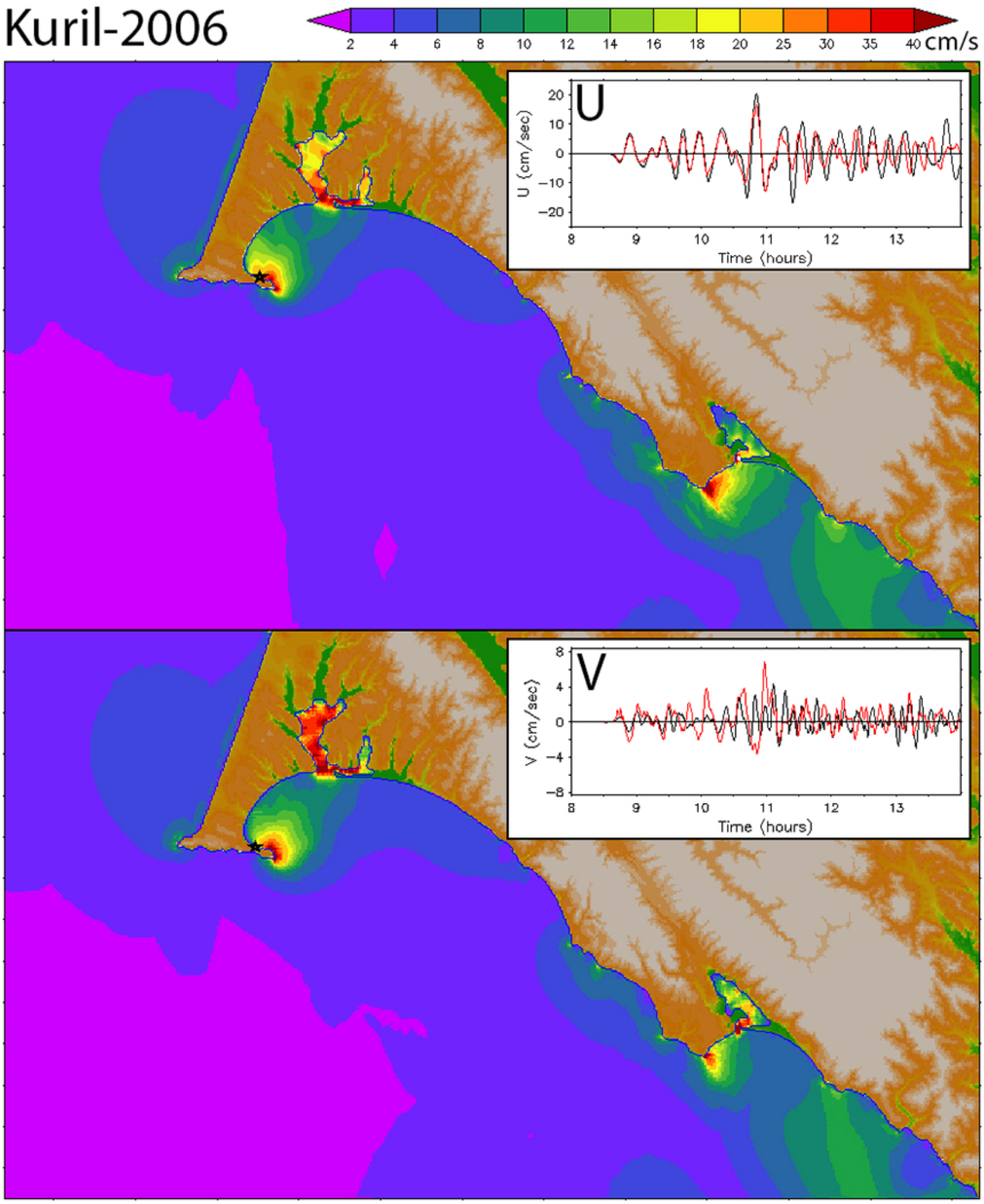

Figure 23 continued. RM and FM comparison, as in Figure 19 but for the Kuril-2006 event.
b) Maximum speed for the RM (upper panel) and FM (lower panel).

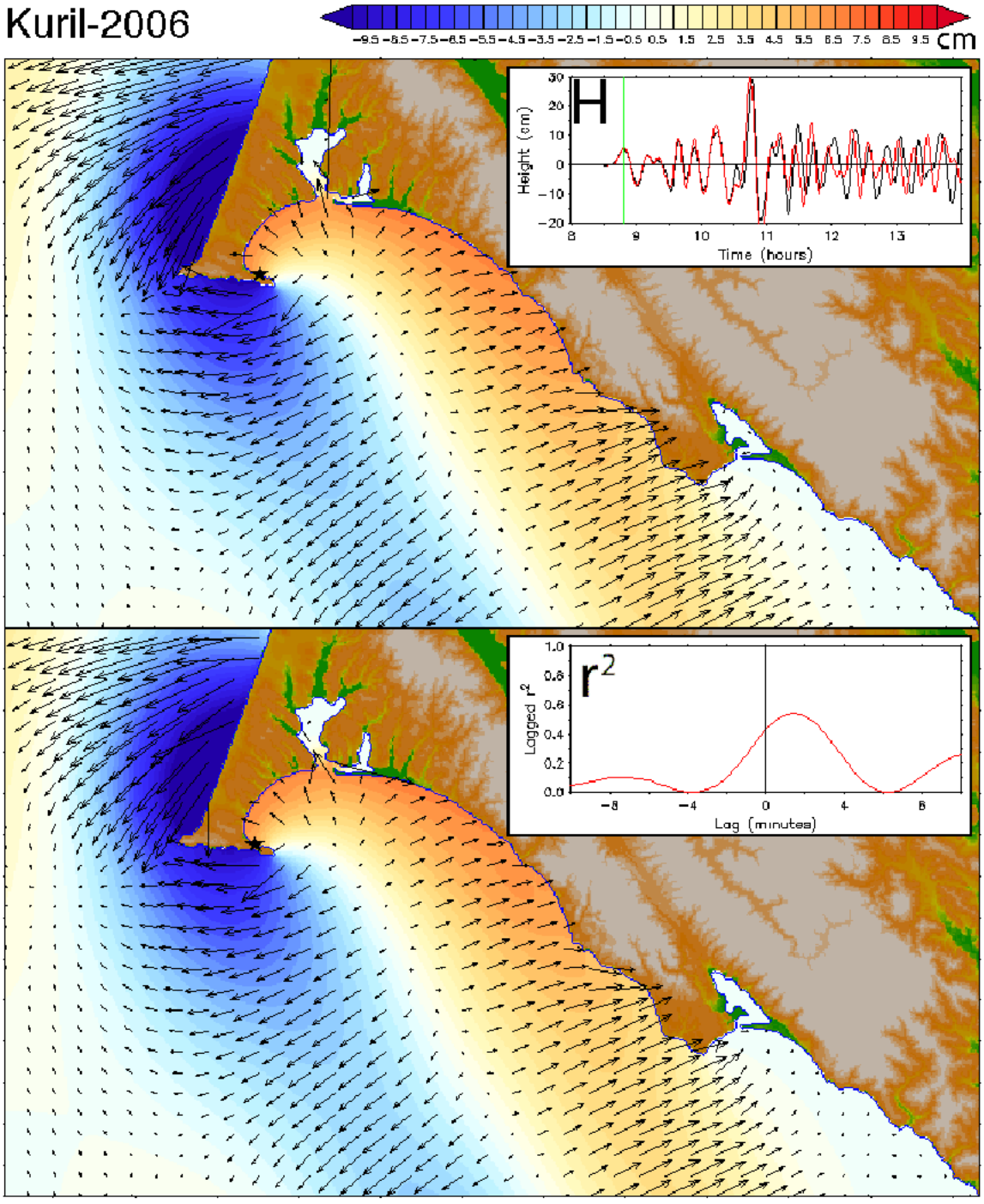

Figure 23 continued. RM and FM comparison, as in Figure 19 but for the Kuril-2006 event.
c) snapshot of amplitude and current at the indicated time.

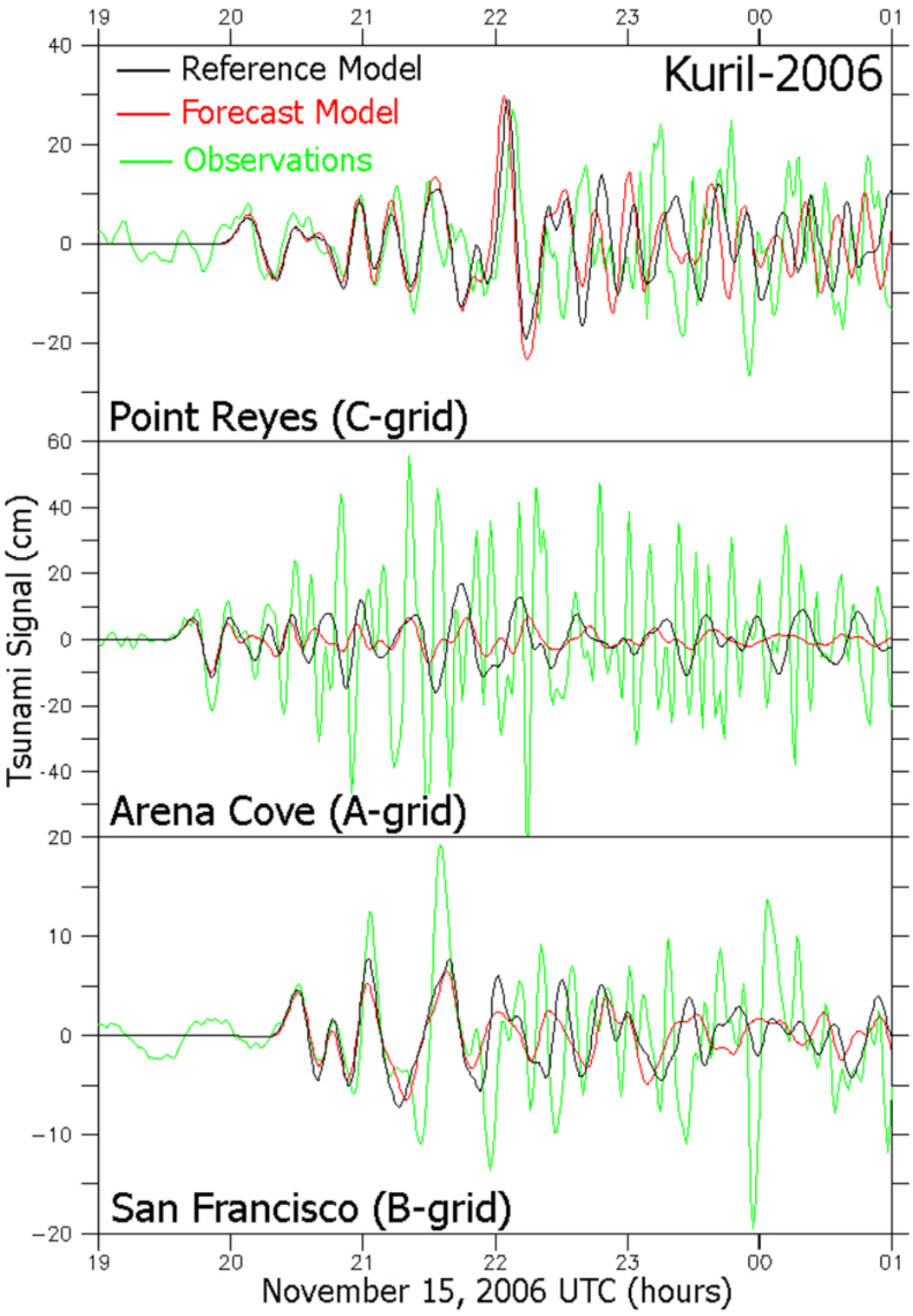

Figure 24. Model and observed time series comparison for the Kuril-2006 event.

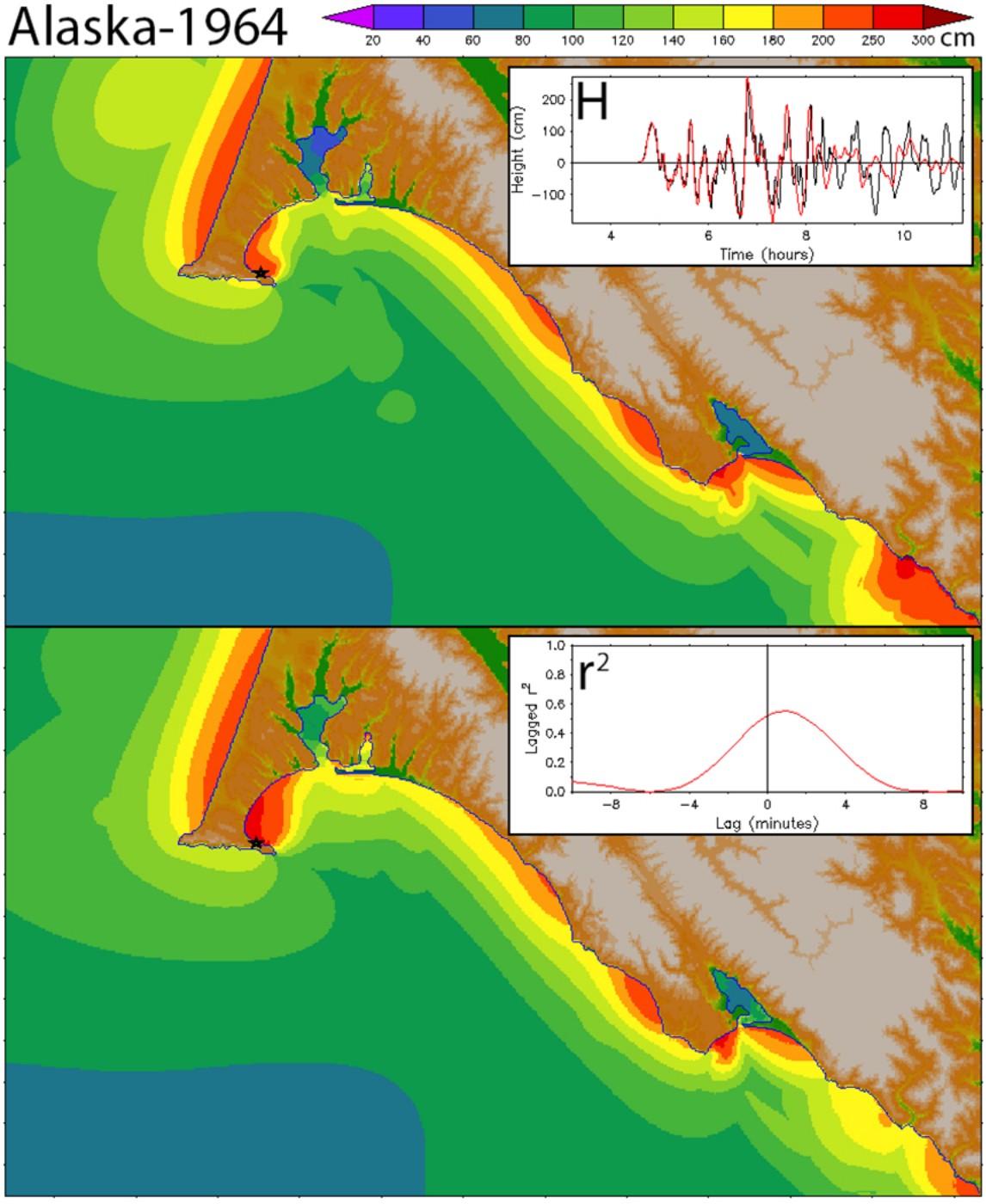

Figure 25. RM and FM comparison, as in Figure 19 but for the Alaska-1964 event.
a) Maximum amplitude for the RM (upper panel) and FM (lower panel).

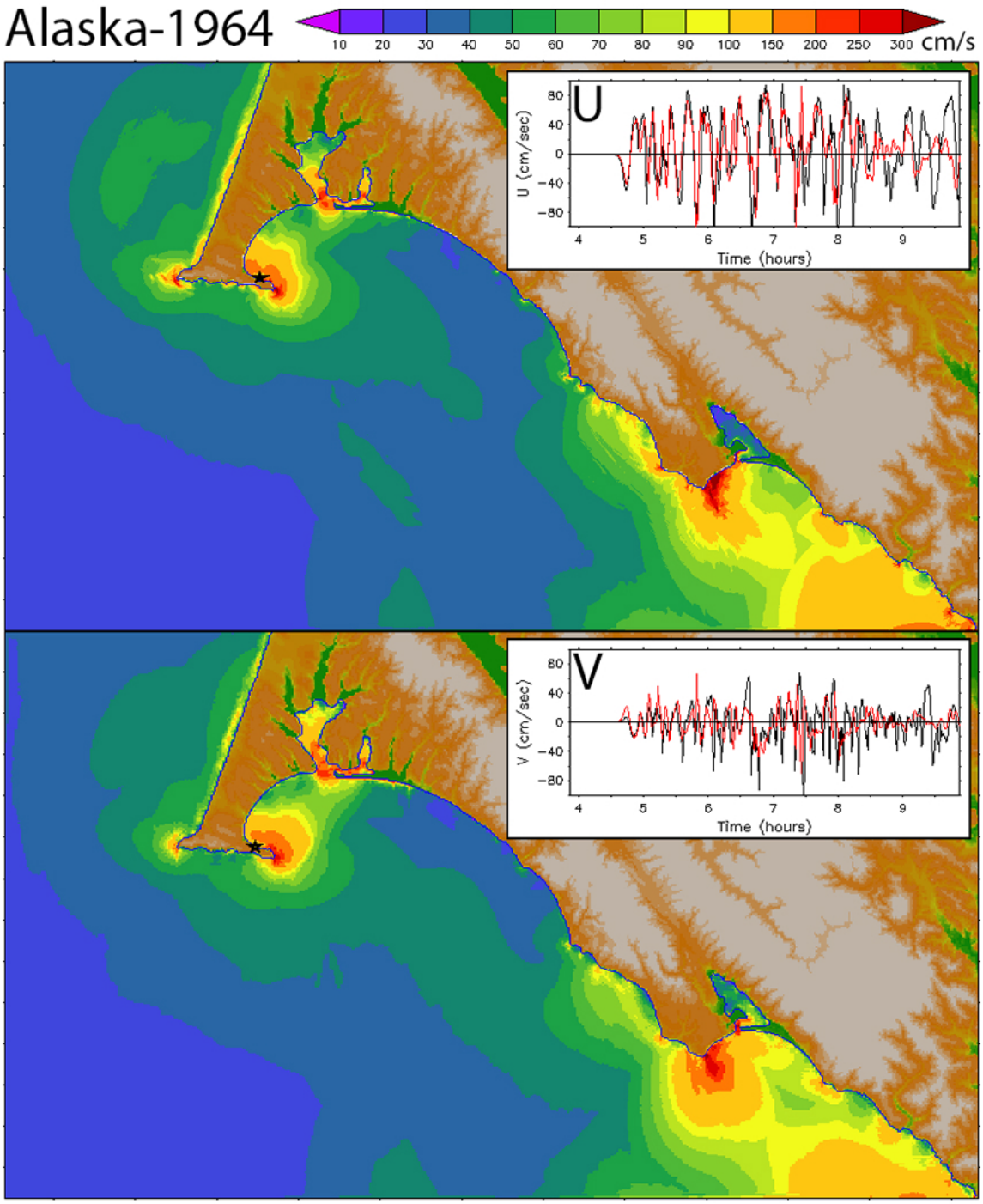

Figure 25 continued. RM and FM comparison, as in Figure 19 but for the Alaska-1964 event. b) Maximum speed for the RM (upper panel) and FM (lower panel).

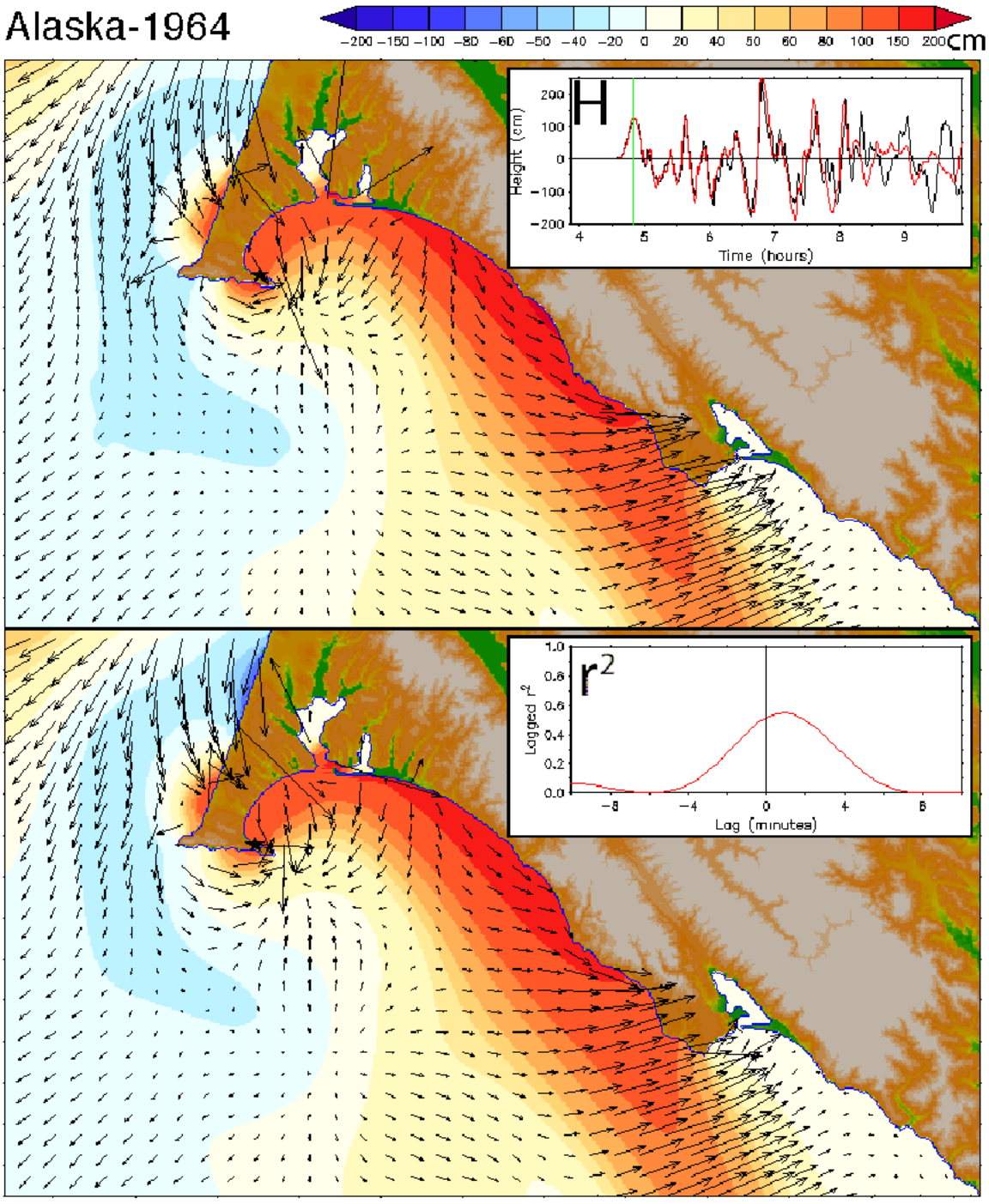

Figure 25 continued. RM and FM comparison, as in Figure 19 but for the Alaska-1964 event. c) snapshot of amplitude and current at the indicated time.

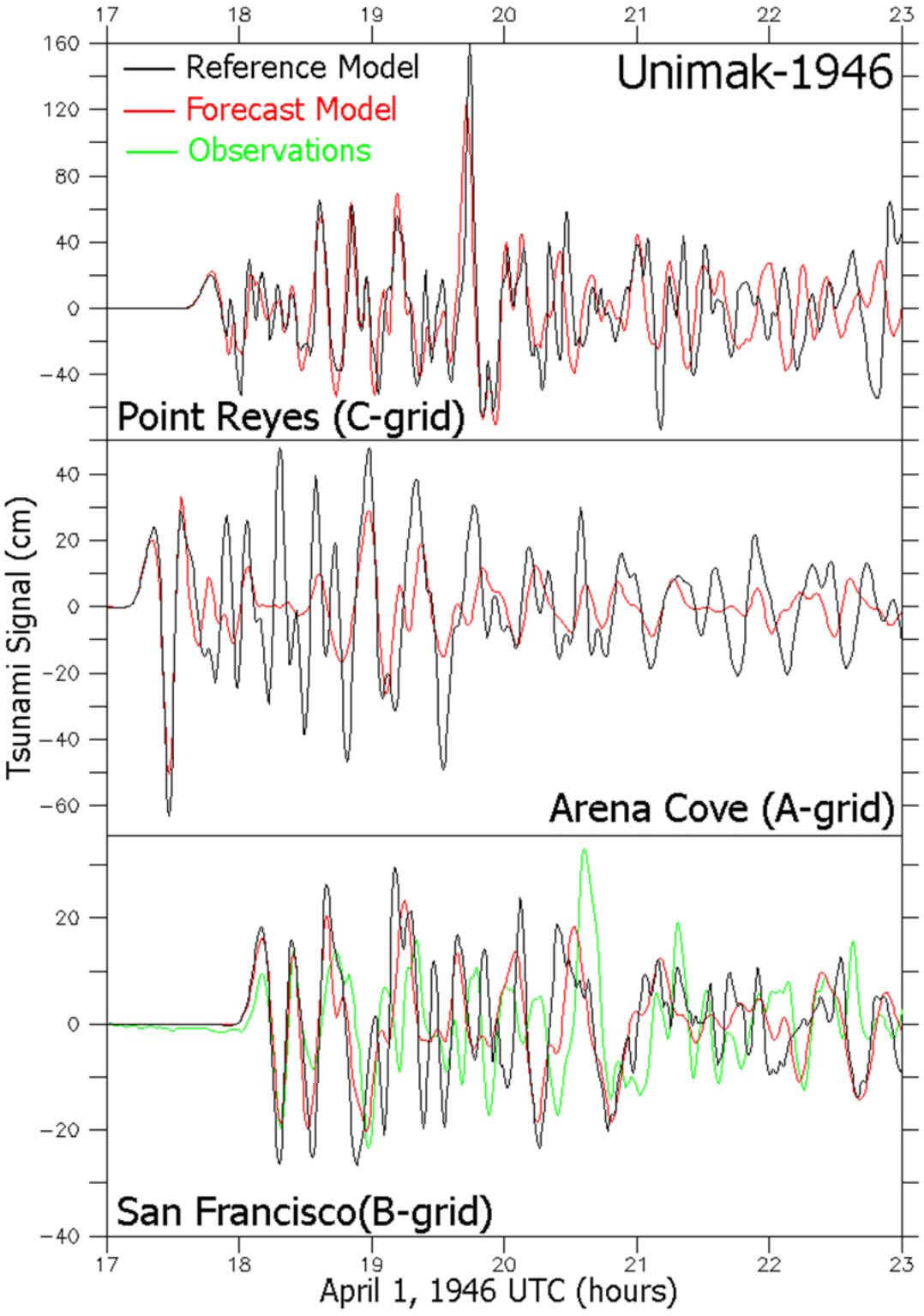

Figure 26. Model and observed time series comparison for the Alaska-1964 event.

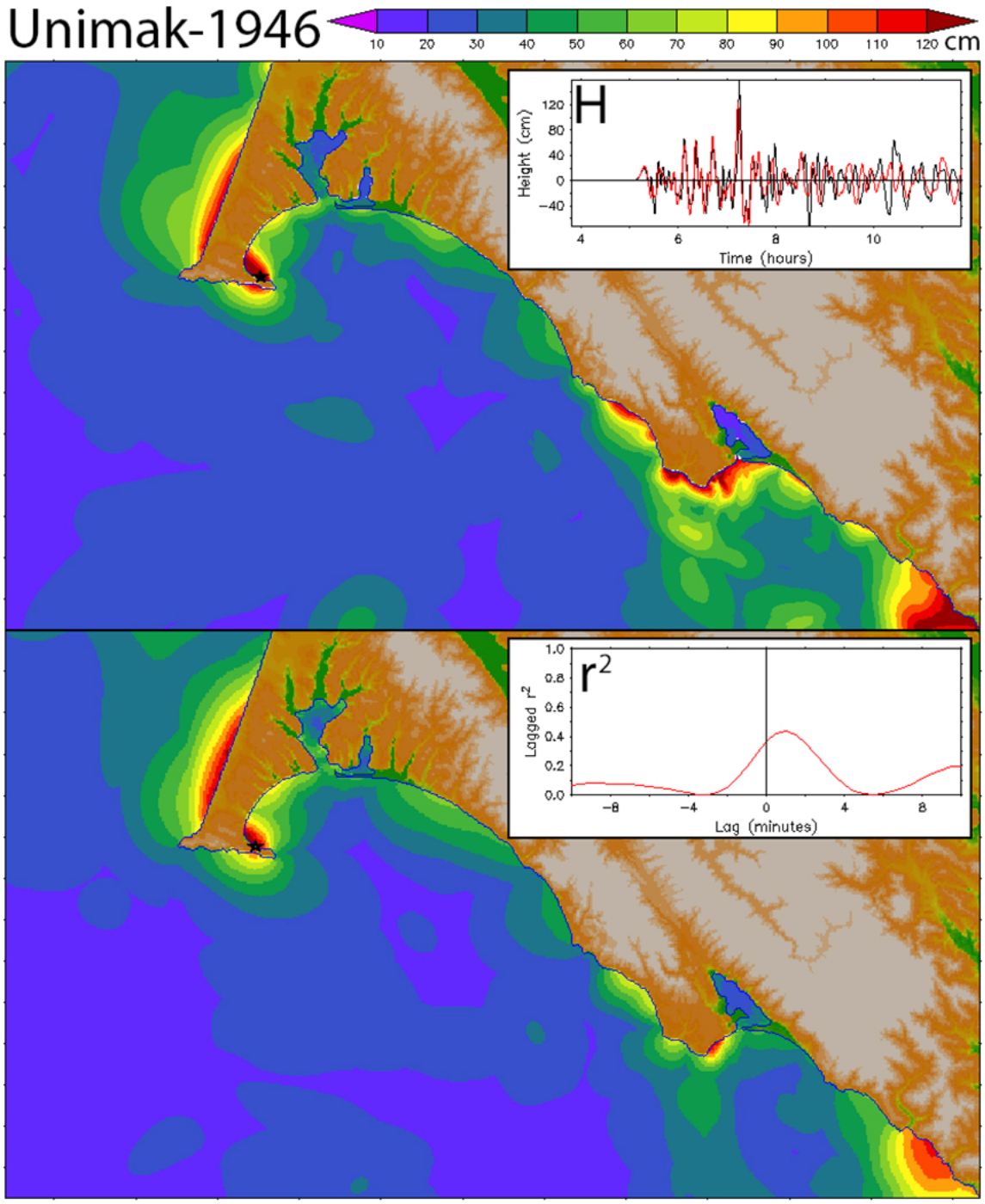

Figure 27. RM and FM comparison, as in Figure 19 but for the Unimak-1946 event.
a) Maximum amplitude for the RM (upper panel) and FM (lower panel).

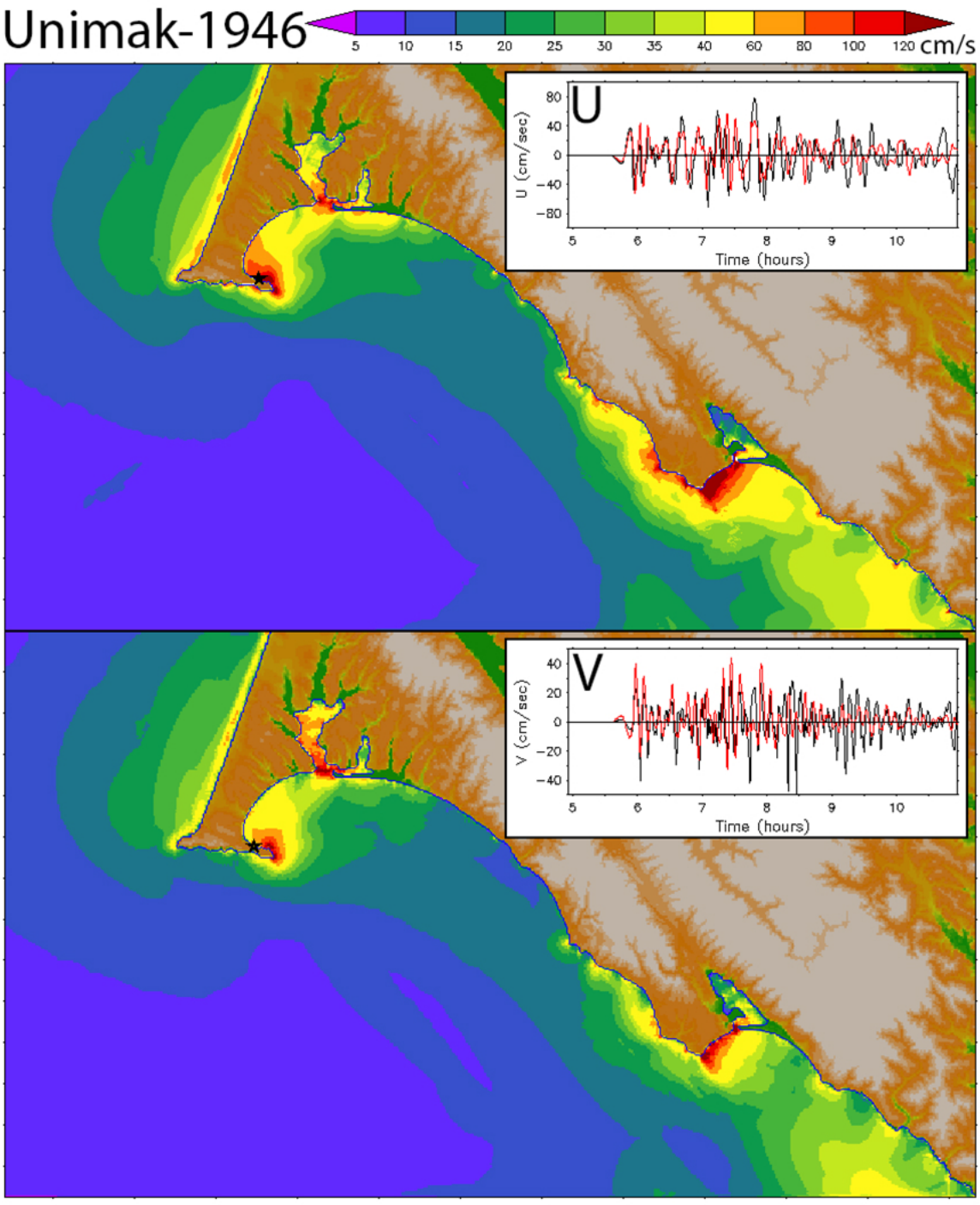

Figure 27continued. RM and FM comparison, as in Figure 19 but for the Unimak-1946 event. b) Maximum speed for the RM (upper panel) and FM (lower panel).

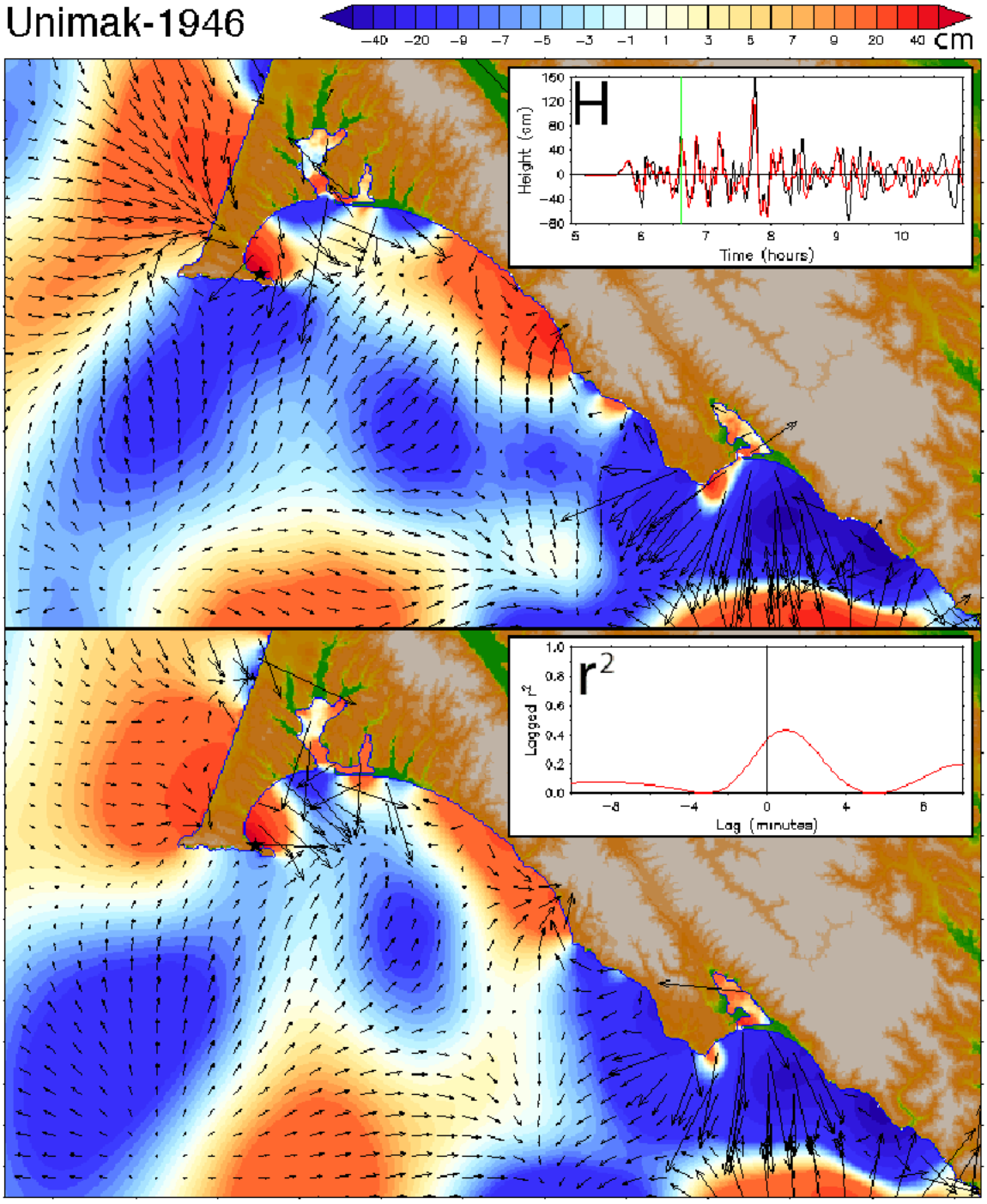

Figure 27 continued. RM and FM comparison, as in Figure 19 but for the Unimak-1946 event. c) snapshot of amplitude and current at the indicated time.

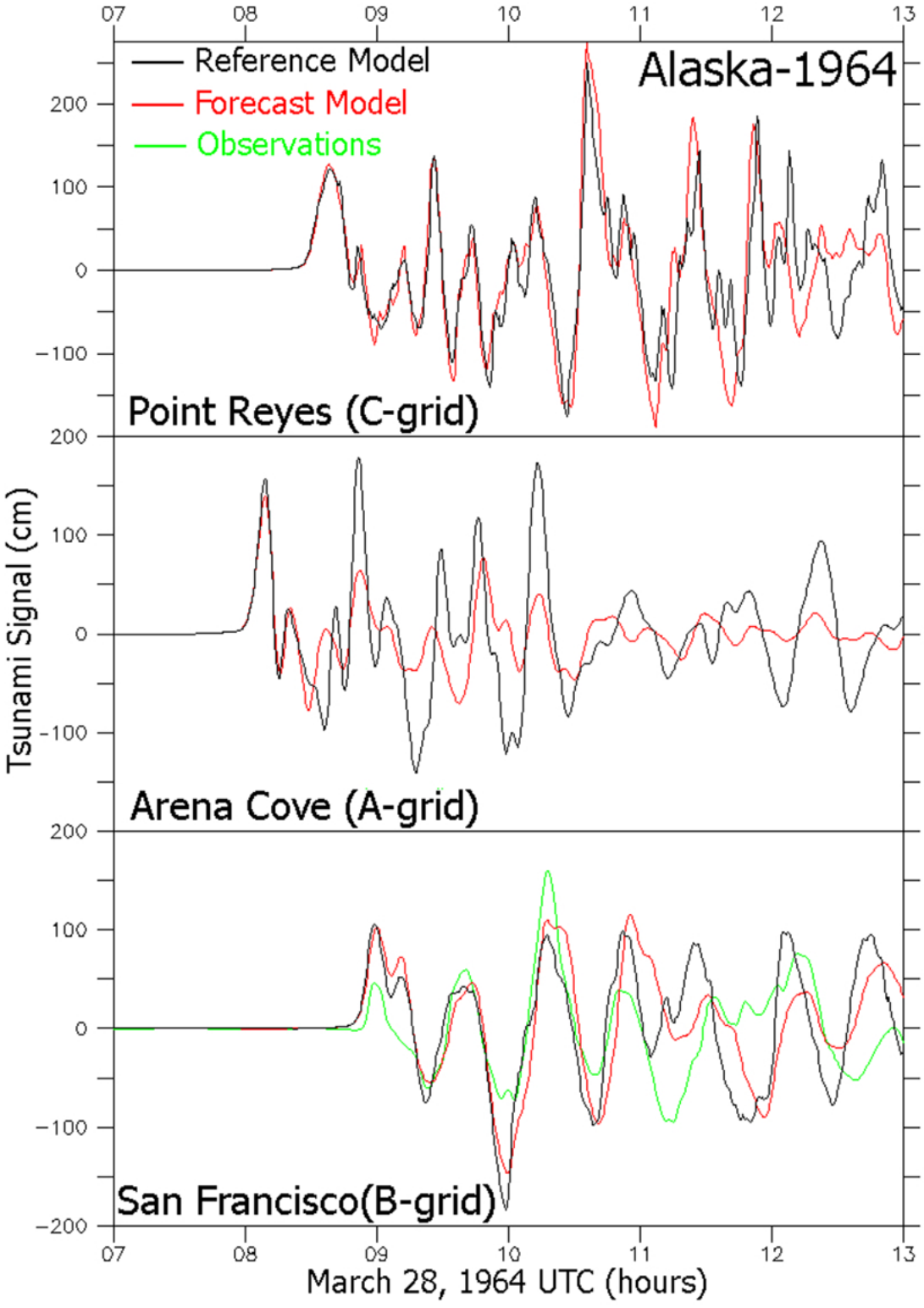

Figure 28. Model and observed time series comparison for the Unimak-1946 event.

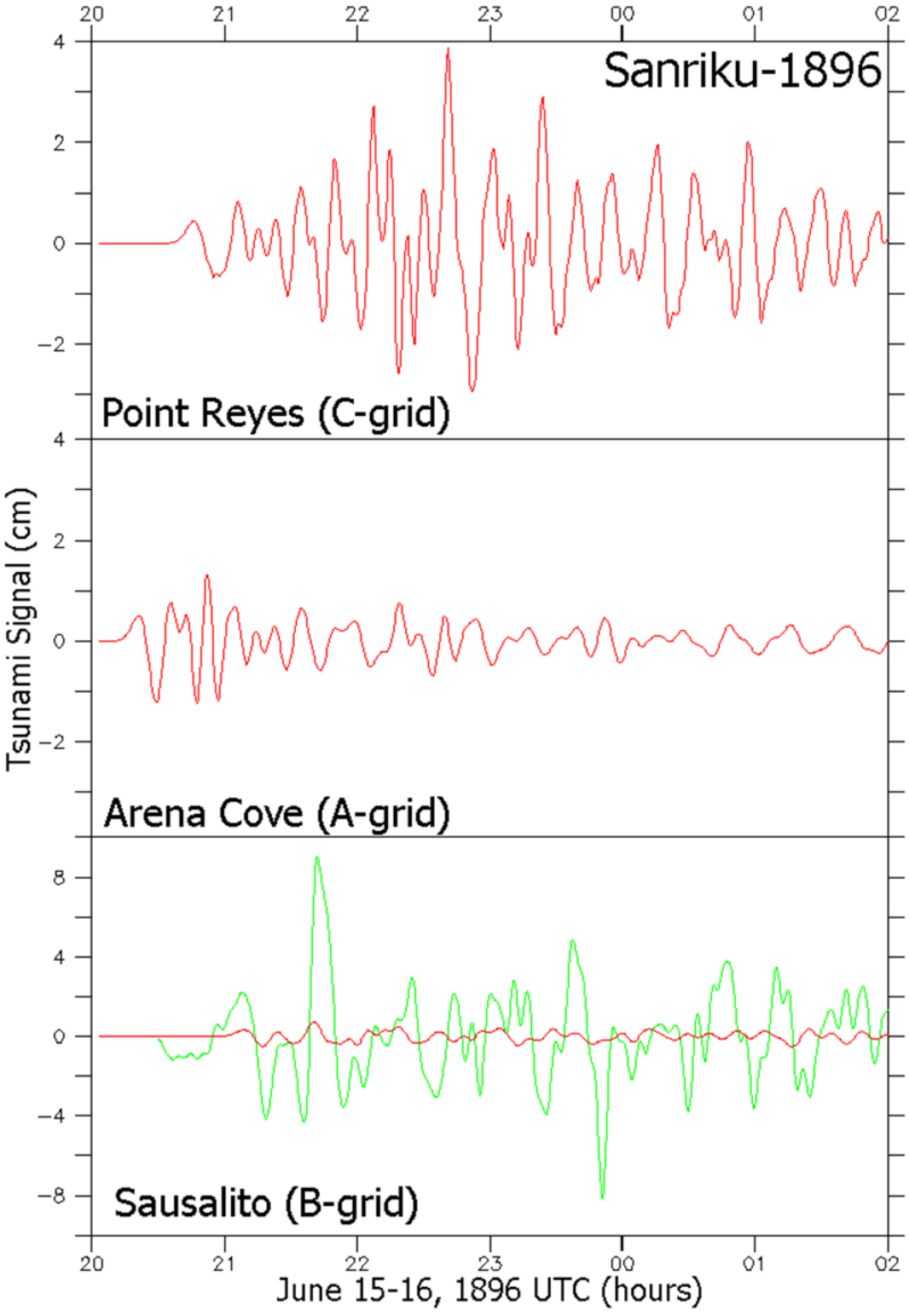

Figure 29. The Sanriku event of June 15, 1896.

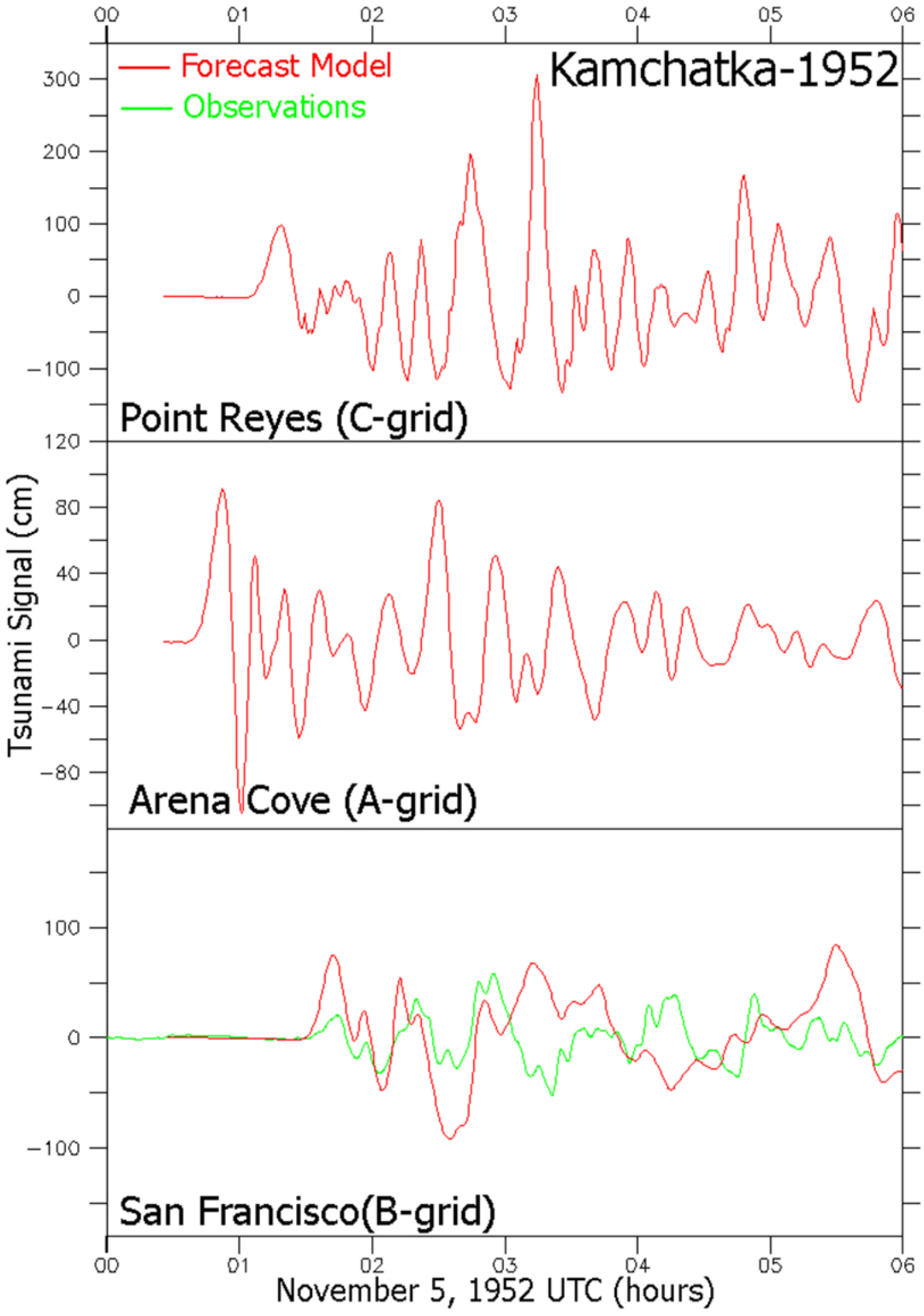

Figure 30. The Kamchatka event of November 4, 1952.

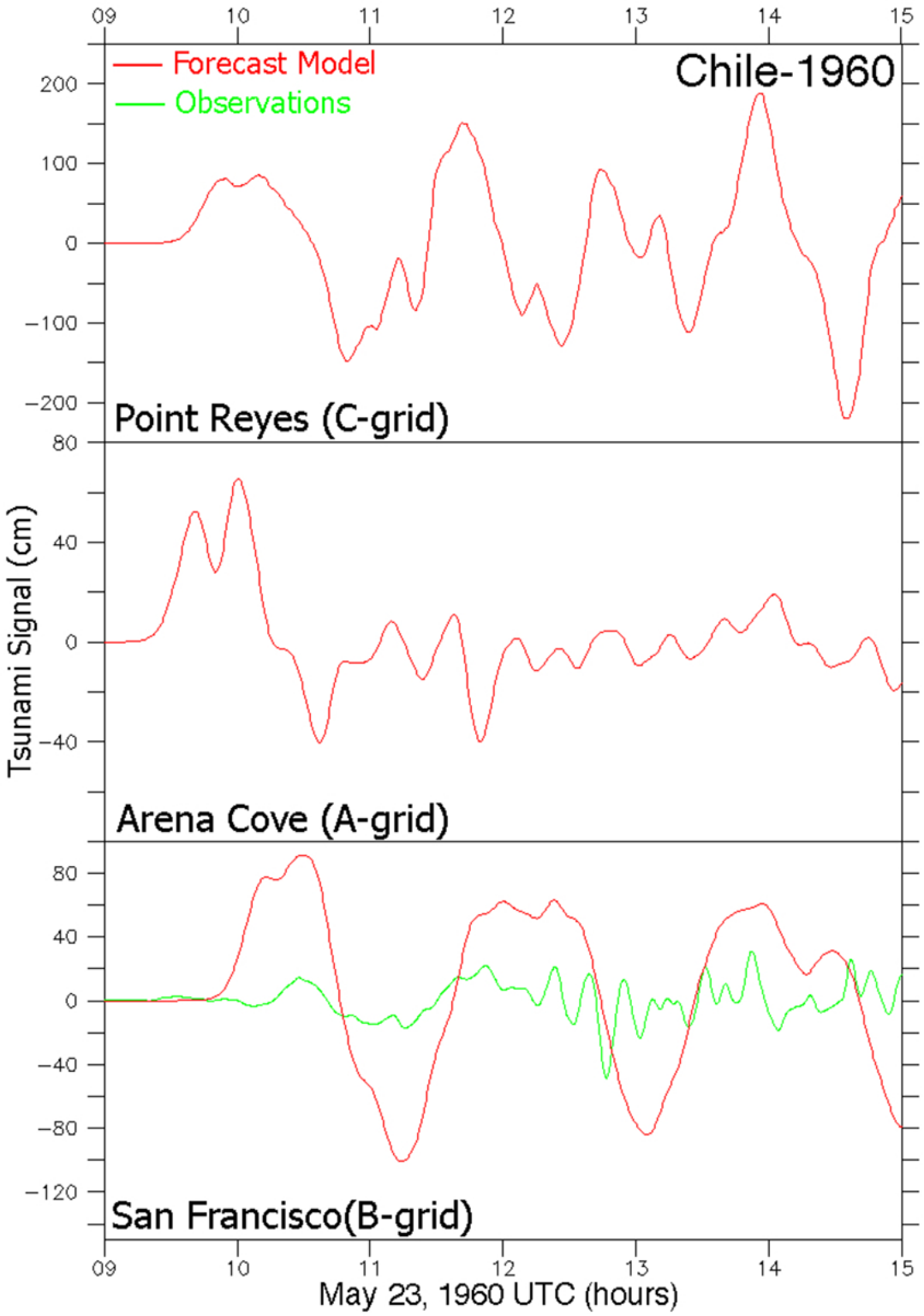

Figure 31. The Chile event of May 22, 1960.

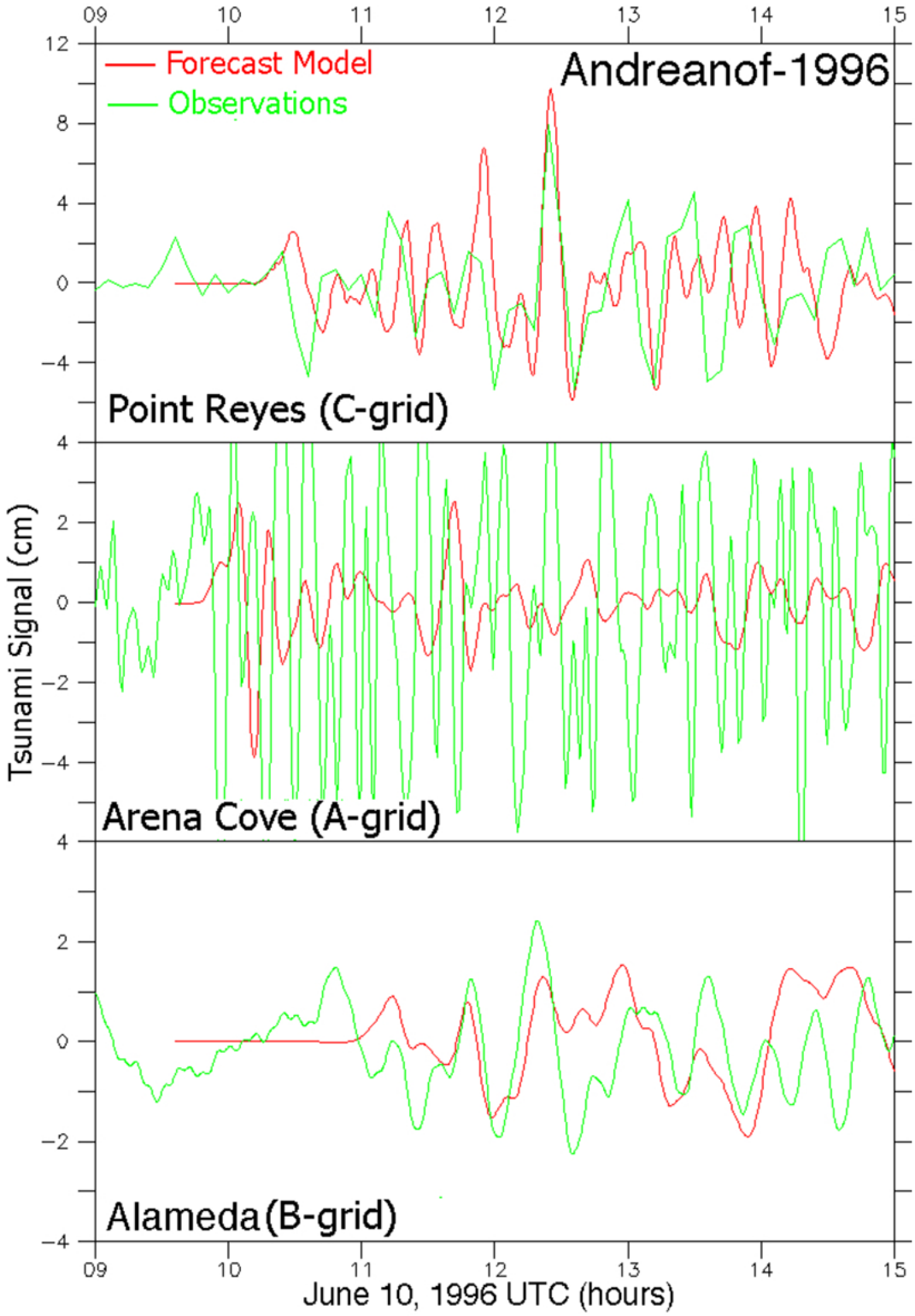

Figure 32. The Andreanof event of June 10, 1996.

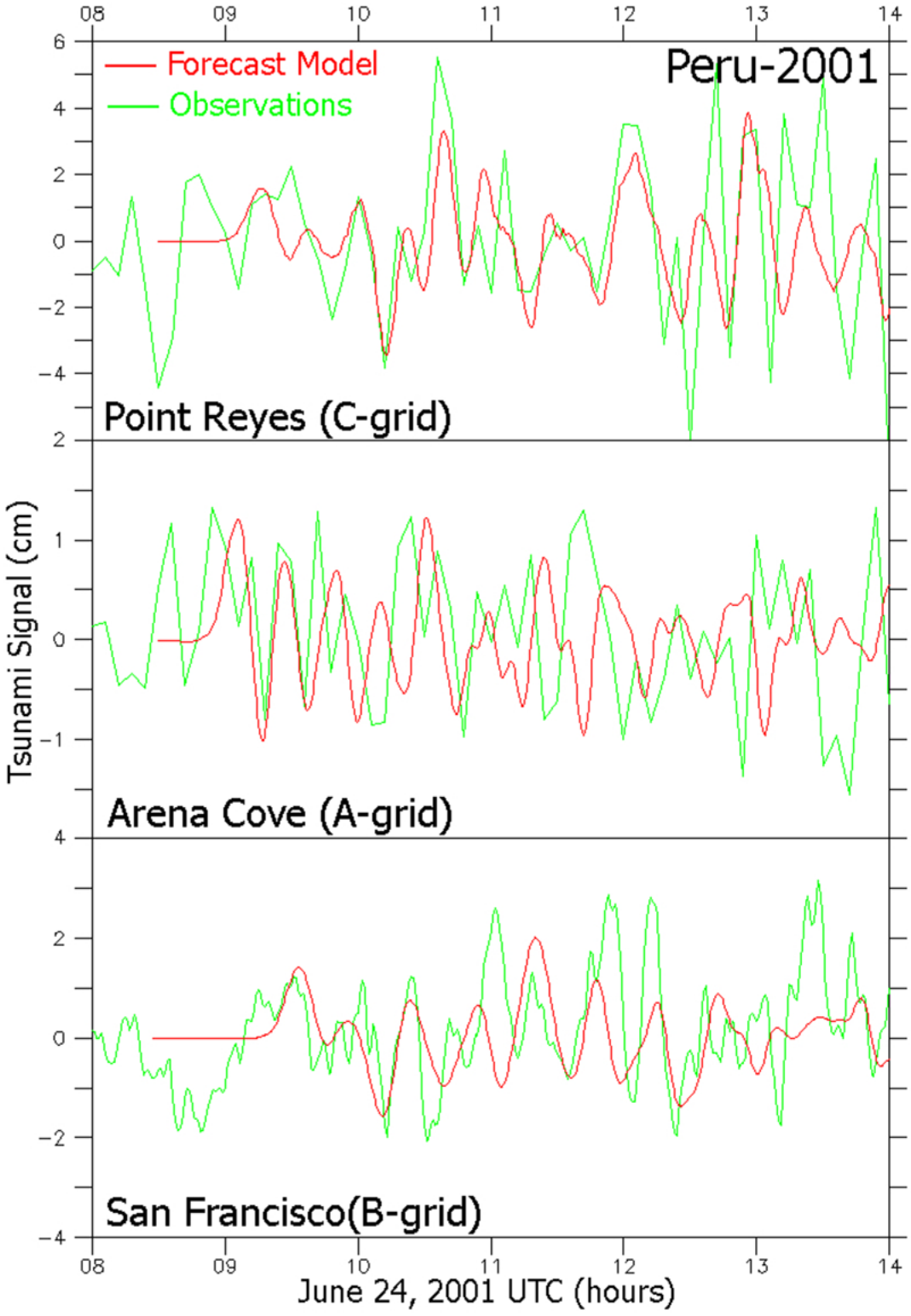

Figure 33. The Peru event of June 23, 2001.

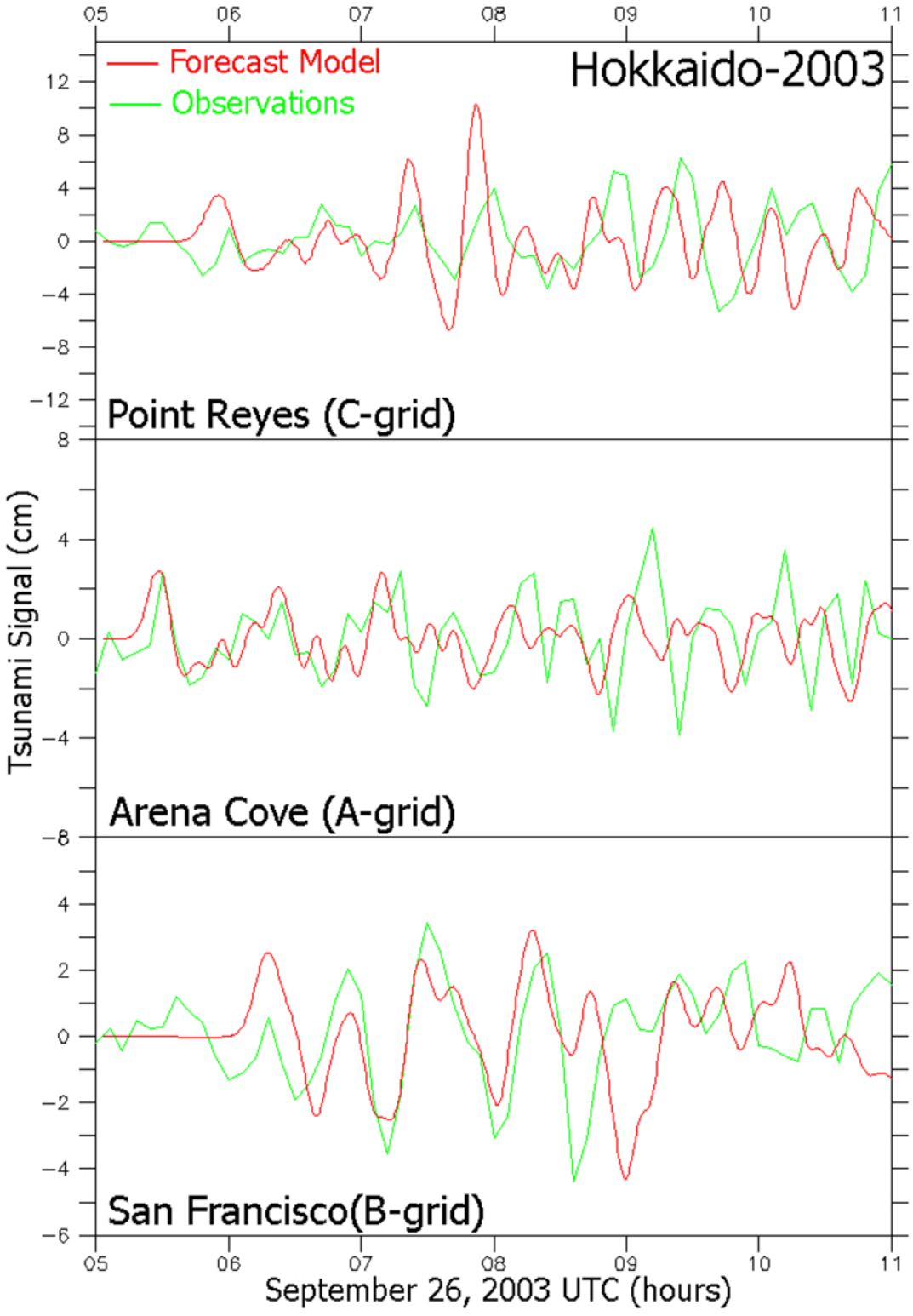

Figure 34. The Hokkaido event of September 25, 2003.

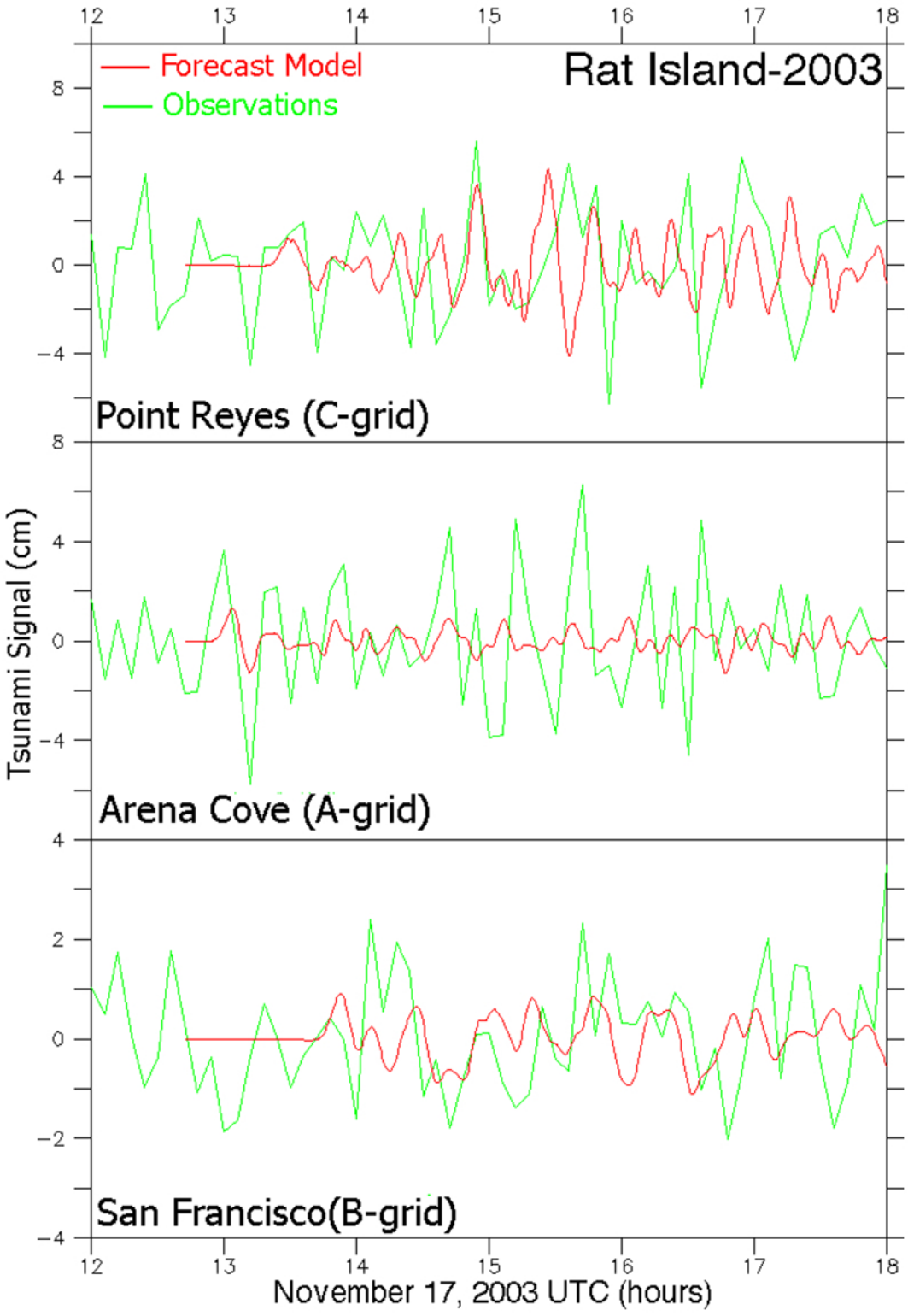

Figure 35. The Rat Island event of November 17, 2003.

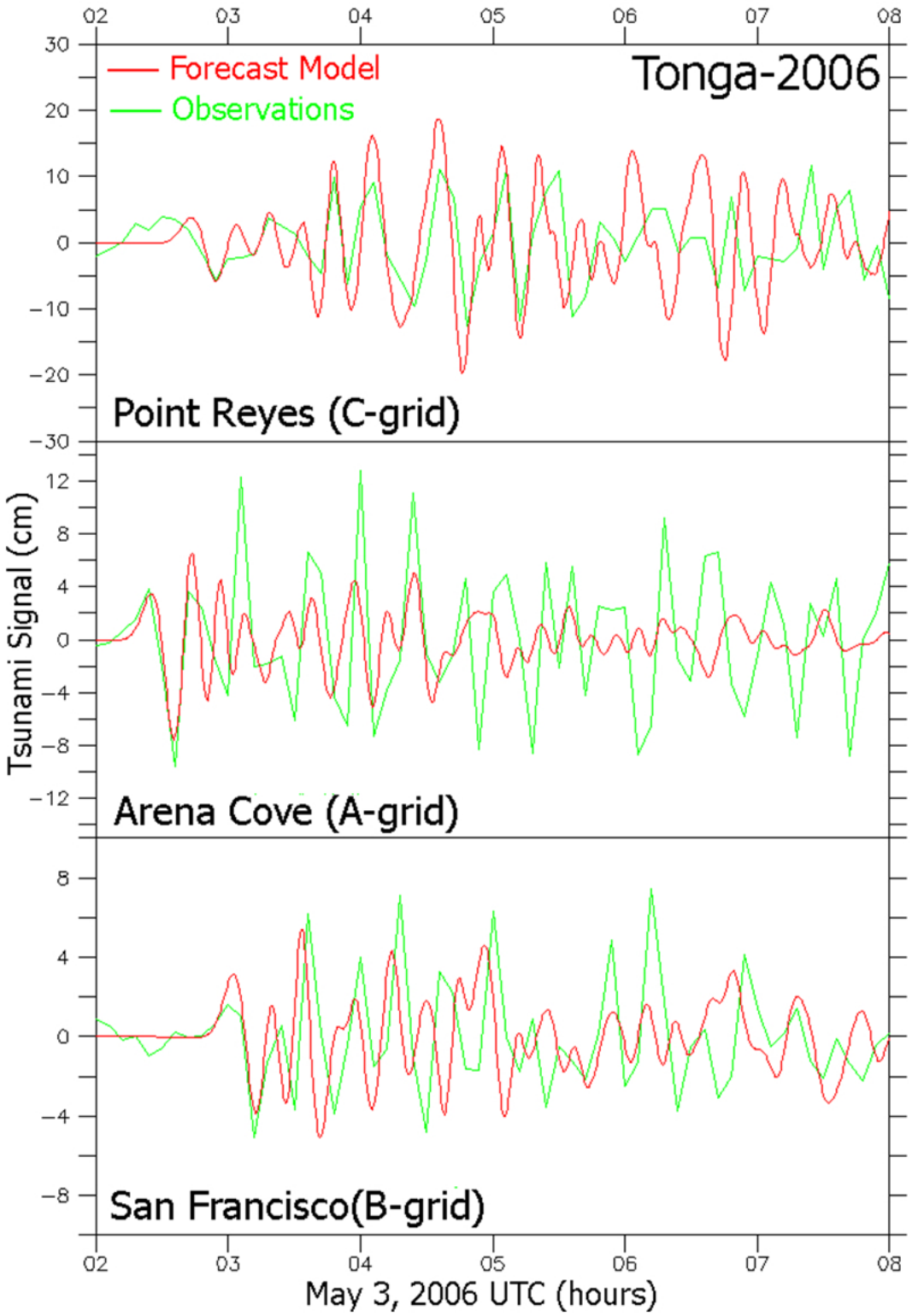

Figure 36. The Tonga event of May 3, 2006.

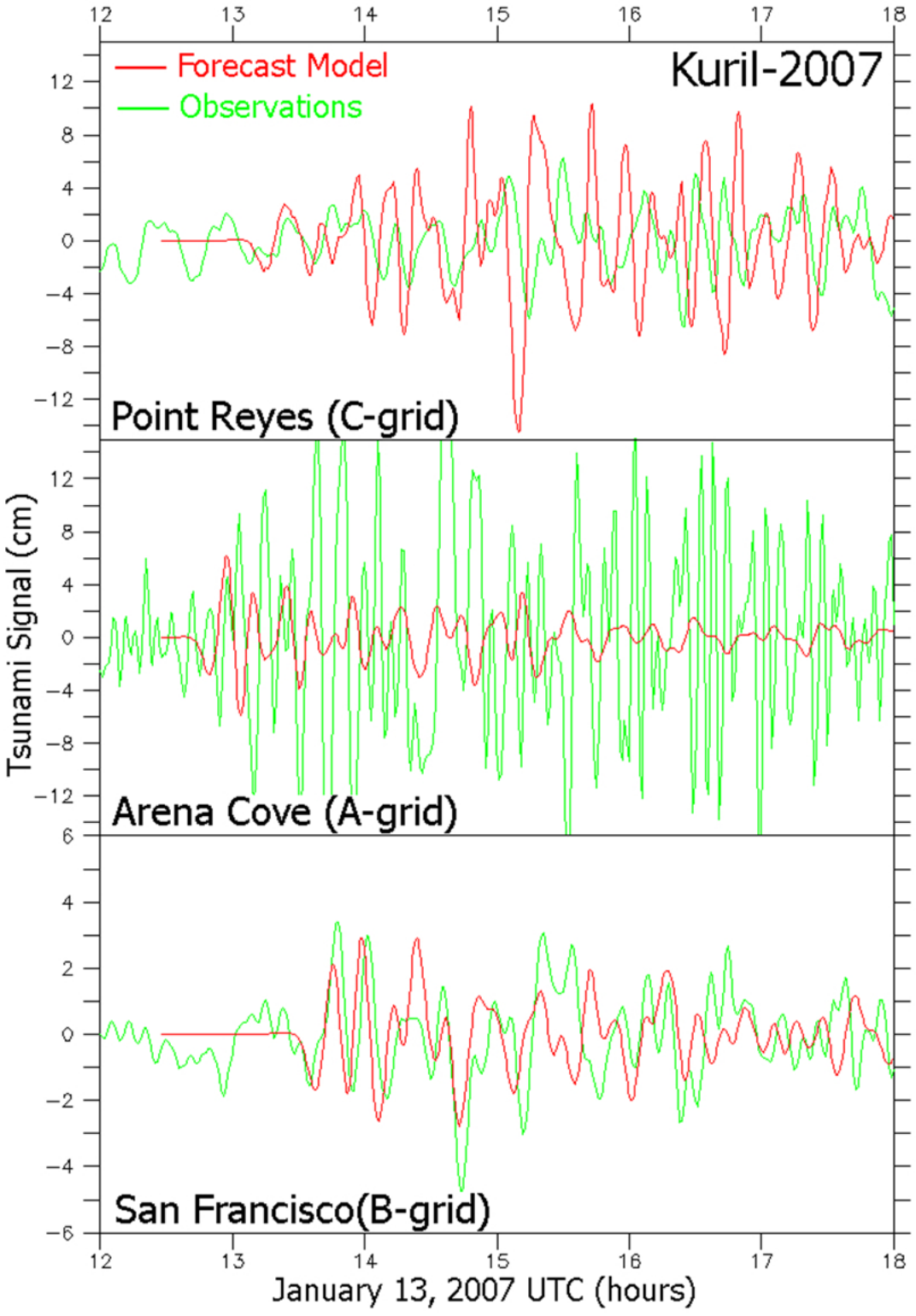

Figure 37. The normal thrust event off the Kuril Islands on January 13, 2007.

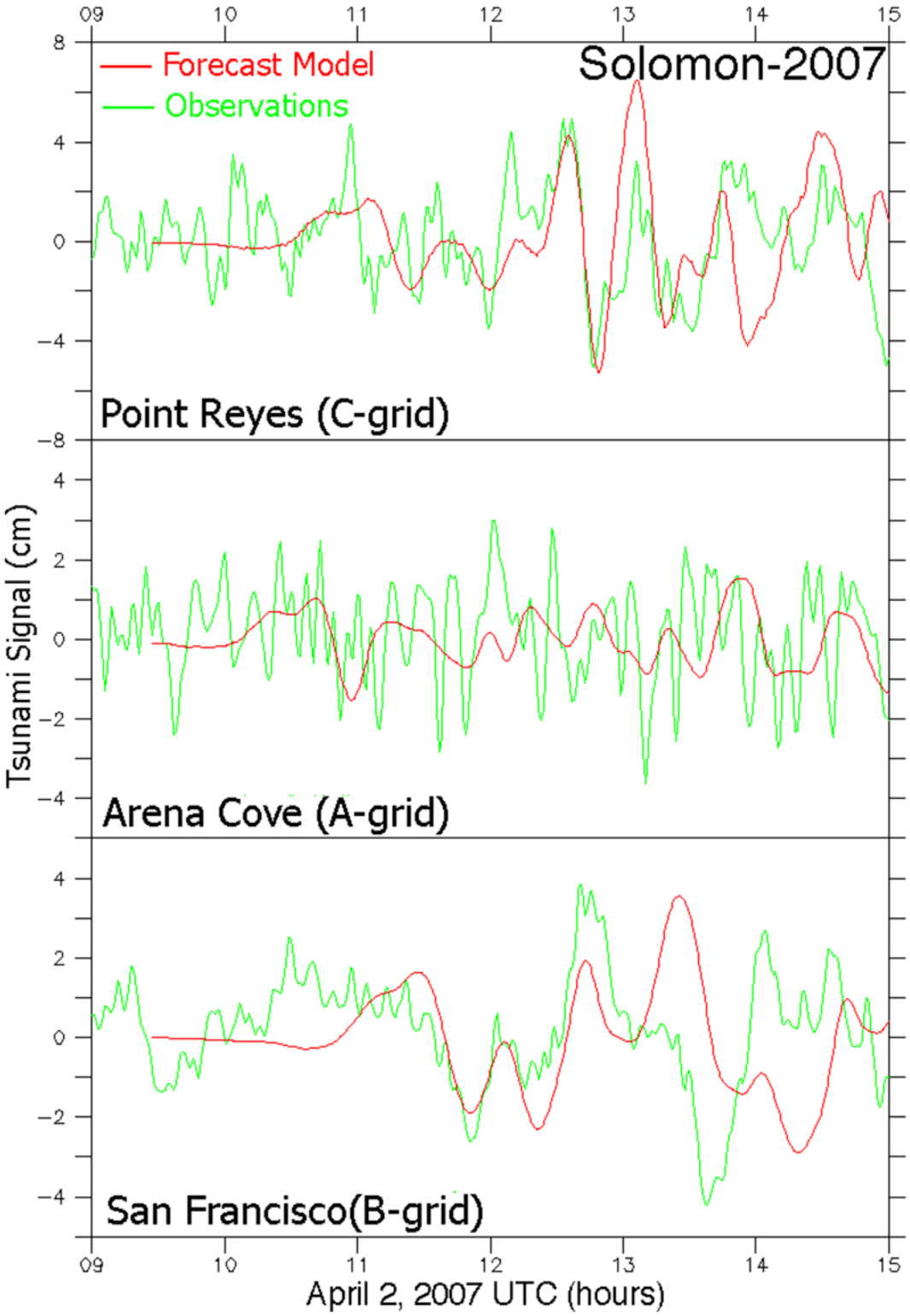

Figure 38. The Solomon event of April 1, 2007.

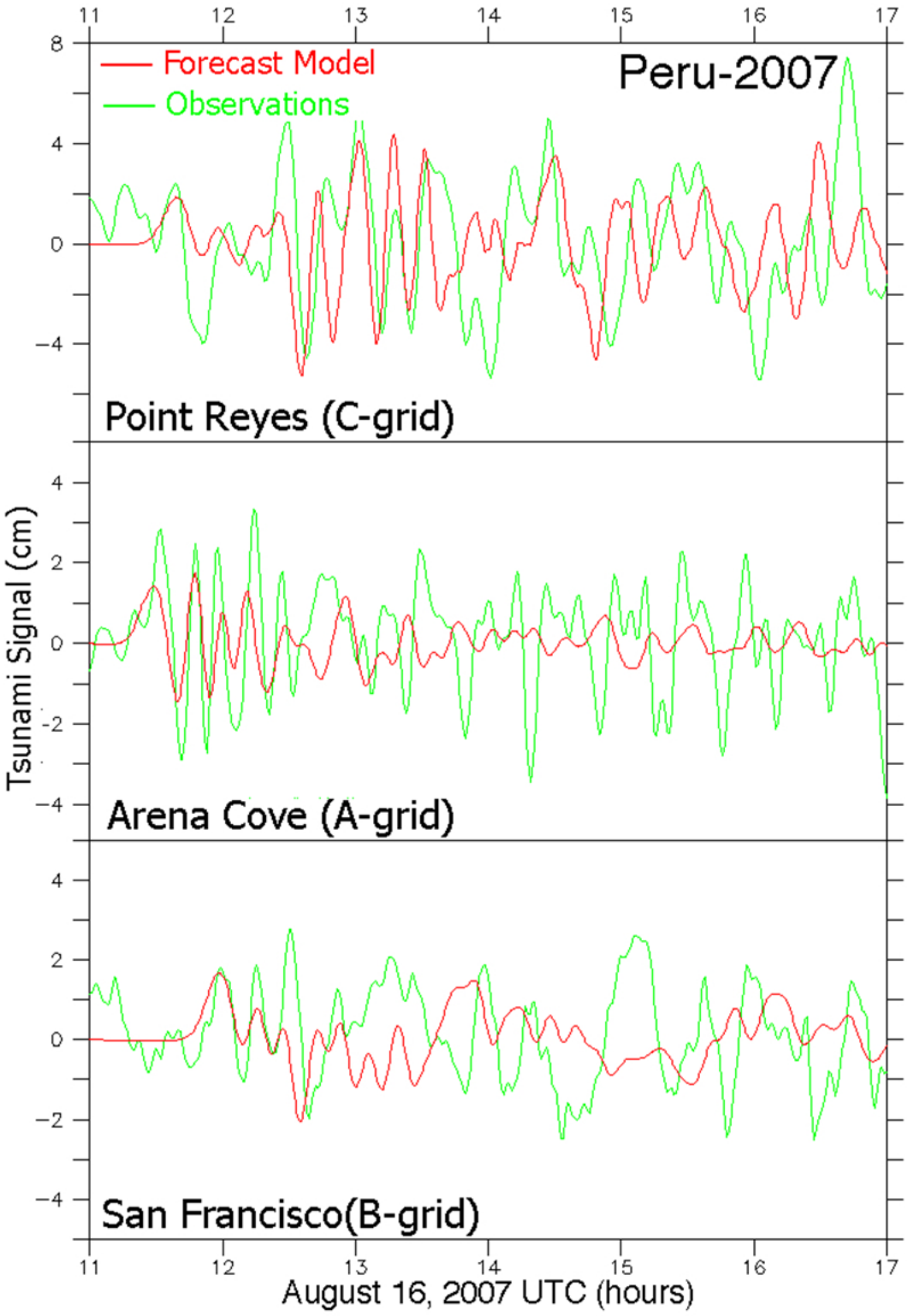

Figure 39. The Peru event of August 15, 2007.

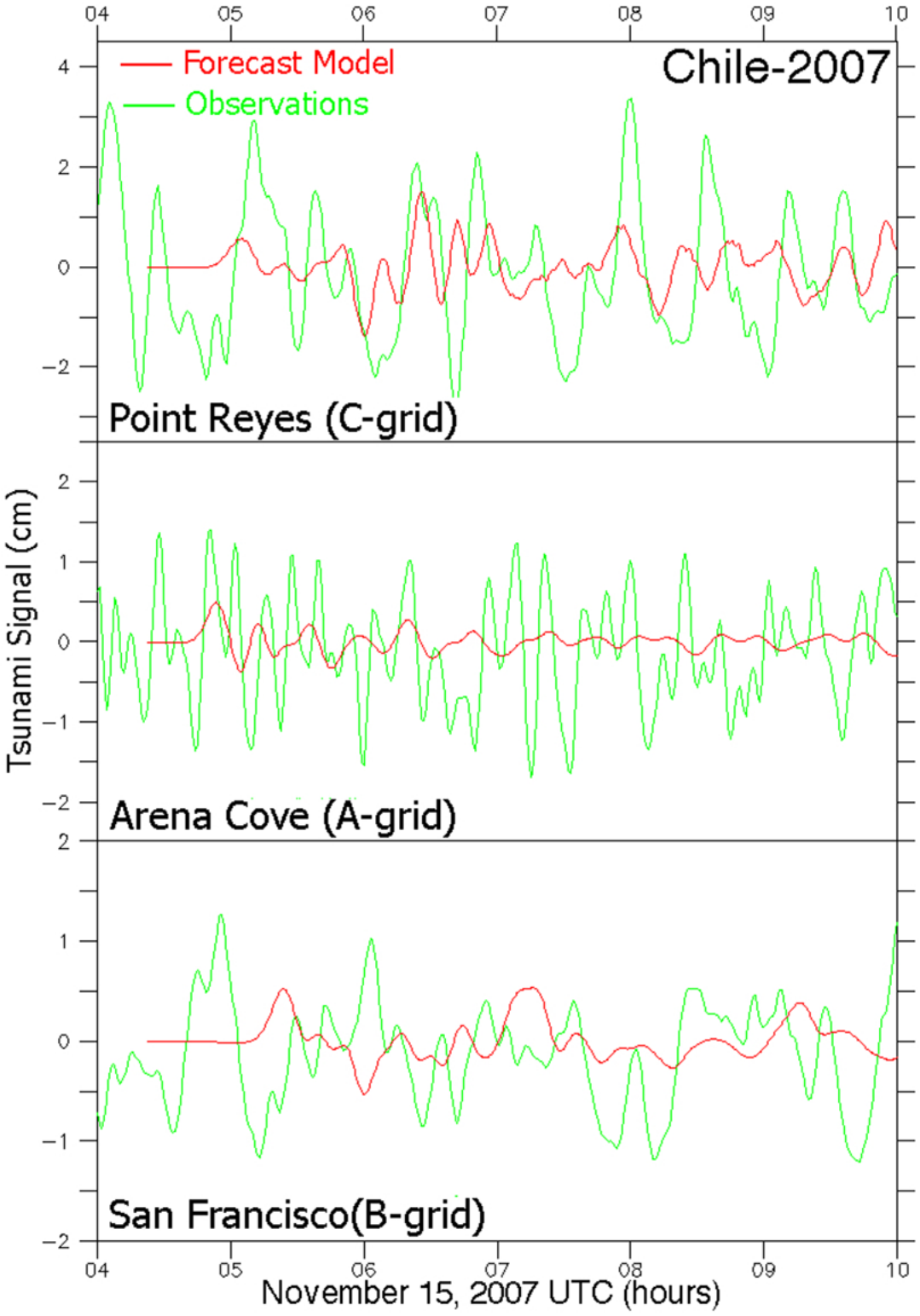

Figure 40. The Chile event of November 14, 2007.

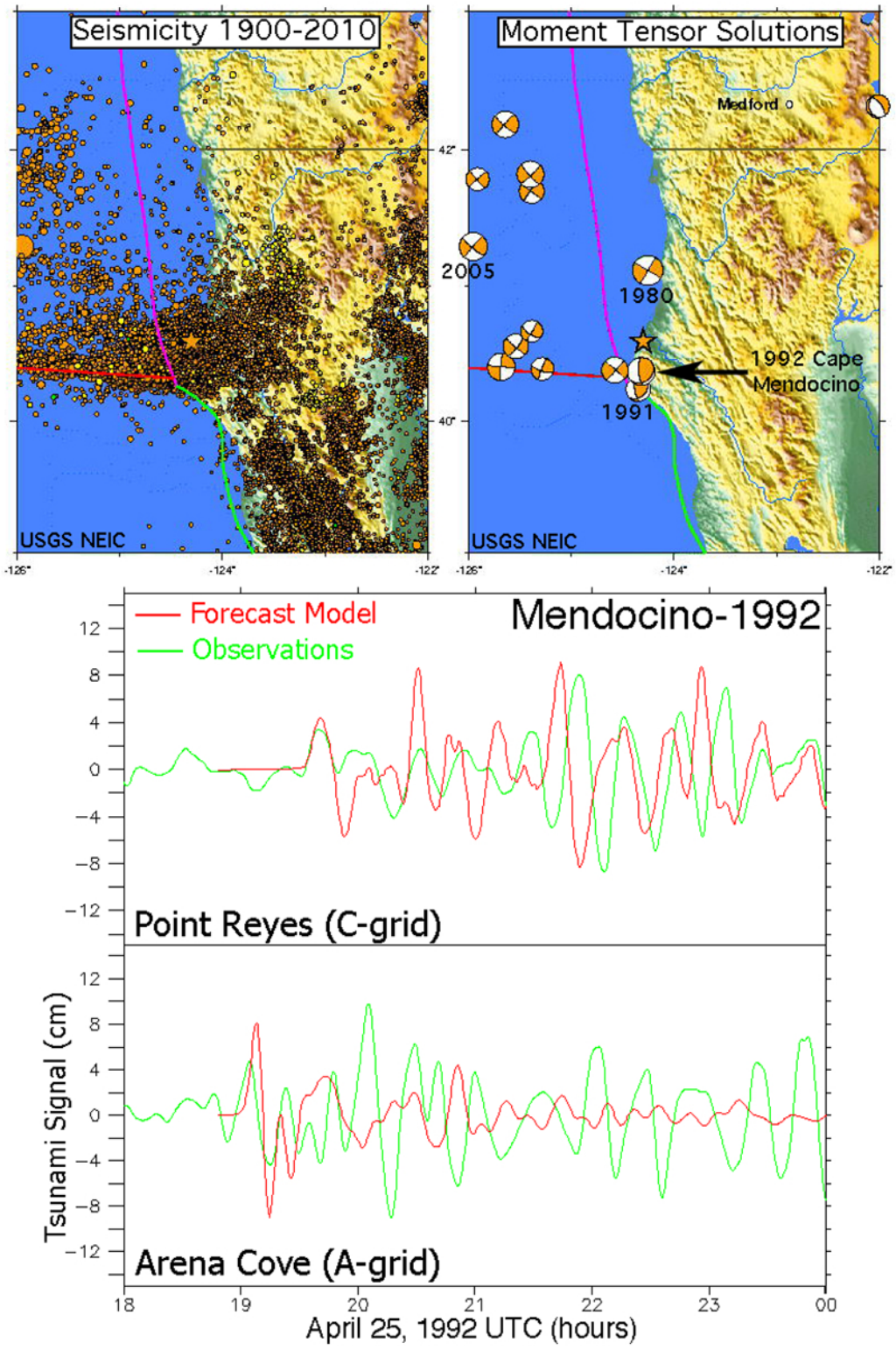

Figure 41. The Cape Mendocino event of April 25, 1992. The upper panels show the frequency of non-thrust events in the vicinity, with only two having a focal mechanism characteristic of subduction. Lower panel: comparison of model with observation at Arena Cove and Point Reyes.

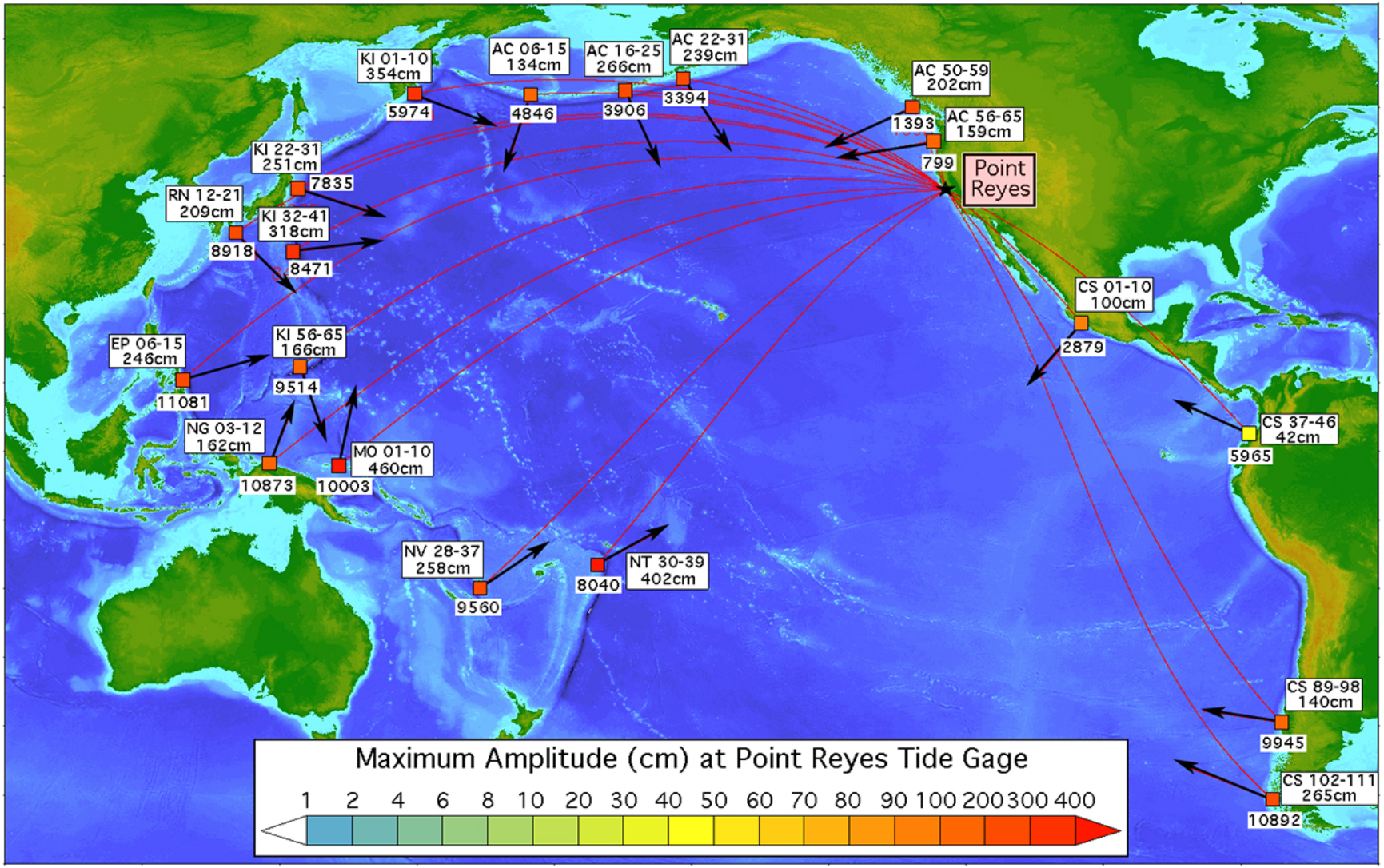

Figure 42. Predicted maximum sea level (from the FM) at the Point Reyes tide gage that might result were “mega-events” to occur at various locations around the Pacific Basin.

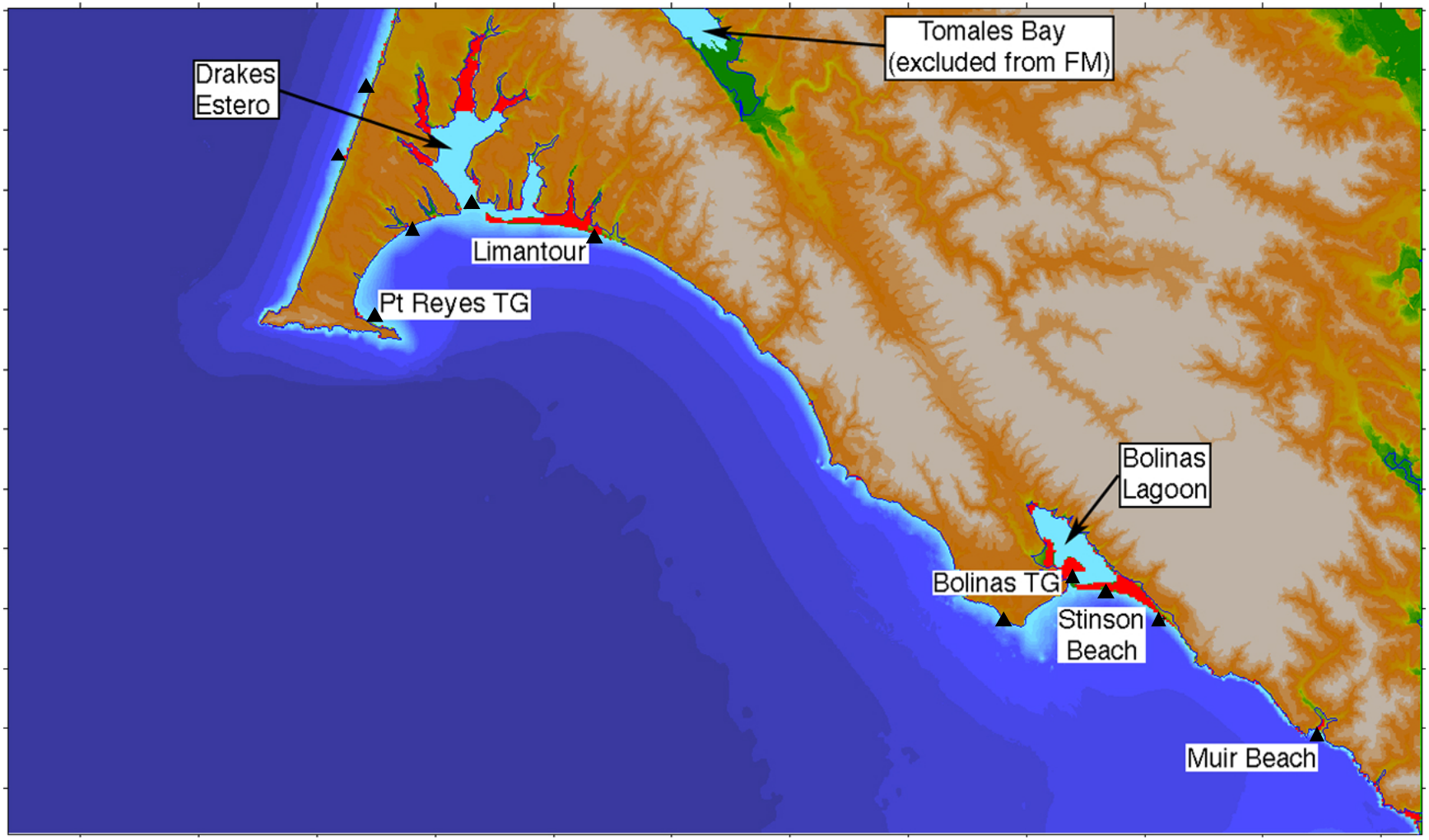

Figure 43. Chart of the area inundated by one or more of the mega-tsunami scenarios modeled with the FM. Shown in blue is the CalEMA inundation line, which is based on a similar ensemble of scenarios.

Appendix A

A1. Reference Model Input (*.in) File for Point Reyes, CA

The following table contains the parameter and file choices used in the input file for the SIFT implementation (most3_facts_nc.in) of the reference model (RM) for Point Reyes, CA.

Parameter/File*	**Purpose**
0.0010	Minimum amp. of input offshore wave (m)
1.5	Minimum depth of offshore (m)
0.1	Dry land depth of inundation (m)
0.0009	Friction coefficient (n**2)
1	Let A-Grid and B-Grid run up
900.0	Max eta before blow-up (m)
0.6	Time step (sec)
48000	Total number of time steps in run
2	Time steps between A-Grid computations
1	Time steps between B-Grid computations
50	Time steps between output steps
0	Time steps before saving first output step
1	Save output every n-th grid point
PtReyesCA_RM_A.most	A-grid bathymetry file
PtReyesCA_RM_B.most	B-grid bathymetry file
PtReyesCA_RM_C.most	C-grid bathymetry file
./	Directory of source files
,/	Directory for output files

* The column headings are not part of most3_facts_nc.in

A2. Forecast Model Input (*.in) File for Point Reyes, CA

The following table contains the parameter and file choices used in the input file for the SIFT implementation (most3_facts_nc.in) of the optimized forecast model (FM) for Point Reyes, CA. When run on an Intel® Xeon® E5670 2.93GHz processor the forecast model produces four hours of simulation in 9.78 minutes, within the desired 10-minute value for this metric.

Parameter/File*	**Purpose**
0.0010	Minimum amp. of input offshore wave (m)
2.5	Minimum depth of offshore (m)
0.1	Dry land depth of inundation (m)
0.0009	Friction coefficient (n**2)
1	Let A-Grid and B-Grid run up
900.0	Max eta before blow-up (m)
2.0	Time step (sec)
14400	Total number of time steps in run
3	Time steps between A-Grid computations
1	Time steps between B-Grid computations
15	Time steps between output steps
0	Time steps before saving first output step
1	Save output every n-th grid point
PtReyesCA_FM_A.most	A-grid bathymetry file
PtReyesCA_FM_B.most	B-grid bathymetry file
PtReyesCA_FM_C.most	C-grid bathymetry file
./	Directory of source files
,/	Directory for output files

* The column headings are not part of most3_facts_nc.in

Appendix B Propagation Database: Pacific Ocean Unit Sources

Appendix C Synthetic Testing Report